USGS
science for a changing world

Prepared in cooperation with the New Mexico Office of the State Engineer

Geophysical Interpretations of the Southern Española Basin, New Mexico, That Contribute to Understanding Its Hydrogeologic Framework

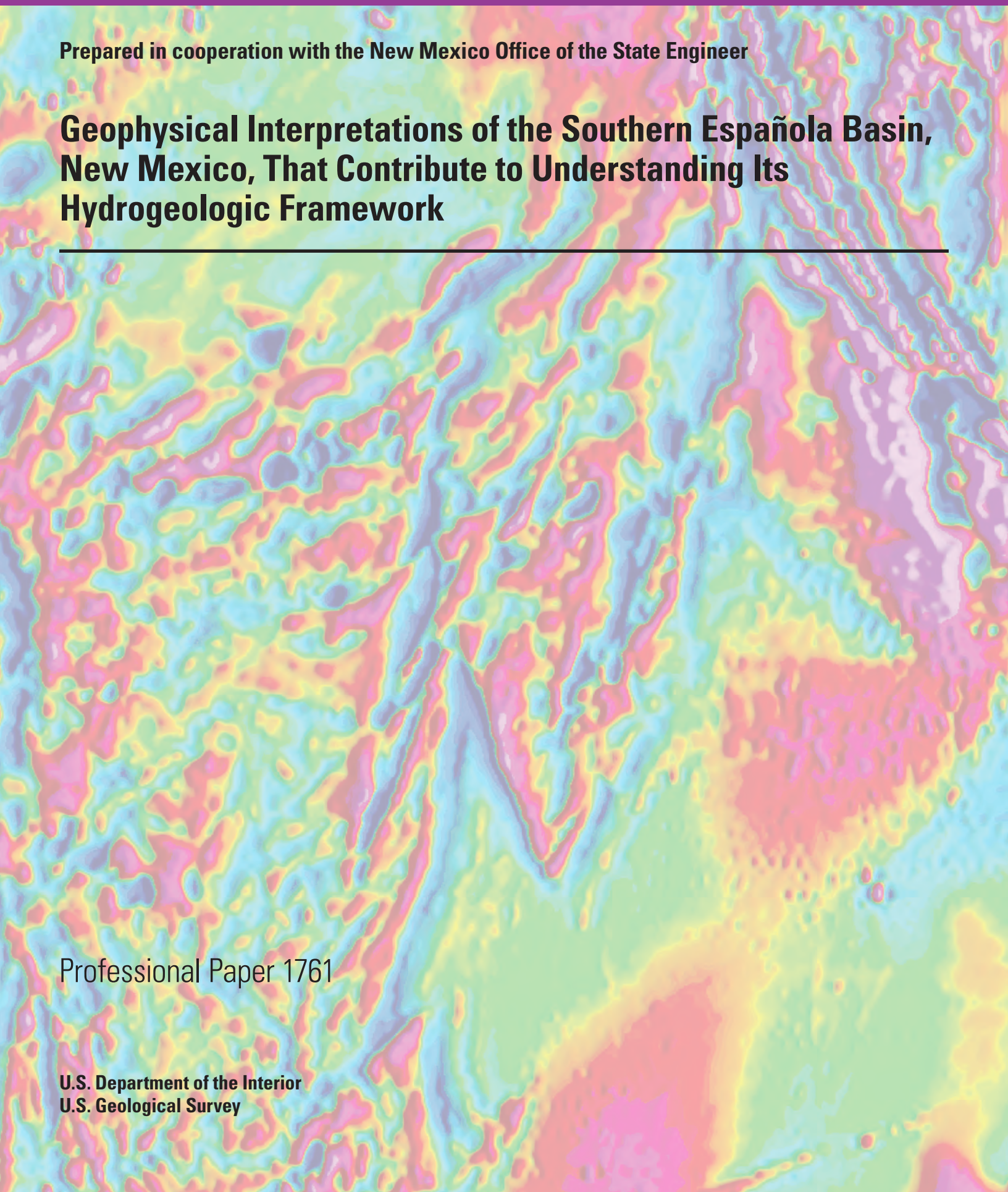

Professional Paper 1761

U.S. Department of the Interior
U.S. Geological Survey

Geophysical Interpretations of the Southern Española Basin, New Mexico, That Contribute to Understanding Its Hydrogeologic Framework

By V.J.S. Grauch, Jeffrey D. Phillips, Daniel J. Koning, Peggy S. Johnson, and Viki Bankey

Prepared in cooperation with the New Mexico Office of the State Engineer

Professional Paper 1761

U.S. Department of the Interior
U.S. Geological Survey

U.S. Department of the Interior
KEN SALAZAR, Secretary

U.S. Geological Survey
Suzette M. Kimball, Acting Director

U.S. Geological Survey, Reston, Virginia: 2009

Suggested citation:
Grauch, V.J.S., Phillips, J.D., Koning, D.J., Johnson, P.S., and Bankey, Viki, 2009, Geophysical interpretations of the southern Española Basin, New Mexico, that contribute to understanding its hydrogeologic framework: U.S. Geological Survey Professional Paper 1761, 88 p.

Contents

Plates

Figures

Tables

Conversion Factors

Multiply	By	To obtain
kg/m^3	0.001	g/cm^3
km	0.621	mi
magnetic susceptibility (SI)	$1/(4\pi) = 0.079577$	magnetic susceptibility (cgs)
m/s	3.2808	ft/sec

Abbreviations Used in This Report

A/m	amperes per meter
cgs	centimeter, gram, second
ft	foot, feet
ft/mi	feet per mile
ft/sec	feet per second
kg/m^3	kilograms per cubic meter
km	kilometer, kilometers
lb/ft^3	pounds per cubic foot
m	meter, meters
m/km	meters per kilometer
m/s	meters per second
mi	mile, miles
nT	nanotesla
2D	two dimensional
3D	three dimensional
CD	compact disk
HGM	horizontal-gradient magnitude
MT	magnetotelluric
N	structural index
NMBGMR	New Mexico Bureau of Geology and Mineral Resources
ohm-m	ohm-meter
SAGE	Summer of Applied Geophysical Experience
SI	Système International

Vertical coordinate information is referenced to the North American Vertical Datum of 1929 (NAVD27).

Horizontal coordinate information is referenced to the North American Datum of 1927 (NAD27).

Altitude, as used in this report, refers to distance above the vertical datum.

Geophysical Interpretations of the Southern Española Basin, New Mexico, That Contribute to Understanding Its Hydrogeologic Framework

By V.J.S. Grauch, Jeffrey D. Phillips, Daniel J. Koning,[1] Peggy S. Johnson,[1] and Viki Bankey

Executive Summary

The southern Española Basin consists of a westward- and northward-thickening wedge of rift fill, composed primarily of Santa Fe Group sediments, that serves as the principal aquifer for the city of Santa Fe and surrounding areas. Detailed aeromagnetic surveys were flown to better understand ground-water resources in this aquifer. This report presents a synthesis of interpretations derived from the aeromagnetic data combined with gravity data and other constraints. The interpretations were accomplished using qualitative interpretation, state-of-art data analysis techniques, and two- and three-dimensional modeling. The results depict the presence of and depth to many geologic features that have hydrogeologic significance, such as shallow faults, different types of igneous units, and basement rocks. The results are presented as map interpretations, geophysical profile models, and a digital surface that represents the base of Santa Fe Group sediments. The following are key points derived from our geophysical interpretations that contribute to an improved understanding of southern Española Basin's hydrogeologic framework.

- The Santa Fe Group aquifer thickens substantially northward across a curvilinear structural feature located south of Santa Fe, called the Rancho Viejo hinge zone. South of the hinge zone, Santa Fe Group sediments overlie the Santa Fe platform and average about 75 meters (250 feet) thick. The platform is composed of generally low permeability volcaniclastic and volcanic rocks of the Espinaso Formation and Cieneguilla volcanic complex. North of the hinge zone, Santa Fe Group sediments thicken markedly by about 130–150 meters per kilometer (700–800 feet per mile) and ultimately reach thicknesses greater than 3 kilometers (10,000 feet) under the Pajarito Plateau west of Española.
- The Santa Fe platform has local irregularities that produce variations in sediment thickness at the base of the Santa Fe Group. These variations are not apparent at the surface. A large, northwest-elongated paleovalley containing as much as 90–150 meters (300–500 feet) of Santa Fe Group sediments is interpreted to be buried in the vicinity of Eldorado at Santa Fe.
- As indicated by the aeromagnetic analysis, in three large areas the low permeability bedrock of the Santa Fe platform is completely missing. In these areas, there may be a direct hydrologic connection between the Santa Fe Group and older, pre-Santa Fe Group sedimentary aquifers.
- Older, pre-Santa Fe Group sedimentary rocks are thickest under the Santa Fe Platform and decrease to a thin veneer of volcanic rocks and limestone overlying crystalline basement north of the Rancho Viejo hinge zone. Thus, deep sandstone aquifers are possible under the platform but are unlikely below the Santa Fe Group in the deeper parts of the basin.
- North of Santa Fe, geophysical modeling supports geologic information showing that the basin floor dips generally westward; dips are moderate (7°–20°) at the mountain front and again about 10–12 km (6.3–7.5 miles) west of the front and are shallow (~5°) in between. The Santa Fe Group aquifer thickens westward in concert with these dips.
- A northerly regional fabric in the basement rocks of the mountain front, expressed in the aeromagnetic data, may influence groundwater flow within the mountain block. This fabric does not extend more than 1–5 kilometers (0.6–3.1 miles) west of the mountain front. Thus, the basement in the subsurface is expected to

[1] New Mexico Bureau of Geology and Mineral Resources

have much different lithologic characteristics and fracturing than is observed in the exposed basement rocks.

- Aeromagnetic interpretations suggest that numerous northerly striking faults offset the basin fill, more than can be recognized at the surface. Moreover, the magnitudes of the observed aeromagnetic anomalies indicate the faults likely juxtapose at least 30 meters (~100 feet) of sediments that have contrasting bulk magnetic properties. These inferences and measured magnetic susceptibilities suggest that (1) significant thicknesses of sediments with differing grain size or volcanic-clast content are juxtaposed at these faults; (2) the juxtapositions may produce permeability contrasts that compartmentalize Santa Fe Group aquifers at depth; and (3) the potential for these permeability contrasts is greater than previously recognized. Conversely, the absence of aeromagnetic expression associated with mapped faults that offset magnetic sediments south of Chimayó suggests that the sediment type, when considered in bulk, does not differ appreciably across these faults.
- Many of the numerous mapped and geophysically inferred faults can be organized into two main fault systems (Agua Fria and Barrancos), which traverse north to north-northwest through the central part of the study area near the communities of Eldorado at Santa Fe, Santa Fe, Pojoaque, and Española. The faults in these systems typically involve basement rocks. The faults may serve as partial barriers, compartmentalize aquifers, or possibly control upwelling of deep ground water from fractured basement rocks. The Agua Fria fault system includes the San Isidro Crossing fault (exposed near the road of the same name at the Santa Fe River), which coincides with a large drop in the water table.
- A north-northeast-trending bedrock high, indicated by gravity and electrical geophysical models, underlies the Cerros del Rio volcanic field. Its steep eastern side may be represented by east-down faults or an east-dipping monocline. It may form a major obstacle to westerly groundwater flow.
- Basalts of the Cerros del Rio volcanic field, included in the uppermost sections of the basin fill, are generally limited in lateral extent to the area of exposure within the study area, on the basis of their aeromagnetic signatures. However, 9 kilometers (5.5 miles) directly west of Santa Fe the basalts are interpreted to underlie sediments of the Ancha Formation at shallow depth. Thus, drilling adjacent to the volcanic field should not encounter particularly thick basalts except in this local area.
- Fracture-dominated granitic rocks in the Cerrillos Hills area form a massive body at depth, on the basis of a strong signature in the aeromagnetic data. The bulk of this intrusive complex has fairly steep sides, encompasses the area of the hills, and extends outside the hills, mostly to the southeast.

The geophysical interpretations also offer insights into the geologic history of the southern Española Basin. The following are some key points.

- A sharp decrease in thickness of the pre-rift sedimentary section inferred from gravity analysis and seismic information follows a 40-kilometer (25-mile)-long northwest trend in the southwestern Española Basin. This trend may mark the southwestern extent of the Laramide uplift previously hypothesized for the area to the northeast.
- The Rancho Viejo hinge zone may represent a long-lived crustal weakness that underwent a reversal of motion from Laramide time (north side up) to Rio Grande rift time (north side down). As the north side went down, strata on the Santa Fe Platform (the south side) were generally eroded. The north-side-down tilting was completed before deposition of the Ancha Formation in Pliocene time.
- Near the Rancho Viejo hinge zone, three-dimensional modeling suggests that the late Eocene–Oligocene Espinaso Formation thickened, and aeromagnetic data delineate associated volcanic vents. This coincidence suggests that magmatism was concentrated along the hinge zone at this time.
- A marked contrast in regional fabrics within the Precambrian basement, apparent in the aeromagnetic data, occurs at a semilinear north-south trend at the mountain front. Comparison with gravity data suggests the contrast is not associated with structural relief, so it likely developed before rifting began.
- The north-northeast-trending bedrock high under the Cerros del Rio volcanic field may have eroded less during Laramide time than adjacent rocks to the east. This interpretation suggests that the modern bedrock high was a structural low in Laramide time that was later inverted to a structural high in rift time.

Introduction

Basin-fill aquifers within the Española Basin and adjoining Santa Fe embayment (fig. 1) are the primary ground-water resource of the City of Santa Fe, Española, six Pueblo nations, and surrounding suburban areas. A better understanding of the subsurface geologic controls on ground-water flow and storage is needed to better define and manage this important ground-water resource. Geophysical investigations using aeromagnetic and gravity data are valuable for improving this understanding. Aeromagnetic data, acquired from aircraft, measure the subtle variations in the Earth's magnetic field due to differences in the naturally occurring magnetic properties of the underlying rocks and sediments. Gravity data, typically acquired from the ground surface, measure small variations in the Earth's gravity field due to differences in bulk densities of the underlying rocks and sediments. Although both aeromagnetic and gravity data are generally insensitive to water, differences in the magnetic properties and densities that they detect can be used to infer many aspects of ground-water-bearing rocks (the "hydrogeologic framework"). In the Española Basin, aeromagnetic and gravity data are used to interpret variations in thickness of basin-fill sediments (the Santa Fe Group aquifer), define major structures and composition of the basin floor, map the distribution of intrusions and volcanic rocks, and locate concealed intrabasin faults.

The impetus for using aeromagnetic and gravity methods for ground-water studies in the southern Española Basin came from a multi-agency study of the Middle Rio Grande Basin during the late 1990s (Bartolino and Cole, 2002) that encompassed the Albuquerque and Santo Domingo Basins to the south. In particular, the aeromagnetic method (previously considered unconventional for ground-water studies) proved successful in the Middle Rio Grande Basin. It efficiently located subsurface hydrogeologic features, knowledge of which ultimately improved the ground-water-flow model for the basin. In anticipation of future ground-water studies to the north, the New Mexico Office of the State Engineer augmented funding to extend the high-resolution aeromagnetic coverage into the southern Española Basin in 1998 (U.S. Geological Survey and others, 1999). Subsequent interpretations of these data provided useful new information on the depth and lateral extent of Precambrian basement rocks, buried intrusive and volcanic rocks, and shallow faults (Grauch and Bankey, 2003; Phillips and Grauch, 2004). This knowledge improved the understanding of aquifer thickness and depths to potential aquifers, and it allowed better prediction of ground-water storage, flow, and quality and better informed choices of drilling sites. The aeromagnetic interpretations benefitted ground-water studies by providing new information used in (1) follow-up drilling and studies by the New Mexico Office of the State Engineer, (2) development of water-use zoning maps for the County of Santa Fe, (3) construction of regional ground-water flow models for the City and County of Santa Fe, and (4) the work of hydrology consultant firms in support of existing and new subdivisions. Because of these benefits, an additional helicopter survey was flown in 2005 to expand the coverage of high-resolution aeromagnetic data for the front of the Santa Fe Mountains (Bankey and others, 2006). Funding was provided by the U.S. Geological Survey, the New Mexico Office of the State Engineer, and Santa Fe County.

In addition to the new aeromagnetic coverage, recent new work by others in the basin has provided motivation to update and expand the scope of the earlier aeromagnetic interpretations of Grauch and Bankey (2003) and Phillips and Grauch (2004). A major objective has been construction of a digital surface representing the base of Santa Fe Group sediments—the base of the basin aquifer system. For this effort, gravity modeling, constrained by lithologic logs from wells and independent geophysical data, has been invaluable for resolving ambiguities in magnetic depth estimates encountered in the earlier work, and it provides most of the information for the deeper parts of the basin.

The organization of this report progresses from introductory material to data descriptions, methods, model construction, and interpreted features arranged by geologic age, and then to a summary. However, the topics are interrelated and they overlap owing to the iterative nature of the geophysical interpretation. For example, as one element in the basin is understood from one geophysical approach, a new understanding of other elements develops or a new approach becomes apparent. Moreover, one commonly must understand the geophysical expression of the subsurface geology below an aquifer of interest before the overlying units can be interpreted. Therefore, final interpretations and all approaches that led to the conclusions are difficult to discuss in a linear fashion, and the geologic units of the least interest hydrogeologically must be discussed first. For this reason, the next section—the geophysical objectives and approach and the relevance of these objectives to the hydrogeologic framework—is provided to help place the following sections in context.

Objectives, Approach, and Hydrogeologic Significance

The objectives of the geophysical interpretations are to characterize and image basin elements that are important for understanding the hydrogeologic framework, especially where those elements are concealed below the ground. The key elements amenable to geophysical interpretation in the southern Española Basin can be divided into geologic units composing basin fill, geologic units composing the basin floor, and structure (fig. 2). For this study, geologic units are grouped into interpretative packages on the basis of similar geophysical expression and representation of key basin elements. Basin-fill units constitute the most important aquifers in the basin, whereas basin-floor units are generally less permeable and form the base of the basin aquifers. Overall basin shape

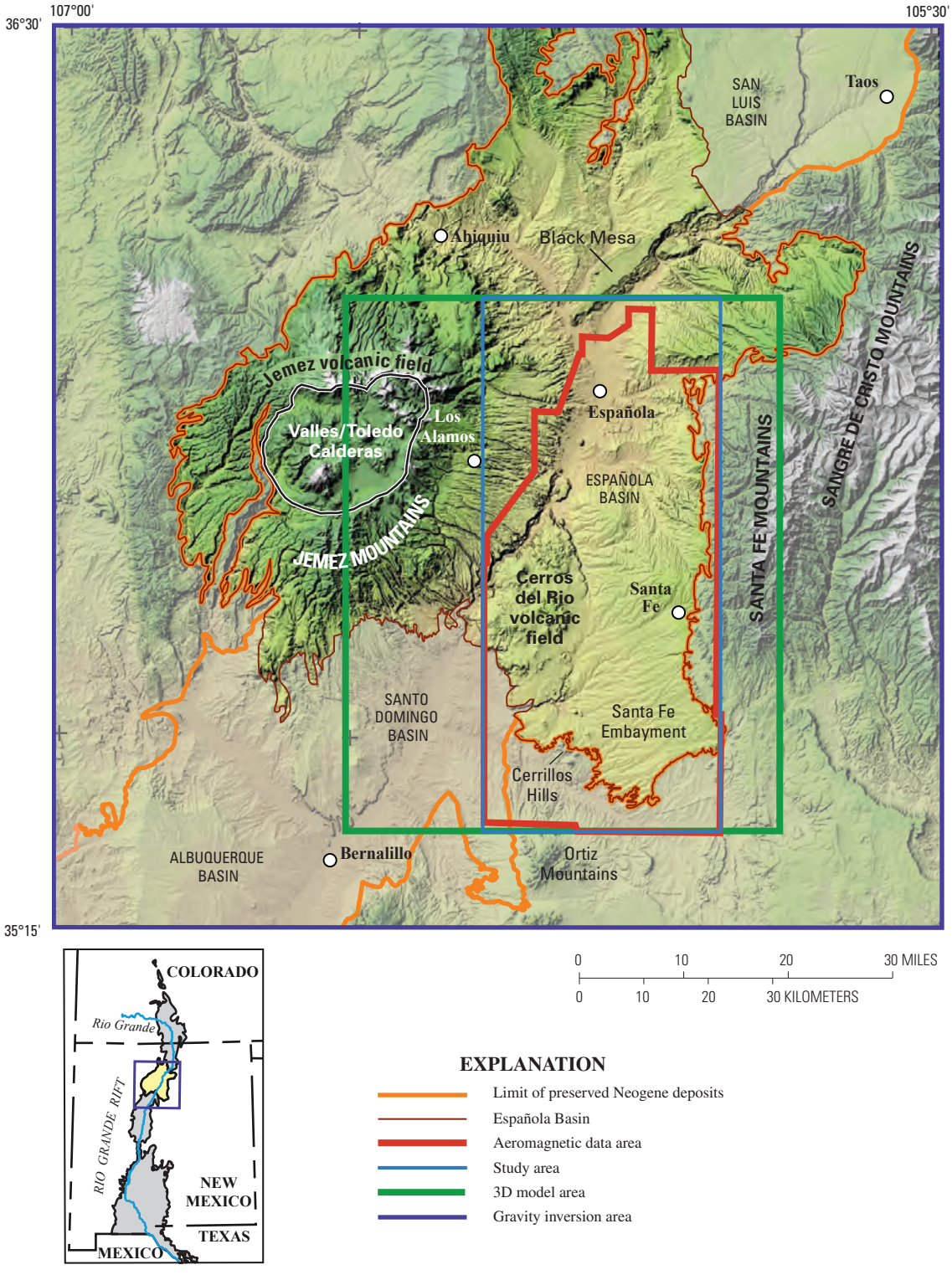

Figure 1. Española Basin and areas used for various analyses. Processed Landsat satellite imagery is from Sawyer (2004). Overall topographic relief within the study area is 1,145 m (3,750 ft).

and irregularities on the top of the basin floor, resulting from faulting or the erosion of ancient landscapes, may bear on the hydrogeology of the overlying basin fill because they affect factors such as sediment type, aquifer thickness, and stratal dip. In addition, faults that cut basin fill can act as partial barriers to fluid flow and juxtapose units of differing permeabilities, which effectively compartmentalize the aquifers.

A different geophysical approach is required to characterize and image each basin element (table 1). The final interpretations take the form of lines on a map (map interpretations) and on digital surfaces derived from three-dimensional (3D) integrated modeling. Interim interpreted products are two-dimensional (2D) geophysical profile models that were incorporated into the 3D model. Map interpretations, cross sections, and contour maps derived from the surfaces are shown for selected areas in the figures cited in subsequent sections. In plate 1 they are plotted together with contours from a digital surface for the whole study area. Digital surfaces related to the model surface of the Santa Fe Group, in georegistered format, can be downloaded from the compact disk (CD) in the pocket.

The following sections summarize the hydrogeologic importance of the key basin elements and what aspects of these elements are determined from the geophysical interpretations in this report. The basin floor is discussed first, because it must be understood before aspects of the overlying basin fill can be addressed. Mapped geologic units that are included in these categories are discussed in the section entitled Geologic Setting.

Elements of the Basin Floor

We generally categorize components of the basin floor as Precambrian basement, pre-rift sedimentary section, Tertiary intrusions, and Tertiary older volcanic rocks. Not all of these units are present throughout the study area. In particular, the pre-rift sedimentary section is thickest at the southern end of the basin, but it was variably removed before deposition of the Santa Fe Group and thins considerably to the north (fig. 2). Moreover, some of the Tertiary intrusions are confined to the vicinity of the Cerrillos Hills, and some are inferred to lie within the pile of older volcanic rocks.

Interpreting the nature of and depth to the Precambrian basement is important for understanding the hydrogeologic framework for several reasons: (1) it closely underlies and thus helps define the base of the basin-fill aquifers throughout most of the area north of the Santa Fe River; (2) it is the main mountain-block aquifer, dominated by flow through fractures; (3) it directly underlies the limestone aquifers southeast of Santa Fe and thus helps define the base of this aquifer; and (4) its internal structure may control the lateral or vertical flow of ground water and influence recharge. Aeromagnetic data and filtered maps were used to qualitatively characterize overall differences in the lithology and structure of the Precambrian basement, especially at the mountain front. In some areas, strong aeromagnetic signatures of the Precambrian basement show elongate structural and lithologic trends that may help predict ground-water flow or patterns of recharge from the mountains. In other places, the Precambrian basement is effectively invisible in the aeromagnetic data because of its very low magnetic susceptibilities. Thus, gravity data were used to constrain the overall form of the basement surface, despite sparse data in the northern part of the area. Qualitative concepts of the shape and nature of the basement were developed using joint gravity and magnetic modeling in two dimensions and limited integrated modeling of subsurface information in three dimensions.

The pre-rift sedimentary section contains Paleozoic through Eocene mostly clastic sedimentary units deposited in a variety of environments. At the top of the uneroded section is an Eocene sandstone-dominated sequence that may locally be important for water storage (Finch, 2008). At the base of the section, a sequence of Paleozoic limestones locally produces water. Below the Eocene sandstones, the low-permeability Mesozoic Mancos Shale is as much as 700 meters (m) thick in the area of the Cerrillos Hills (Sawyer and Minor, 2006a). Although none of the clastic units in the pre-rift section has overall permeabilities and yields as high as those of the Santa Fe Group sediments (Lewis and West, 1995), they may be important where the overlying Santa Fe Group is thin or where uplift has brought the limestones near the surface, such as near the mountain front southeast of Santa Fe. The thickness of the pre-rift section is interpreted by using limited seismic and well-log information, supplemented by indirect inferences that can be made from gravity data analysis. The pre-rift section is considered as one package, because gravity and aeromagnetic data cannot distinguish individual units. Inferences about the presence of individual units underlying the Santa Fe Group were made in a few local areas, where well data exist.

Tertiary intrusions are important in the hydrogeologic framework because they represent a fracture-dominated rather than a porous medium. Dikes and sills emanating from the bodies may locally divert or obstruct ground-water flow paths and may influence ground-water quality. Small intrusions are located under the Cerros del Rio volcanic field and within the sequence of Tertiary older volcanic rocks. A larger intrusive complex, which is associated with turquoise and metal deposits (Giles, 1995), is located in the vicinity of the Cerrillos Hills (fig. 2). Inspection and analysis of the aeromagnetic data provides the best definition of the overall lateral extents of these intrusions at depth. No attempt was made to estimate depths to the top of the Cerrillos intrusion from the geophysical data because (1) in many places the intrusive rocks cannot be distinguished from overlying, magnetic, Tertiary older volcanic rocks; (2) weakly magnetic pre-rift sedimentary rocks cannot be distinguished from overlying Santa Fe Group sediments; and (3) gravity data and subsurface information from other sources are not adequate.

The Tertiary older volcanic rock package is an important element of the hydrogeologic framework because (1) the rocks directly underlie Santa Fe Group sediments in most of the southern part of the study area; (2) they generally form

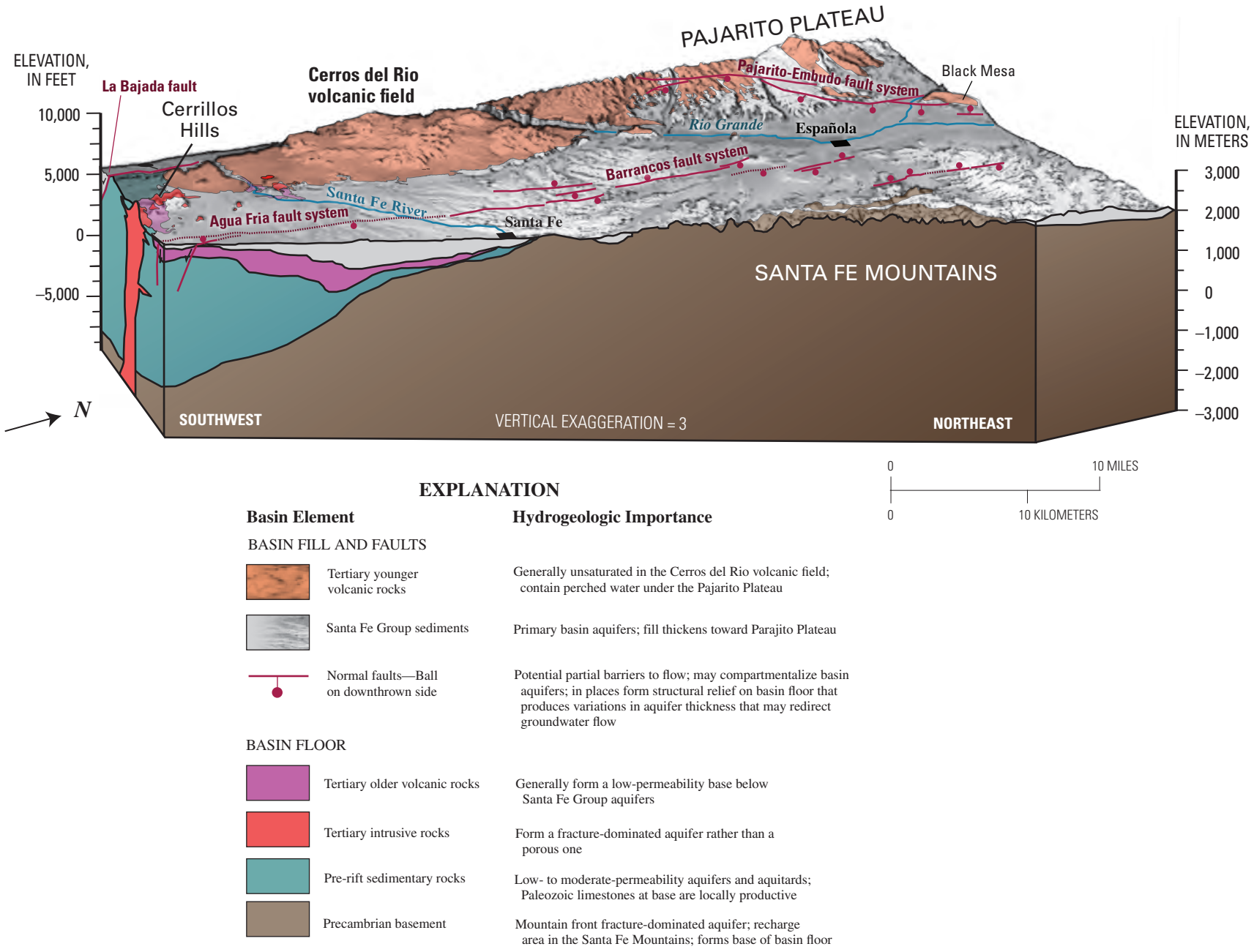

Figure 2. Key basin elements addressed by geophysical interpretations and their roles in the geologic and hydrogeologic frameworks.

Table 1. Interpretation approach and constraints for key basin elements.

[Approaches and data constraints involved in geophysical interpretation of aspects of basin elements illustrated in figure 2. Methods described more fully in the sections entitled "Methods of Data Analysis" and "Model Construction." 2D, two-dimensional; 3D, three-dimensional]

Basin element	Interpreted aspect	Interpretation approach and constraints
		Elements of basin fill
Tertiary younger volcanic rocks [units Qbt, QTv, fig. 3].	Lateral extent of Cerros del Rio volcanic field.	Interpret magnetic maps by recognizing anomaly patterns. Exact boundaries determined by the horizontal gradient magnitude of magnetic data.
	Isolated volcanic vents	Interpret magnetic maps by recognizing circular anomalies. Boundaries determined by the horizontal gradient magnitude of magnetic data. More detailed interpretations of geologic unit and age can be found in Thompson and others (2006) and Grauch and others (2006).
	Region of thick volcanic rocks and numerous vents.	Interpretation derived from Grauch and Bankey (2003), who inspected magnetic anomaly patterns in comparison with mapped vents and used magnetic depth estimation techniques on profile data to indicate areas of thick magnetic sources.
	Areas of thin basalt	Interpretation derived from Grauch and Bankey (2003), who used magnetic depth estimation techniques to indicate areas underlain by thin magnetic sources.
Santa Fe Group sediments [units QTsf, Tsf, fig. 3].	Elevation of base surface	3D integrated model developed from grid-based magnetic depth estimates, basin-fill thickness results from gravity inversion, well information, geologic cross sections, 2D geophysical models, magnetotelluric pseudoboreholes derived from 2D resistivity models, and depth picks from seismic horizons. Modeled in conjunction with surfaces representing the tops of Tertiary older volcanic rocks, pre-rift sedimentary section, and Precambrian basement.
	Thickness	Subtract interpreted Santa Fe Group base elevation surface from a topographic surface.
	Differences in magnetic lithology.	Interpret maps by inspecting correlations between the shapes of magnetic anomalies with topography in areas where Santa Fe Group is mapped.
		Elements of basin floor
Tertiary older volcanic rocks [units Tomv, Te, fig. 3].	Elevation of top surface	3D integrated model developed from grid-based magnetic depth estimates, basin fill thickness results from gravity inversion, well information, geologic cross sections, and isolated depth picks from seismic horizons in deep parts of the basin. Modeled in conjunction with surfaces representing the base of Santa Fe Group sediments and the tops of pre-rift sedimentary section and Precambrian basement. This surface is included in the 2D geophysical models, but it is not well constrained except near the mountain front.
	Elevation of base surface	3D integrated model using isolated depth picks from seismic horizons and limited well information. In some places, the surface was interpreted to be parallel to grid-based magnetic depth estimates that presumably show internal structure.
	Lateral extent underneath Santa Fe Group sediments.	Interpret maps by recognizing unique anomaly patterns. Incorporated into the 3D integrated model from map interpretations, well information, and grid-based magnetic depth estimates in relation to basement interpretations.
	Thickness	Subtract the interpreted base from the interpreted top surface of Tertiary older volcanic rocks.
Tertiary intrusions [units Ti, fig. 3; inferred vents related to Te].	General lateral extent of Cerrillos intrusion.	Interpret magnetic anomalies in relation to mapped intrusive rocks. Boundaries mapped using the horizontal gradient magnitudes of magnetic and pseudogravity data.
	Locations of buried volcanic vents probably associated with Espinaso Formation.	Recognize and interpret circular negative magnetic anomalies on maps. Boundaries mapped using the horizontal gradient magnitude of magnetic data. Use magnetic depth estimates to interpret depths of burial and geologic affiliation, supported by magnetic property measurements.

Table 1. Interpretation approach and constraints for key basin elements. —Continued

[Approaches and data constraints involved in geophysical interpretation of aspects of basin elements illustrated in figure 2. Methods described more fully in the sections entitled "Methods of Data Analysis" and "Model Construction." 2D, two-dimensional; 3D, three-dimensional]

Basin element	Interpreted aspect	Interpretation approach and constraints
		Elements of basin floor—Continued
Pre-rift sedimentary section [units Tgd, MzPzu, Pap, fig. 3].	General differences in total thickness.	Interpret trends in the bedrock gravity map resulting from gravity inversion. Inspect 2D geophysical models constrained by gravity data, limited information from magnetotelluric pseudoboreholes derived from 2D resistivity models, and deep wells.
	Buried bedrock high	3D integrated model developed from basin fill thickness results from gravity inversion, 2D geophysical models, magnetotelluric pseudoboreholes derived from 2D resistivity models, and depth picks from seismic horizons.
	Differences in magnetic lithology.	Inspect magnetic maps in relation to mapped contacts in areas where pre-rift sedimentary rocks are exposed.
Precambrian basement [unit pC, fig. 3].	Elevation of basement surface.	2D geophysical models and profile-based magnetic depth estimates. 3D integrated model developed from 2D geophysical models, depth picks from seismic horizons and well information. Additional information near the mountain fronts provided by geologic cross sections, grid-based magnetic depth estimates, and basin fill thickness results from gravity inversion. Modeled in conjunction with surfaces representing the base of Santa Fe Group sediments and the tops of Tertiary older volcanic rocks and pre-rift sedimentary section.
	Regional magnetic character.	In mountain areas, inspect patterns in magnetic and first-vertical-derivative maps in relation to topography and mapped geology. In basin areas, inspect patterns in magnetic and lowpass-filtered maps in relation to gravity data.
	Major intrabasement boundaries.	Inspection of magnetic maps in relation to gravity maps to determine magnetic anomaly differences that are unrelated to modern structural relief.
		Structure and miscellaneous
Normal faults	Fault traces based on magnetic expression.	Interpretations from Grauch and Hudson (2007), who used horizontal-gradient magnitudes of magnetic data after local trends were removed within a moving data window. As part of the procedure, linear trends solely related to topography are discarded. Locations cannot be mapped near Santa Fe, where there is too much interference from anthropogenic sources.
	Fault traces based on gravity expression.	Map interpretation derived from the horizontal-gradient magnitude of gravity data. Poor data coverage precluded these interpretations in much of the study area.
	Major fault systems	Determined by inspection of geophysically interpreted and geologically mapped faults and other structures in comparison to seismic reflection records.
Basin geometry	Structural relief on the basin floor.	Derived from relief on interpreted base of Santa Fe Group surface.
Miscellaneous	Linear features of undetermined origin.	Lines drawn along crests of linear magnetic anomalies on maps that may represent normal or strike-slip faults; linear contacts, such as the strike of dipping strata; other linear geologic features, such as narrow paleovalleys or narrow structural blocks; or regional metamorphic fabric of Precambrian basement.

a relatively impermeable base (Spiegel and Baldwin, 1963), although permeabilities may be moderate in local areas; (3) they contain information about faults that may influence the overlying Santa Fe Group sediments; (4) their absence indicates areas where the overlying Santa Fe Group and underlying pre-rift section have hydraulic connection; and (5) they likely contribute locally to poor ground-water quality. The Tertiary older volcanic rocks are one of the most important targets of the geophysical interpretations owing to their unique aeromagnetic signature and their position at the top of the basin floor. Using magnetic depth analysis and gravity modeling to locate the top of these rocks is equivalent to locating the depth to the base of the overlying Santa Fe Group; it places important constraints on maximum aquifer thickness. In addition, interpretations were derived from aeromagnetic maps to delineate the limits of these rocks in plan view and constrain their configuration in the 3D model.

Elements of Basin Fill

We generally categorize geologic units that compose the basin fill as Santa Fe Group sediments and Tertiary younger volcanic rocks. Santa Fe Group sediments form the primary aquifers for domestic and agricultural water supplies in the southern Española Basin. The aeromagnetic and gravity data can provide information about the maximum thickness of this sediment and suggest where major lithologic contrasts occur. To determine the Santa Fe Group's maximum thickness, information from analysis and modeling of the gravity and aeromagnetic data were integrated with other types of subsurface information and with geologic cross sections to develop a 3D-model surface representing the base of Santa Fe Group sediments. Documentation of variations in basin-fill thickness provides water-storage constraints for regional ground-water flow models and identifies potential structures at the base of the section. Major contrasts in lithology, as represented by different magnetic properties, suggest the locations of potential contrasts in aquifer properties that can influence ground-water flow. Because the geophysical data cannot readily distinguish between the formations or other lithostratigraphic divisions of the Santa Fe Group, the sediments are considered as a collective package.

In the study area, Tertiary younger volcanic rocks generally lie at or near the top of basin fill and are much thinner relative to the bulk of the sediments that compose the Santa Fe Group. The volcanic rocks are generally unsaturated in the Cerros del Rio volcanic field (Sawyer and Minor, 2006b), but under the Pajarito Plateau they form perched aquifers that provide horizontal flow paths (Robinson and others, 2005). The younger volcanic rocks have strong signatures in the aeromagnetic data, but the complexity of these signatures limits interpretations to qualitative determinations of thickness in the Cerros del Rio volcanic field and mapping their presence under shallow sediment cover. More extensive use of the aeromagnetic data to interpret volcanostratigraphy and map units in the Cerros del Rio volcanic field are presented in Grauch and others (2006) and Thompson and others (2006).

Structure

Faults and basement structures are important elements of the hydrogeologic framework for several reasons. First, faults that offset basin aquifers may partition aquifers if the sediments on either side have different hydraulic characteristics. Second, ubiquitous, impermeable, clay-rich fault zones in the northern Albuquerque and Española Basins suggest that intrabasin faults in these basins commonly are partial barriers to flow (Minor and Hudson, 2006; Caine and others, 2008). Finally, basement structures may affect lateral or vertical flow at depth and can control connectivity between adjacent basins. Faults that cut the basin fill are expressed in the aeromagnetic data throughout much of the study area, but a more comprehensive view of their patterns and extent is gained by combining information from geologic mapping and limited seismic reflection data. Integrating these data sets allows identification of two major deformation zones that extend the length of the study area, which we call the Barrancos and the Agua Fria fault systems (fig. 2). The Agua Fria and Barrancos fault systems are the subjects of geophysical interpretation presented in this report. Two other previously known fault systems included in the 3D modeling commonly serve as convenient boundaries in regional ground-water models. The Pajarito-Embudo fault system forms the master system of normal faults that bounds the west-dipping half graben of the Española Basin. The La Bajada fault, which forms a topographic escarpment on the southwest side of the Cerros del Rio volcanic field, is commonly viewed as the boundary between the Española and Santo Domingo Basins (Minor, 2006).

Geologic Setting

The Española Basin is one of a series of basins composing the Rio Grande rift, which formed during crustal extension that was active from late Oligocene to the present. It is located at a major right step in the Rio Grande rift and has the general form of a west-dipping half graben. It adjoins the east-dipping San Luis Basin on the northeast and the transitional Santo Domingo and east-dipping Albuquerque Basins to the southwest (fig. 1). The Rio Grande flows through these basins. The river and its tributaries drain the primary watershed of the area. The boundary of the Española Basin has been defined in a variety of ways in the literature (Baltz, 1978; Kelley, 1978; Manley, 1979; Wilkins, 1998); we use the limit of Neogene units because that limit encompasses a convenient area for gravity modeling. "Santa Fe embayment" is a name introduced informally by Kelley (1952, 1978) to indicate a tectonic element surrounded by the southward protrusion of

the Española Basin margin east of the Santo Domingo Basin (fig. 1). However, we use this term solely to indicate the general locality, following its common usage.

This study focuses on the southern Española Basin and the Santa Fe embayment; it provides only limited evaluation of the area south of the basin margins. The southern Española Basin is bounded on the east by the Santa Fe Mountains and on the west by the Jemez Mountains (fig. 1). The Santa Fe Mountains are composed primarily of Precambrian basement rocks (unit pЄ on fig. 3), with limited exposures of Paleozoic rocks (Read and others, 2003, 2004). Precambrian basement rocks are predominantly granitic with subordinate schist, gneiss, and amphibolite. The rocks are highly brecciated in many localities (Spiegel and Baldwin, 1963; Read and others, 2004).

Pre-rift sedimentary units of the basin floor are exposed outside of the basin in the southern part of the study area (fig. 3). These units include Paleozoic to Eocene sedimentary rocks (units lPap, MzPzu, Tgd) and Eocene to Oligocene igneous and volcaniclastic rocks (units Ti through Tomv). Paleozoic-Mesozoic rocks (unit MzPzu) form a sedimentary section as much as 2,000 m (6,560 feet (ft)) thick that generally correlates with sections in the Colorado Plateau (Sawyer and Minor, 2006a). Unconformably overlying the Paleozoic-Mesozoic section are the late Paleocene-Eocene Galisteo and Diamond Tail Formations (unit Tgd), which accumulated in basins at the southern and southwestern margins of the present Española Basin in the late stages of the Laramide orogeny (Cather, 1992, 2004; Lucas and others, 1997). The entire pre-rift sedimentary section is variably eroded within the basin (fig. 2). Only the basal, limestone-dominated portion of the Paleozoic section (unit lPap) is preserved in isolated exposures in the Santa Fe Mountains (fig. 3) and in the subsurface north of the Santa Fe River (Myer and Smith, 2006). Northeast of Pojoaque, the Mesozoic-Paleozoic section may be totally absent in the subsurface, on the basis of well data and geologic inference (Koning, Nyman, and others, 2005).

Eocene and Oligocene intrusions related to a porphyry belt (the Ortiz porphyry belt) are represented by monzonite and monzonite porphyry rocks exposed in the Cerrillos Hills (unit Ti, fig. 3). Laccolithic sills that emanated from the intrusive rocks domed overlying sedimentary deposits (Maynard and others, 2002); the sills have been encountered in boreholes (Grant, 1999). Intrusive episodes of several different ages and rock types are recognized as part of this intrusion (Maynard and others, 2002).

At the top of the basin floor, the late Eocene and Oligocene Espinaso Formation (unit Te) and the Cieneguilla volcanic complex (unit Tomv) overlie the Cerrillos intrusion and the pre-rift sedimentary section (fig. 3). The Espinaso Formation is a heterogeneous unit composed primarily of volcaniclastic sandstones, conglomerates, boulder conglomerates, near-vent volcaniclastic breccias, and minor intermediate-composition lava flows (Kautz and others, 1981; Smith and others, 1991; Thompson and others, 2006). Speigel and Baldwin (1963) describe rocks related to the Espinaso Formation as a series of latite flows and breccias. Kautz and others (1981) and Erskine and Smith (1993) interpret the Espinaso Formation as an extensive apron of volcaniclastic debris as much as 400 m thick that accumulated next to volcanic centers associated with the emplacement of the Ortiz porphyry belt. The overlying Cieneguilla volcanic complex is composed of basanite and nephelenite lava flows and interbedded sediments, as much as 200 m (660 ft) thick. The term Cieneguilla basanite replaces the previously used term Cieneguilla limburgite (Sawyer and others, 2002). Ages range from 36–29 Ma for the Espinaso Formation (Sawyer and others, 2002; Baldridge and others, 1980; Sauer, 1999) to 24–27 Ma (probably 25–26 Ma) for the Cieneguilla basanite (Baldridge and others, 1980; Kautz and others, 1981; Koning and Hallett, 2001).

Basin-fill sediments that formed in response to extension of the Rio Grande rift from Oligocene to Pleistocene time are collectively placed in the Santa Fe Group. These clastic sediments form important basin aquifers for ground water in the region. The primary aquifers in the Santa Fe area are the Oligocene-Miocene Tesuque Formation and the Plio-Pleistocene Ancha Formation (fig. 3). The Tesuque Formation, which represents the bulk of the basin fill north of Interstate 25, is composed primarily of pink to tan sandstone and silty-clayey sandstone with minor conglomerate, siltstone, and claystone (Spiegel and Baldwin, 1963; Borchert and others, 2003; Koning and Maldonado, 2003; Read and others, 2005; Koning, Connell, and others, 2005). The Tesuque Formation can be subdivided into lithostratigraphic units deposited in unique paleolandscape positions in the Española Basin having different sediment source areas, as follows. Sediment deposited on the alluvial slope (or piedmont slope) along the foot of the Sangre de Cristo Mountains and on the basin floor to the west has been called lithosomes A and B, respectively, by Cavazza (1986). Lithosome S applies to reddish, sandy sediment with a slightly higher proportion of quartzite and Paleozoic detritus compared with lithosome A, which was deposited by an ancestral Santa Fe River as an alluvial fan near Santa Fe (Koning, Read, and others, 2005). Volcaniclastic, alluvial fan sediment that was eroded from paleohighlands near the source vents of the Espinaso Formation and Cieneguilla basanite forms a subsurface unit southwest of Santa Fe called lithosome E (Koning and Johnson, 2006).

Coarser grained basin fill that postdates about 13 Ma has been subdivided into various members of the Chamita and Tesuque Formations (Koning and Aby, 2005; Koning, Connell, and others, 2005). The Cuarteles and Cejita Members of the Tesuque Formation east of the Rio Grande are similar to the underlying lithosome A and B units of the Tesuque Formation, respectively, in their source areas and general composition. In the lower Tesuque Formation, the volcaniclastic Bishops Lodge Member has recently been interpreted as a distal equivalent of the Espinaso Formation (Smith, 2000; Read and others, 2003). The late Pliocene to early Pleistocene Ancha Formation is composed of poorly consolidated sand, gravel, and clayey-silty sand, fining to the west. It forms a

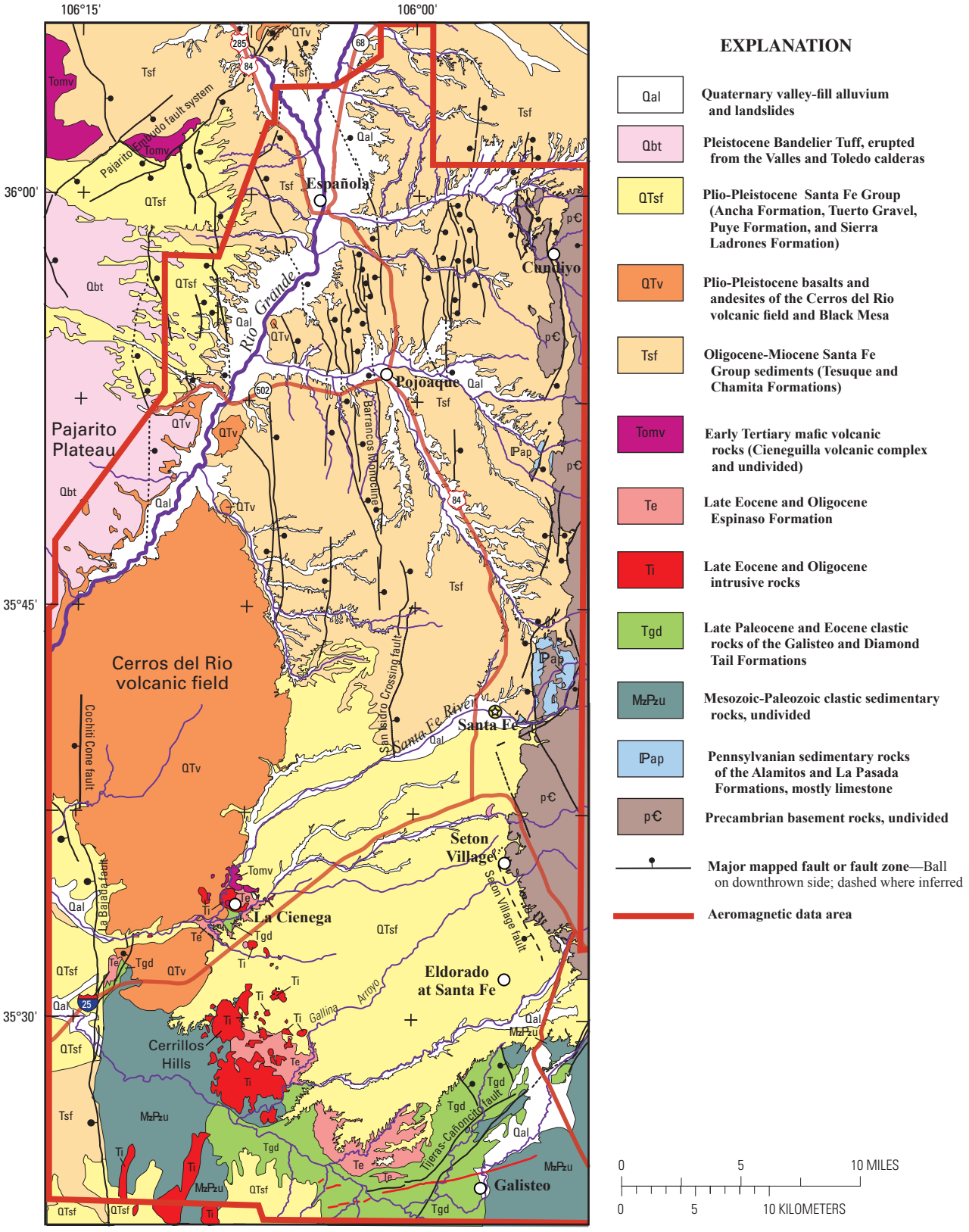

Figure 3. Generalized geology and geography of the study area. Geologic contacts are generalized from Read and others (2004), Minor (2006), New Mexico Bureau of Geology and Mineral Resources (2003), Koning (2005b), and Koning, Nyman, and others (2005). The irregular outline of the extent of mapped Santa Fe Group units (units QTsf and Tsf) is used for location purposes in many subsequent figures.

thin (10–90 m (33–295 ft)) blanket over older units (Koning, Connell, and others, 2002). West of the Rio Grande, the gravelly Puye Formation occupies a stratigraphic level similar to that of the Ancha Formation, and it is overlain by basaltic rocks and tuff of Pliocene-Quaternary age (Kelley, 1978; Dethier, 2003, Dethier and Koning, 2007).

The basin fill also includes Plio-Pleistocene basalts of the Cerros del Rio volcanic field and the silicic volcanic rocks that erupted from the Valles and Toledo calderas in the late stages of the Jemez volcanic field. In the study area, these rocks overlie the bulk of the Santa Fe Group sediments, as determined by examination of well and geophysical data from the Pajarito Plateau (Broxton and Vaniman, 2005; Los Alamos National Laboratory, 2006) and the Cerros del Rio volcanic field (Minor, 2006). They generally overlie the Plio-Pleistocene Santa Fe Group sediments on the west side of the study area, but locally the two units interfinger. Speigel and Baldwin (1963) included these volcanic rocks in the definition of the Santa Fe Group. We distinguish them as Tertiary younger volcanic rocks in this report because of their contrasting physical properties with the Santa Fe Group sediments.

The southern Española Basin is structurally bounded on the northwest by the Pajarito-Embudo fault system and on the southwest by the La Bajada fault (fig. 2). On the Pajarito Plateau, the Pajarito-Embudo fault system is represented by the northerly striking Pajarito fault that bounds the west-tilted half graben of the eastern Española Basin (Golombek, 1983). On the southeast side of Black Mesa (fig. 1), the fault system is represented by the northeast-striking Embudo transfer fault, which extends northeastward outside of the study area. The Embudo fault transfers strain between the west-tilted Española and east-tilted San Luis Basins (Muehlberger, 1979; Faulds and Varga, 1998) (fig. 1). The Pajarito fault links with the Embudo fault at a complexly faulted area in the northwest part of the study area. For simplicity, we consider these faults together as part of the Pajarito-Embudo fault system (fig. 3). The La Bajada fault is a major down-to-the-west normal fault that is commonly considered as the boundary between the Española and Santo Domingo Basins (Minor, 2006) (fig. 1). North of the Santa Fe River where the La Bajada fault curves to the west, regional gravity gradients suggest that most of the down-to-the-west displacement is accommodated instead by the north-south Cochiti Cone fault (fig. 3; Minor and others, 2006). Thus, for purposes of this report, the basin-bounding fault system in this area is considered as a combination of the La Bajada and Cochiti Cone faults. Numerous normal faults are exposed in the Tesuque Formation (unit Tsf) in the middle of the basin; whereas very few faults deform the over-lying Ancha Formation (unit QTsf) on the south (fig. 3). The concealed Seton Village fault (fig. 3) south of Santa Fe was previously inferred from geophysical evidence (Speigel and Baldwin, 1963). Many more concealed faults are revealed by the geophysical interpretations in this report and are introduced in subsequent sections.

Data Types and Descriptions

Magnetic and gravity data are measurements that show variations in the Earth's magnetic and gravity fields, respectively. Aeromagnetic data are magnetic data that are collected from aircraft. Once known field variations are removed, the remaining measured variations provide clues to the geology that underlies the surface. These clues are based on an understanding of the behavior of subtle fields produced by differences in the distribution and nature of the physical properties of rocks and sediments. For magnetic data, the applicable physical property is magnetization, which is determined by naturally occurring magnetic minerals in rocks and sediments. For gravity data, the applicable physical property is bulk density, which is the overall mass per unit volume of rocks, sediments, and their pore spaces.

Aeromagnetic and gravity interpretation involves indirect investigation of physical properties to infer the geology of the subsurface. To minimize ambiguities and subjectivity, a variety of additional data are commonly considered during analysis and interpretation. For this study, these additional data included measurements of physical properties, geologic mapping, subsurface well lithology, seismic-reflection geophysical data, and deep-looking electrical geophysical models.

Physical Properties

The physical property germane to aeromagnetic interpretation is total magnetization, which is the vector sum of remanent and induced components. The induced magnetization is defined as the magnetic field spontaneously produced in a volume of rock by the action of an applied field (Bates and Jackson, 1984). The ratio of the induced magnetization to the applied field (the present-day Earth's magnetic field in this case) is defined as magnetic susceptibility. A dimensionless number in the SI system, magnetic susceptibility is mainly a function of the quantity of magnetic minerals (commonly magnetite). Rock types typically containing the greatest abundance of magnetic minerals are mafic and ultramafic igneous and metamorphic rocks. Sedimentary rocks and sediments typically contain the least abundance (Reynolds and others, 1990). The remanent component, commonly called remanent magnetization, represents the vector sum of all permanent magnetizations held by the magnetic minerals, which have fixed directions irrespective of applied magnetic fields (Bates and Jackson, 1984). An important contribution to the remanent magnetization is acquired at the time the rock forms, which results in a record of the direction of the Earth's magnetic field at the time of formation. Remanent magnetization can be large but highly variable in magnitude in volcanic and metamorphic rocks but is commonly negligible in sedimentary rocks and sediments (Reynolds and others, 1990). Traditionally, magnetic susceptibility is reported rather than its associated vector quantity, induced magnetization. In contrast, remanent

magnetization is commonly reported as intensity in amperes per meter (A/m in Système International (SI)) with a given orientation (declination and inclination).

Reconnaissance measurements of magnetic susceptibility and limited information about remanent magnetization are available for many geologic units in the Española Basin and nearby areas (fig. 4). These measurements guide the interpretations but are not intended to represent a rigorous study of rock magnetic properties. The large variability of these properties is readily apparent within individual units and between units (fig. 4); note that magnetic susceptibility is presented on a log scale. In general, the volcanic rocks have the greatest magnetic susceptibilities, whereas the sedimentary rocks have the least, as expected. Precambrian basement rocks have the greatest variability. Total magnetizations for the volcanic rocks are likely very large because remanent components are typically much greater than the induced components in these rocks. The opposite is true for the sedimentary rocks, giving rise to low total magnetizations.

The physical property germane to gravity interpretation is bulk density. Bulk density correlates fairly well with rock type, but it is also affected by porosity and cementation related to diagenesis, compaction, and degree of fracturing. Density measurements from single samples and from borehole density logs are available for the Española and nearby Albuquerque Basins (fig. 1, table 2). Several deep oil exploration wells in the Española Basin, and more in the Albuquerque Basin, provide valuable information about the densities of geologic units. This information is especially important for basin-fill sediments, which become denser with depth owing to compaction. The results show that the Santa Fe Group is considerably less dense compared with the other rock types (differences greater than 140 kilograms per cubic meter (kg/m^3)), even to depths of 3.75 kilometers (km) (12,300 ft). This relation and the small overall volume of volcanic rocks compared with the volume of sediments in the study area allow robust application of a gravity inversion technique (discussed in a subsequent section) to separate the gravity effect of sediments from that of other rock types.

Because robust geophysical interpretation relies on good contrast between physical properties, the physical properties ascribed to rocks in the study area generally formed the basis for dividing the geologic units into interpretative packages (table 1). For example, the low densities of the Santa Fe Group sediments set them apart from all other rock types, although individual formations within the Santa Fe Group cannot be distinguished. On the other hand, the Tertiary younger volcanic rocks are considered separately from the Santa Fe Group sediments for map interpretation and modeling in the study area, but they are lumped with the sediments for the basin-scale gravity inversion, where their volume is small compared with that of fill in the whole basin. Tertiary older volcanic rocks are considered as a package because the Cieneguilla volcanic complex (unit Tomv, fig. 3) closely overlies the Espinaso Formation (unit Te) and they have similar densities and magnetic properties. In contrast, Precambrian basement is discussed as one package despite its wide variation in magnetic properties and a density similar to that of the Paleozoic limestones. Precambrian rocks that have very low magnetic susceptibilities cannot be distinguished by density or magnetic properties from Paleozoic limestones. On the other hand, they are easily distinguished in seismic-reflection records which, combined with well data, constrain the models in limited areas.

Aeromagnetic Data

Aeromagnetic surveys measure the total intensity of the Earth's magnetic field from an aircraft as it follows a regular pattern of flight lines. The collected data are processed to remove time-varying external fields and are corrected for noise from aircraft movements. The effects of Earth's primary magnetic field are removed to produce "magnetic anomaly data" or "magnetic data" that isolate subtle variations related to geology. The processed data are gridded at an interval commensurate with the flight-line spacing before they are displayed on magnetic anomaly maps. High-resolution surveys are flown closer to the ground and with narrower line spacing than conventional aeromagnetic surveys. The low flight path allows better detection of weak magnetic sources near the surface. The narrow line spacing increases sampling of the magnetic field and thus provides better definition of sources with limited lateral extent, and it improves the overall resolution of details in map view.

Four surveys provide high-resolution aeromagnetic data for the southern Española Basin study area (fig. 5). All but the Santa Fe East survey (which used a helicopter) were flown using fixed-wing aircraft. The Sandoval–Santa Fe survey, which covers most of the area, was flown using east-west lines spaced 150 m (500 ft) apart and a magnetometer height nominally 150 m (500 ft) above ground (U.S. Geological Survey and others, 1999). The Cochiti survey was flown with 400 m (1,310 ft) line spacing at a nominal 73 m (240 ft) above ground and the Pajarito Plateau survey with 100–200 m (330–660 ft) line spacing at a nominal 75 m (246 ft) above ground. For the latter two surveys, the wide line spacing relative to the ground clearance was not optimal for aeromagnetic map interpretation, but it was required because the primary purpose of both surveys was to collect electromagnetic geophysical data (Deszcz-Pan and others, 2000; Sweeney and others, 2002; Cole and others, 2006; Baldridge and others, 2007). The Santa Fe East survey was flown with 200 m (660 ft) line spacing at a nominal 150 m (500 ft) above ground (Bankey and others, 2006). To minimize analytical problems caused by regions that lacked data, areas not covered by these four surveys were filled with data from a regional grid compiled for the state of New Mexico (Kucks and others, 2001).

After flight-line data from the four surveys were processed to remove Earth's field variations and reduce ordinary data-acquisition errors, the data were analytically

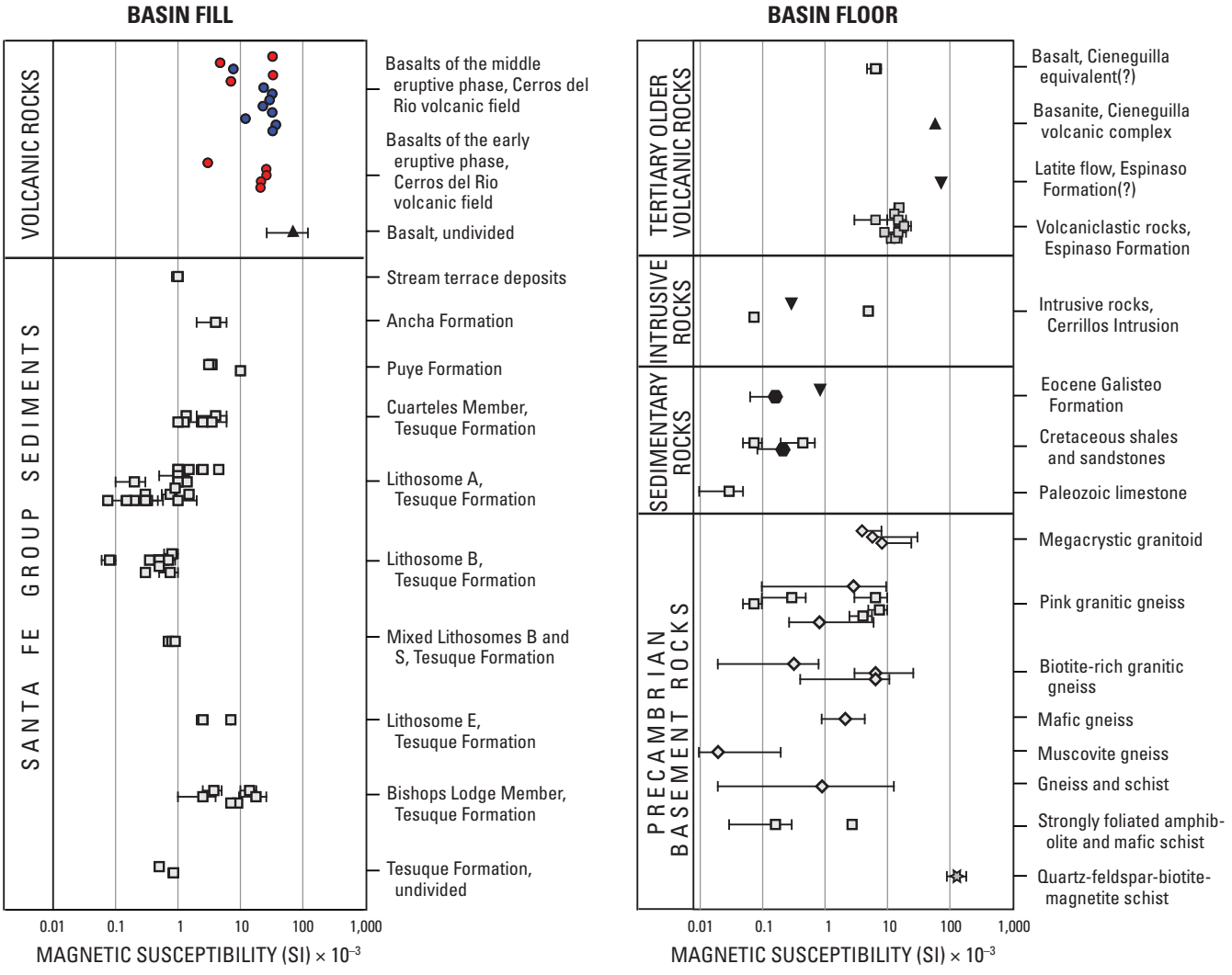

Figure 4. Magnetic-property information for geologic units in the study area. Diagrams show magnetic susceptibility (SI) measured for volume on a logarithmic scale; symbols indicate available information about the ratio of remanent to induced magnetization and direction (see explanation). Different symbols reflect different data sources, sampling procedures, and types of reported data. The data set primarily represents reconnaissance measurements, which should not be considered statistically robust.

Table 2. Densities of geologic units.

[Measured and estimated bulk densities of geologic units in the Española Basin and equivalent units in the Albuquerque Basin and vicinity to the south. ft, feet; m, meter; N/A, not applicable; NR, not reported]

Geologic unit or rock type	Bulk density[1] (kilograms/cubic meter)			Number of samples or wells[2]	Data source
	Minimum	Maximum	Mean		
Basin fill volcanic rocks					
Basalt	2,540	2,810	2,660	3	Laboratory samples (Spiegel and Baldwin, 1963).
Volcanic rocks of the Jemez volcanic field.	N/A	N/A	2,350	N/A	Estimated from gravity modeling of Valles Caldera (Nowell, 1996).
Basin fill sedimentary units					
Ancha Formation of the Santa Fe Group.	N/A	N/A	1,700	N/A	Estimated from geophysical analysis (Spiegel and Baldwin, 1963).
Tesuque Formation of the Santa Fe Group.	N/A	N/A	2,100	N/A	Estimated (unexplained analysis by Speigel and Baldwin, 1963).
Santa Fe Group, undivided, 0–1,250 m (0–4,100 ft) depth.	2,090	2,260	2,170	12	Borehole density logs from Albuquerque and Española Basins.
Santa Fe Group, undivided, 1,250–2750 m (4,100–9,020 ft) depth.	2,230	2,400	2,300	3	Borehole density logs from Albuquerque and Española Basins.
Santa Fe Group, undivided, 2,750–3,750 m (9,020–12,300 ft) depth.	2,300	2,450	2,380	1	Borehole density log from Albuquerque Basin.
Santa Fe Group, undivided, 3,750–4,250 m (12,300–13,940 ft) depth.	2,500	2,580	2,540	1	Borehole density log from Albuquerque Basin.
Basin floor volcanic rocks					
Cieneguilla volcanic rocks	NR	NR	3,080	2	Laboratory samples (limburgite of Spiegel and Baldwin, 1963).
Cieneguilla volcanic rocks	2,350	2,640	2,480	2	Borehole density logs from the Española Basin.
Flow latite	2,690	2,690	2,690	1	Laboratory sample (Spiegel and Baldwin, 1963).
Brecciated latite	2,180	2,180	2,180	1	Laboratory sample (Spiegel and Baldwin, 1963).
Espinaso Formation	2,320	2,540	2,430	3	Borehole density logs from Albuquerque and Española Basins.
Basin floor intrusive rocks					
Intermediate-composition intrusive rocks.	2,470	2,500	2,485	2	Laboratory samples (andesite dike and monzonite of Spiegel and Baldwin, 1963).
Basin floor sedimentary units					
Eocene Galisteo Formation (sandstone).	2,400	2,450	2,425	6	Laboratory samples (Spiegel and Baldwin, 1963).
Eocene and Oligocene clastic rocks, undivided, 0–1,750 m (0–5,740 ft) depth.	2,380	2,390	2,390	2	Borehole density logs of Oligocene and Eocene clastic rocks from the Albuquerque and Española Basins.

Table 2. Densities of geologic units.—Continued

[Measured and estimated bulk densities of geologic units in the Española Basin and equivalent units in the Albuquerque Basin and vicinity to the south. ft, feet; m, meter; N/A, not applicable; NR, not reported]

Geologic unit or rock type	Bulk density[1] (kilograms/cubic meter)			Number of samples or wells[2]	Data source
	Minimum	Maximum	Mean		
Basin floor sedimentary units—Continued					
Eocene and Oligocene clastic rocks, undivided, 1,750–3,250 m (5,740–10,660 ft) depth.	2,500	2,560	2,530	2	Borehole density logs of Oligocene and Eocene clastic rocks from the Albuquerque and Española Basins.
Eocene and Oligocene clastic rocks, undivided, 4,750–6,500 m (15,580–21,330 ft) depth.	2,610	2,670	2,630	1	Borehole density log of Oligocene clastic rocks from the Albuquerque Basin.
Cretaceous Mancos Shale	NR	NR	2,590	8	Laboratory samples (Spiegel and Baldwin, 1963).
Jurassic Wingate and Entrada sandstones.	2,640	2,640	2,640	1	Laboratory sample (Spiegel and Baldwin, 1963).
Mesozoic sedimentary rocks, undivided, 0–2,500 m (0–8,200 ft) depth.	2,400	2,500	2,440	10	Borehole density logs from Albuquerque and Española Basins.
Mesozoic sedimentary rocks, undivided, 2,500–3,250 m (8,200–10,660 ft) depth.	2,500	2,550	2,530	3	Borehole density logs from Albuquerque and Española Basins.
Mesozoic sedimentary rocks, undivided, 3,250–4,500 m (10,660–14,760 ft) depth.	2,509	2,670	2,620	1	Borehole density log from Albuquerque Basin.
Permian sedimentary rocks, undivided, 0–3,250 m (0–10,660 ft) depth.	2,510	2,660	2,600	10	Borehole density logs from Albuquerque and Española Basins.
Pennsylvanian sedimentary rocks, undivided, 0–3,250 m (0–10,660 ft) depth.	2,550	2,690	2,630	9	Borehole density logs from Albuquerque and Española Basins.
Precambrian basement rocks					
Precambrian crystalline rocks	2,490	2,990	2,690	5	Laboratory samples (Spiegel and Baldwin, 1963).
Precambrian crystalline rocks	2,570	2,700	2,620	5	Borehole density logs from Albuquerque and Española Basins.

[1]For samples measured in the laboratory, range and average bulk densities are reported for the number of samples measured. For all but densities for basin floor volcanic rocks obtained from borehole density logs, typical densities throughout 250-m (820-ft)-depth intervals were estimated by inspection of each borehole log and were assigned to the appropriate geologic unit. Then, for each geologic unit within the indicated overall depth range, densities were averaged for all applicable 250-m (820-ft)-depth intervals from all boreholes. Overall depth ranges were determined by inspection of major differences in density with depth. Where multiple samples were unavailable or densities were estimated, a single value is listed as the mean.

[2]Number of laboratory samples measured or number of wells for which borehole density logs were inspected for the geologic unit and depth range specified. Number of samples is not applicable for bulk densities that were estimated by geophysical modeling.

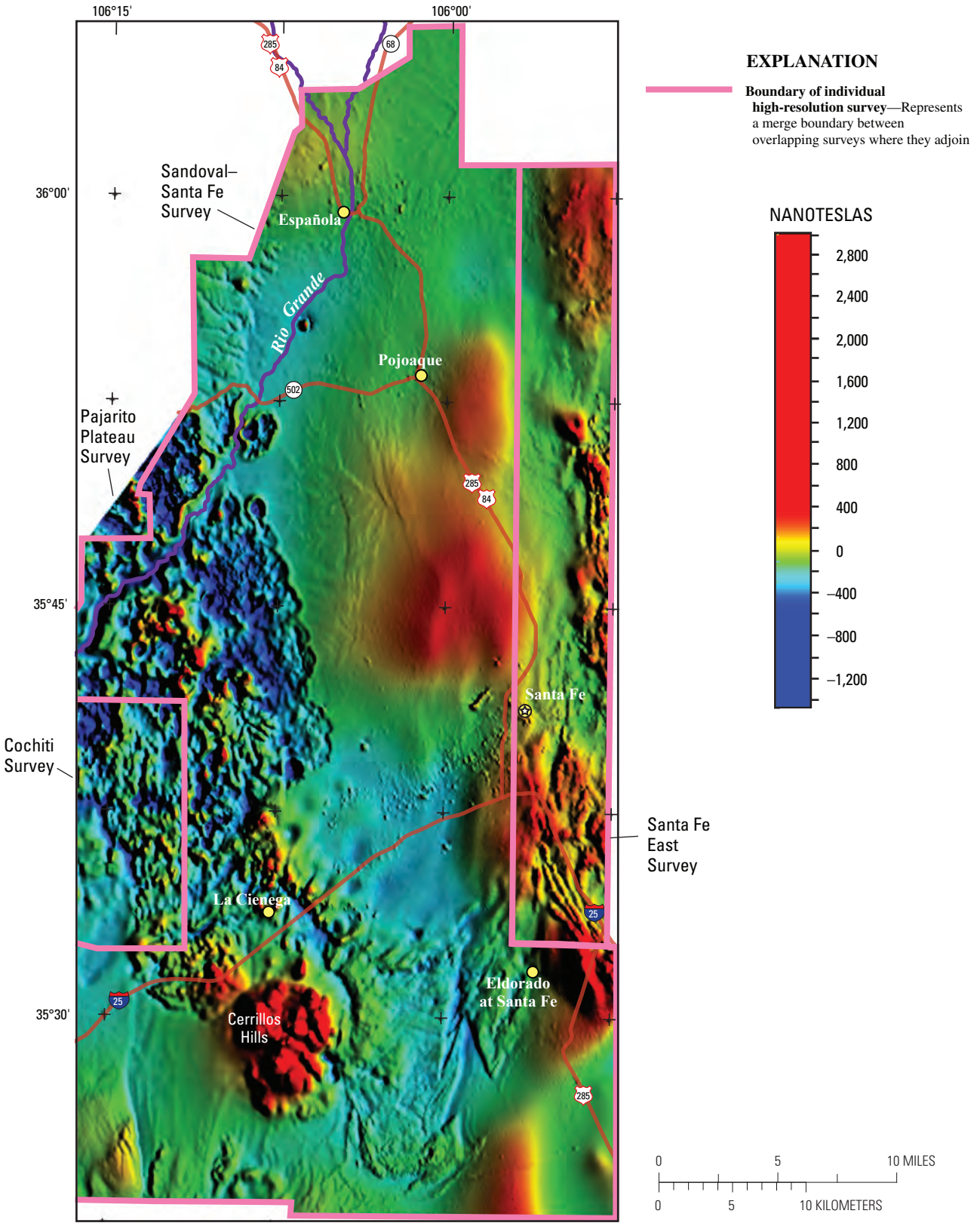

Figure 5. Aeromagnetic map showing coverage of high-resolution surveys. Reduced-to-pole aeromagnetic data are shown after final data processing and merging of data from individual surveys (pink lines). Image is color-shaded relief with illumination from the east. The Pajarito Plateau survey covers a larger area than shown here; it extends as much as 5 km northwest of its boundary on this map.

continued from the variable observation surfaces to a common surface draped 100 m (330 ft) above ground and digitally merged with regional magnetic data into a 50-m (160-ft)-interval grid, following procedures described in Sweeney and others (2002) and Grauch and Hudson (2007). The gridded data were then transformed to reduced-to-pole data, a standard geophysical operation applied to data collected in areas of high latitude (Blakely, 1995). Reduction-to-pole transformations correct for shifts of anomalies away from the centers of their magnetic sources; these shifts are an effect of the oblique orientation of the measured magnetic field with respect to Earth's surface. If not corrected, positive aeromagnetic anomalies for the study area would be offset to the southwest of their causative sources and partial rings of negative anomalies would occur on the northeast. A related technique, called the pseudogravity transformation (or computation of the magnetic potential), also minimizes these shifts while enhancing the broad features of the data. The pseudogravity transformation is used in this report solely as an interim step during application of interpretative techniques (discussed below). The reduced-to-pole and pseudogravity transformations are best utilized in areas where the total magnetizations of sources are generally collinear (within 25°) with Earth's main field (Bath, 1968). General collinearity is a reasonable approximation for most of the study area because of the Neogene age of volcanic units, which are the ones most likely to have consistently strong remanent magnetization. The reduced-to-pole magnetic data for the central Rio Grande rift incorporate the assumption that Earth's field has declination=11° and inclination=63°.

Figure 5 is a color shaded-relief image of the final, reduced-to-pole aeromagnetic data. This image uses color to display the broad variations in the data and shading (analogous to illumination by the sun) to enhance many subtle details obliquely oriented to the direction of illumination.

Gravity Data

Gravity data throughout the Española Basin and surrounding region come from Kucks and others (2001), from unpublished data collected by an educational group called Summer of Applied Geophysical Experience (SAGE) (Jiracek and others, 2008) during the period 1997–2002 (Shawn Biehler, University of California, Riverside, written commun., 2002), and from a web database maintained by the Pan-American Center for Earth and Environmental Studies (*http://research.utep.edu/Default.aspx?tabid=37229*) accessed in 2006. The third database contains decades of data collected by numerous previous workers. Data from these three sources were merged, reconciled for discrepancies and duplicate stations, and edited to remove station data with large discrepancies compared with data at surrounding stations. Standard Bouguer corrections were applied using a reduction density of 2,670 kg/m^3. Terrain corrections were applied within a 167 km (104 miles (mi)) radius to the data at each station using digital terrain data with a resolution as fine as 30 m. The station data were then interpolated onto a grid at a 250 m interval.

In order to focus on density variations within the upper crust, an isostatic regional field was removed from the terrain-corrected Bouguer gravity values by using parameters established for New Mexico by Heywood (1992). The resulting "*isostatic residual gravity* map" (fig. 6) generally isolates the gravity effects produced by sources within the upper 10 km of the crust (Simpson and others, 1986).

Reliability of the features depicted on the isostatic gravity residual map is highly dependent on station spacing, which is unevenly distributed across the region (fig. 6). Resolution of anomalies is excellent in areas south of Santa Fe, where station spacing is 1 km (0.625 mi) or less. However, gaps in data coverage in the northern part of the study area can span 8 km (5 mi) or more. In these areas, only gradients orthogonal to profile data are fairly well defined. These data may not properly resolve irregular boundaries or the expression of local variations underlying the regional gradients.

Other Data

Additional data incorporated into interpretations of the gravity and aeromagnetic data include geologic cross sections, lithologic picks in well data, electrical resistivity models from magnetotelluric (MT) soundings, and interpreted picks of seismic-reflection horizons. Geologic cross sections and geologic concepts come from several sources, including published maps and cross sections (Koning and Maldonado, 2003; New Mexico Bureau of Geology and Mineral Resources, 2003; Koning, 2005b; Koning, Nyman, and others, 2005; Read and others, 2005; Shroba and others, 2005; Sawyer, Minor, Grauch, and others, 2006; Sawyer, Minor, Thompson, and others, 2006), unpublished cross sections (Daniel Koning, New Mexico Bureau of Geology and Mineral Resources, 2008), and consultation with other geologists who have worked in the area (David Sawyer, Scott Minor, Jonathan Caine, and Ren Thompson, U.S. Geological Survey, and Adam Read, New Mexico Bureau of Geology and Mineral Resources).

Interpretations of borehole logs and cuttings are available from water wells and exploration wells, mostly from the southern part of the study area. Lithologic picks in more than a hundred of these wells were compiled by Peggy Johnson and Daniel Koning at New Mexico Bureau of Geology and Mineral Resources (NMBGMR). These picks and those from other sources are listed in appendixes 1 and 2. Many more wells exist in the basin with excellent lithologic information pertinent to the internal stratigraphy of the Santa Fe Group (for example, Frost, 2006; Los Alamos National Laboratory, 2006), but they are not included here because they have limited use in the deeper parts of the basin. Although the NMBGMR database includes much lithologic information, only a few lithologic picks were used as constraints for gravity

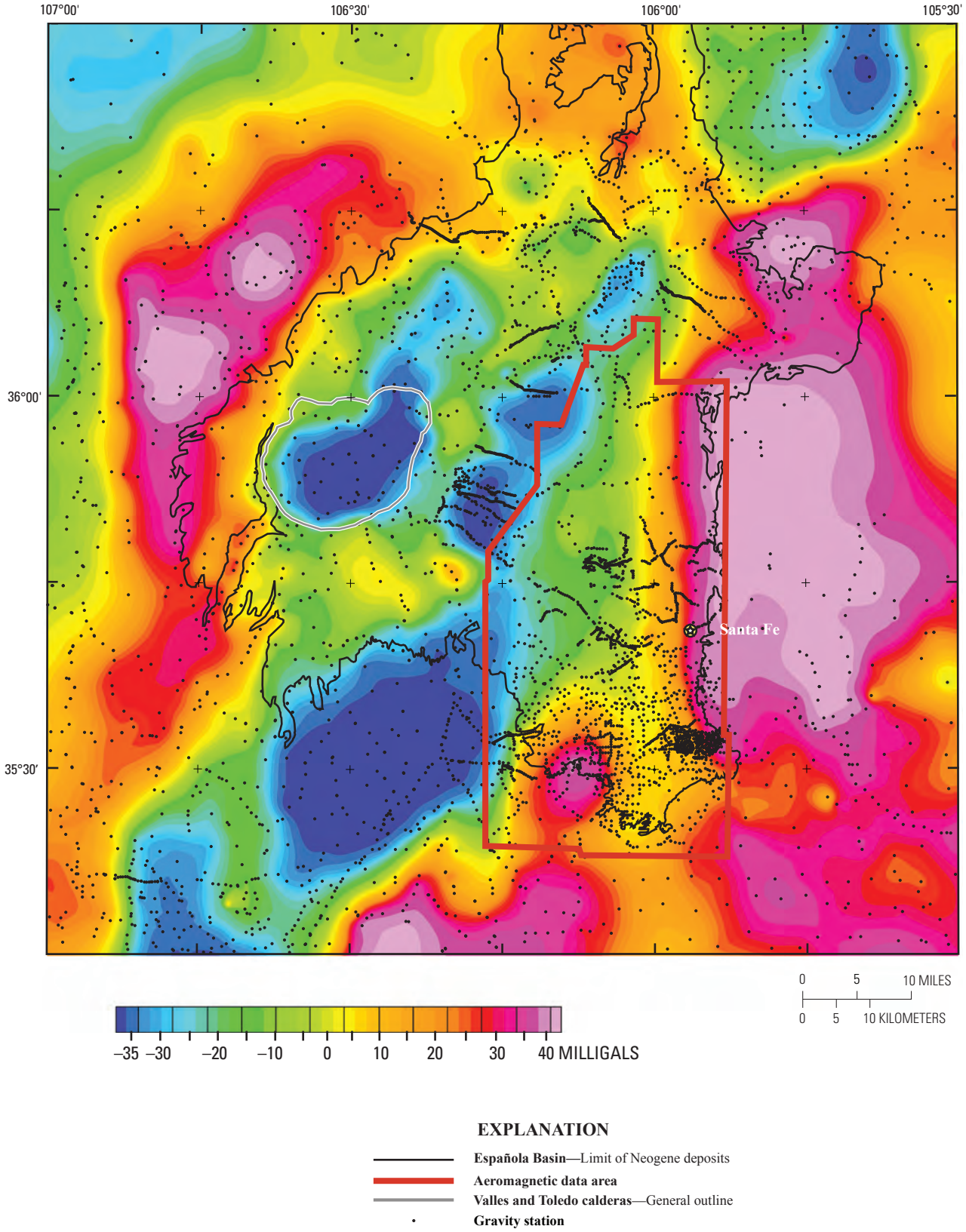

Figure 6. Isostatic residual gravity map of the area of gravity analysis.

inversion and 3D modeling: the top of Tertiary older volcanic rocks (Espinaso Formation and overlying Cieneguilla volcanic complex if present), the top of the pre-rift sedimentary section (lower Tertiary through Paleozoic sedimentary section), and the top of Precambrian basement (appendix 1).

Magnetotelluric data are available for the southwestern part of the study area as part of recent investigations by the U.S. Geological Survey. Preliminary models of these data, derived from 2D resistivity inversions, are reported in Rodriguez and others (2006). Since that study, revised and new models incorporating 13 additional MT soundings have been developed (Rodriguez and Sawyer, 2007; Brian Rodriguez, U.S. Geological Survey, written commun., 2007). The 2D inverse models show discrete resistivity layers that are interpreted as different geologic units on the basis of comparisons with electrical resistivity logs in boreholes and geologic cross sections. At the location of each MT sounding, the resistivity layers defined by the 2D inversion were assigned different depth ranges, as though the sounding was a borehole that penetrated layers of different electrical resistivities. These pseudoboreholes could then be used in this study to guide modeling of geologic surfaces. Two important results were obtained from the MT modeling: the detection of a conductor directly under moderately low resistivities associated with Santa Fe Group sediments, and resistive layers at the base of the electrical resistivity model that represent Paleozoic strata or Precambrian basement. Some ambiguities exist in the interpretation of the conductor, because it could represent Mesozoic Mancos or Chinle Formations at the top or middle of the pre-rift sedimentary section, respectively; Espinaso Formation within the package of Tertiary older volcanic rocks; or the clay-rich base of the Santa Fe Group (Brian Rodriguez and David Sawyer, U.S. Geological Survey, oral commun., 2008). However, consistencies between individual MT models and correlations with geologic maps provide some confidence in interpreting the resistivity layers in terms of trends and general depths to the base of the Santa Fe Group and top of the Paleozoic section.

Seismic information comes from data acquired and interpreted by the SAGE group. Some of the data and interpreted sections are published (Biehler and others, 1991; Baldridge and others, 1994; Ferguson and others, 1995). Only the interpreted model of Biehler and others (1991) is located within the study area, but the other data were used to constrain the basin-wide gravity inversion. The SAGE group has also had access to industry seismic reflection data from the 1970s in the form of paper copies of processed, common-midpoint stacked sections. Reflection data for several of these lines were first published (without locations or time scales) by Black (1984). The data and preliminary interpretations have been presented orally (Baldridge and others, 2001; Ferguson and others, 2007), but a final synthesis is pending. In the meantime, depth picks and images of some of the sections depicted in Ferguson and others (2007) were generously provided to the senior author by John Ferguson, University of Texas at Dallas, in 2007. (Note that Ferguson's picks represent a different interpretation of the model presented in Biehler and others (1991), which was developed before the industry seismic data had been acquired.) The picks and images, which did not include all seismic data, were used as guides in our interpretation and 3D modeling but cannot be presented here.

Methods of Data Analysis

Data analysis, the first step in interpreting magnetic and gravity data, applies mathematical techniques to investigate the shapes of and depths to magnetization and density sources. The methods used for this study include edge detection, magnetic anomaly separation, and magnetic depth estimation. Edge detection is the application of techniques that locate the edges of causative sources that have near-vertical boundaries. Magnetic anomaly separation applies techniques to magnetic data in order to isolate various wavelength components. The separation helps investigators assess relations between regional, local, shallow, and deep features. Magnetic depth estimation includes techniques that estimate the depths to the tops of magnetic sources. For this study, edge detection methods were applied to both gridded gravity and magnetic data; magnetic anomaly separation techniques were applied to gridded magnetic data; and several depth estimation techniques were applied in different ways to both gridded and profile magnetic data.

Edge Detection

Abrupt lateral contrasts in rock properties, such as those that occur at faults or steeply dipping contacts, correspond with the steepest slopes of their associated gravity or magnetic anomalies. Although several alternative techniques exist (Nabighian, Ander, and others, 2005; Nabighian, Grauch, and others, 2005), we use the horizontal-gradient method to locate edges related to faults. In this method, the steepest gradients can be located by computing the local maxima of the horizontal-gradient magnitudes (HGM) of gravity data, pseudogravity data, or reduced-to-pole magnetic data. The procedure is analogous to taking a derivative to find the value of the slope at the inflection point of a curve. For gridded data, the HGM is computed as a separate grid, and edges are located along HGM maxima that appear as ridges.

Although many geophysical edges detected from HGM grids correspond directly with underlying faults, the interpretation is not always straightforward. First, steep gradients can be caused by steeply dipping surfaces other than faults, such as homoclines, dipping beds truncated by erosion, intrabasement or igneous lithologic contacts, and high-relief topography. Although the nature of geophysical edges usually becomes apparent during interpretation, the origins of some may remain ambiguous. Second, mapping the surface projections of faults from geophysical edges is affected by the dip of the interface and the location of the contrast in physical

property at depth along the interface. In both gravity and magnetic cases where dip is less than vertical, the maximum of the HGM migrates downdip farther away from the surface projection as depth to the magnetic contrast increases (Grauch and Cordell, 1987; Grauch and Hudson, 2007). The most serious problems are caused by basement-related contrasts at depths >1 km (0.6 mi), where maxima can be offset from the surface projection of associated faults by 500 m (1,640 ft) or more. Finally, in magnetic data, multiple maxima can be associated with one magnetic interface. These complications were resolved previously (Grauch and Hudson, 2007) by inspection of the aeromagnetic data used in this study area. Major gravity gradients representing regional features in the Española Basin were presented previously by Grauch and others (2006). More detailed gradients, representing individual faults or steep basement slopes in the vicinity of Eldorado at Santa Fe, are discussed in the section entitled Interpreted Structure.

Magnetic Anomaly Separation

Because magnetic anomalies become broader as distance between the magnetometer and the source increases, it is common practice to apply digital filters to gridded aeromagnetic data to separate broad (long-wavelength) anomalies from narrow (short-wavelength) ones in order to investigate source depths. Although anomaly wavelengths also depend on the shapes of sources, anomaly separation filters allow qualitative examination of detailed (as opposed to regional) features that may otherwise be difficult to see. Several standard geophysical techniques can separate anomalies (Nabighian, Grauch, and others, 2005). For this study, we used the first vertical derivative and lowpass filtering.

The first vertical derivative computes how rapidly the magnetic field decreases with distance from the sources following principles of potential-field theory (Blakely, 1995). The procedure is common practice because it enhances anomalies caused by shallow sources that are depth limited and generally brings out detail that is otherwise difficult to see (fig. 7). On the other hand, it also enhances data noise.

Lowpass filtering was accomplished by a filter designed using matched filtering (Syberg, 1972; Phillips, 2001), followed by application of an upward continuation filter using a continuation distance of 2 km (3.2 mi). These filters are designed to reduce the amplitudes of short-wavelength anomalies while minimizing filtering artifacts. The reader is referred to Blakely (1995) for more detailed discussion of this type of digital filter analysis. The result of the lowpass filtering (fig. 8) isolates the regional features of the data. Although deep sources generally cause regional features such as these, not all broad anomalies represent deep sources. For example, the broad region of negative magnetic anomaly values throughout the Cerros del Rio volcanic field is caused by shallow and exposed basalts within the field (Grauch and others, 2006). These anomalies coalesce to form a broad negative anomaly in the lowpass map that masquerades as a deep-source anomaly. Likewise, broad magnetic highs within the volcanic field may also be due to sources within the volcanic field. Comparison of anomalies between the original (fig. 5), the first vertical derivative (fig. 7), and the lowpass (fig. 8) maps shows that some anomalies have expression in both short- and long-wavelength components. Overlap of expression at different wavelength components was also apparent from more extensive matched filtering on the earlier aeromagnetic data compilation (Grauch and Bankey, 2003). The overlap of expression in areas outside of the Cerros del Rio volcanic field may indicate that the sources occupy a wide range of depths.

Magnetic Depth Estimation

Methods for estimating depth to magnetic sources from aeromagnetic data build on edge detection methods that locate magnetic edges in three dimensions. The methods rely on the general principle that shallow sources produce anomalies with steep gradients, whereas deep sources produce anomalies with broad gradients. However, the configuration of magnetic edges (source shape) also affects anomaly gradients and creates many unknown variables. To deal with unknown source shape, depth-estimation methods commonly consider idealized magnetic sources that are represented by a variable called the structural index (N). An infinite step (commonly called a “magnetic contact”) is represented by N=0; it extends to infinity in four directions (for example, north, south, east, and down). A magnetic sheet source is represented by N=1; it has zero thickness and extends to infinity in three directions (for example, north, south, and east for a horizontal sheet or north, south, and down for a vertical sheet, commonly called a “dike”). A magnetic line source (commonly called a “pipe”) is represented by N=2; it extends to infinity in two horizontal directions (for example, north and south). A magnetic point source, or dipole, which does not extend in any direction, is represented by N=3.

Depth-estimation methods generally solve for the 3D coordinates of the top edge of one of these source types (or point location in the case of the point source) using the observed magnetic data and the magnetic-field equation appropriate for the source type. For the infinite step and sheet cases, many methods also solve for the dip of the step or dip of the sheet, respectively. The value of N has a large effect on the outcome of the resulting depth solutions. The shallowest solutions arise from N=0 and the deepest from N=3. Without any prior knowledge of source shape, common practice is to compare the solutions for different values of N. The primary end-member source types considered for geology are infinite steps (N=0) and thin sheets (N=1). The infinite step is used to represent a fault with large offset or the edge of a pluton. The thin sheet is used to represent horizontal or vertical sources, such as a basalt flow (observed at a distance much greater than its thickness) or a thin dike. In practice, shapes are likely to

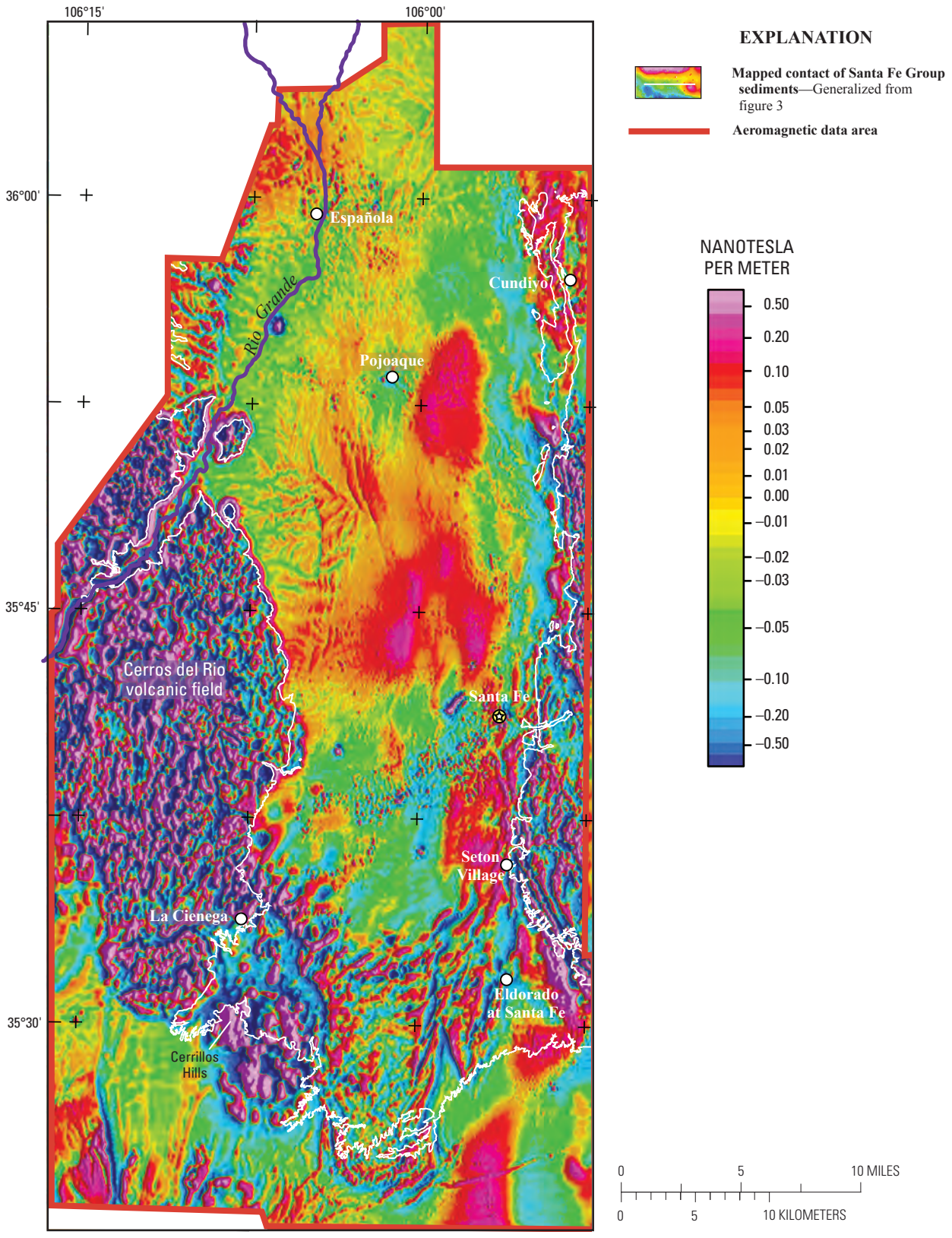

Figure 7. First vertical derivative of reduced-to-pole aeromagnetic data. The resulting map enhances detailed anomalies related primarily to shallow, depth-limited sources. Note linear anomaly patterns in the Precambrian basement along the eastern mountain front. The tiny circular features extending southwest from Santa Fe are caused by buildings. Image is color-shaded relief illuminated from the east.

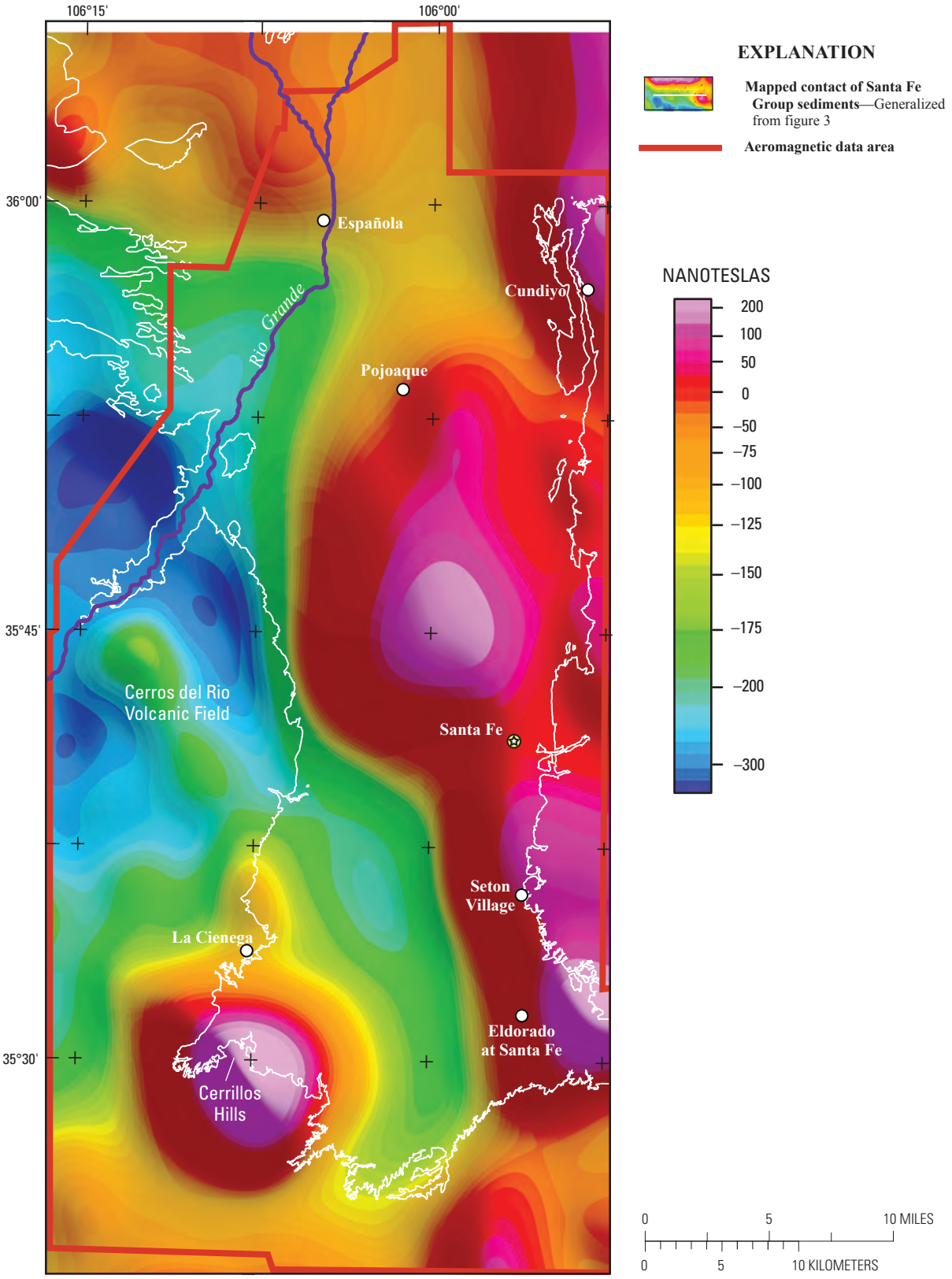

Figure 8. Lowpass-filtered magnetic map that enhances broad anomalies. The strong gradient extending west from Española may in large part be influenced by artifacts related to the poor resolution data in the northwest corner of the figure. Image is color-shaded relief illuminated from the east.

represent a case between the end-member shapes (0<N<1), such as a fault with moderate offset, or have more complexity, such as a fold or a gradational contact. In these cases, the structural index N is not an integer, and it will vary as distance to the source changes. For example, the magnetic field due to a finite-width dike behaves as though N=1 at distances much greater than the width of the dike, but behaves as though N=0 at distances very close to one of the dike edges. As a consequence, depth solutions must be examined in context with other information, because the actual depths to the edges of sources may commonly occur somewhere between the shallower solutions using N=0 and the deeper solutions using N=1.

Magnetic depth-estimation methods can be applied either to grids or to profiles extracted from the aeromagnetic data across selected anomalies. In both cases, a window is passed across the data, which results in multiple depth solutions, one from the analysis of each window of data. The results are generally considered robust when solutions cluster around one location. For this study, both profile-based and grid-based methods were applied and compared.

Profiles were analyzed by using the computer program PDEPTH (Phillips, 1997), which incorporates a variety of methods so that results can be examined together. The approaches giving the best results for this study are multisource Werner (Hansen and Simmonds, 1993), Euler deconvolution (Thompson, 1982), and local wavenumber or source parameter imaging (Thurston and Smith, 1997; Smith and others, 1998). These profile-based methods and their assumptions, strengths, and limitations are described in more detail in appendix 3. Except for the local wavenumber method, which computes the structural index directly, the methods require prior selection of N=0 or N=1. The multisource Werner method generally provided the most robust results for profiles. Solutions from this method (for both N=0 and N=1) are shown in subsequent figures in comparison with the geophysical profile models.

Gridded data were analyzed using an adaptation of the local wavenumber method (Thurston and Smith, 1997; Smith and others, 1998) by Phillips and others (2007). Previous results from the application of a two-step extended Euler method to the southern part of the study area (Phillips and Grauch, 2004) were compared during construction of the model. Descriptions of these grid-based applications are also included in appendix 3. A major advantage of the local wavenumber method is that it solves directly for N, unlike other methods in which multiple values of N must be tested separately. A major disadvantage is that it is sensitive to data noise, which produces scattered or spurious results (Phillips, 2000). To overcome the noise problem, the method was applied to the magnetic data after application of the pseudogravity transformation. By inspection along several profiles, solutions using pseudogravity data had similar depths compared with those from the reduced-to-pole data, where they were focused on the same magnetic source. To further reduce scatter, a median filter was applied that moved a window across the solution points and computed the median for as many as 50 neighboring points. The resulting solutions still densely cover the entire area and represent a wide range of depths (more than 64,000 points).

The Euler method is better suited to noisy data than the local wavenumber method, but N must be chosen before application. The two-step modification to the Euler method seeks to overcome the need to test different values of N by testing the solutions for N=0 against a user-defined minimum depth surface (Phillips and Grauch, 2004). When solutions are initially above the surface, N is increased until the solutions fall on the surface. Solutions that end up with unreasonable values of N are then discarded. In the previous study, the minimum depth surface was constructed from preliminary well data. For the present study, solutions from the local wavenumber and two-step extended Euler methods have similar results when compared in detail along profiles. However, the solutions from the local wavenumber method using pseudogravity and median filtering have less scatter, tend to provide more information on dipping interfaces, and are independent of any user-defined surfaces.

Although depth estimates related to an individual source may have errors as much as 20 percent of the estimated depth (Milsom, 1989), greater sources of error are the assumptions about the geologic origins of the magnetic source. Multiple types of magnetic sources at many depths in this study area make it difficult to predict which are represented by the depth estimates. In addition, where multiple sources are stacked vertically, the methods provide results only for the shallowest magnetic source.

Model Construction

Building on the results of our data analysis, we developed models to investigate various aspects of the gravity and magnetic data and integrate these results with information from other sources. We used a gravity inversion technique designed specifically to estimate the base of basin fill, joint gravity and magnetic modeling in 2D (profile) form to determine major sources of anomalies, and 3D integrated modeling to develop specific model surfaces across the basin. The results of the gravity inversion and modeling are discussed in the sections on interpreted subsurface geology. This section describes steps in the development of various models and how all information was integrated into a 3D model.

Gravity Inversion

The isostatic residual gravity data are most sensitive to the contrast in density between bedrock and poorly consolidated sediments, so they strongly constrain the general configuration of the basin floor. Deep gravity lows are closely associated with the thickest accumulation of sediment (fig. 6). However, gravity lows at the Valles caldera are instead caused

by a thick accumulation of volcanic tuff that is less dense than surrounding rocks. Underlying variations in density, thickness, and structural relief of basin-floor rocks are expected to produce notable overprints on the overall gravity map, but they are difficult to predict because they are buried.

To isolate the gravity effects of the basin fill alone, we used an iterative gravity inversion technique developed specifically for sedimentary basins by Jachens and Moring (1990), described by Blakely (1995), and that is very similar to the method of Ferguson and others (1988). The technique is based on separation of observed data into regional and residual components, where the residual component represents the gravity effects of the basin fill. A regional field is initially constructed using data only from stations located on bedrock not considered to be basin fill. This field is subtracted from the observed data to give a starting approximation of the residual field. Inversion techniques are then iteratively applied to vary the thickness of basin fill and modify the regional-residual separation to reach good fits to the observed data and to other independent constraints, such as well information. The two primary products are a model of basin-fill thickness (thickness model) and the final regional field, which represents the gravity effects of the bedrock (bedrock gravity) and includes the gravity effects of the both the basin floor and the bedrock of the flanking uplifts. The method is most successful where gravity data cover bedrock on all sides of the basin, where the density-depth function of basin fill compared with bedrock can be estimated, and where drill holes are available to help constrain the modeled thickness at depth. All three criteria for successful application of the gravity inversion technique are met for the Española Basin, except in the area of the Valles and Toledo calderas (fig. 1), where a separate approach is required. Because the study area skirts the caldera area, we elected to use the same approach throughout the basin and then ignore the results in that area. The steps of the gravity inversion are described as follows.

First, we expanded the area of analysis to include a large area surrounding the Española Basin. Gravity station coverage is fairly good at this scale except for a large region northeast of Santa Fe, which is mountainous (fig. 9). To begin the inversion, the area is divided into areas mapped as bedrock and areas mapped as Neogene and younger sedimentary and volcanic basin fill. Gravity stations within the areas considered as bedrock are separated out (blue circles on fig. 9) and used to develop the first regional bedrock gravity field in the iterative process.

Second, within the area considered as basin fill, a simple density-depth function must be defined. A plot of the densities derived from borehole density logs in the Albuquerque and Española Basins from table 2 provide a way to view how densities of different units vary with depth (fig. 10). The Santa Fe Group consistently possesses much lower densities at a given depth than any other unit. This markedly lower density provides the rationale for using the Santa Fe Group, along with the small-volume Tertiary younger volcanic rocks, to represent the basin fill and for all the other units to be considered bedrock. The density-depth function provided to the gravity inversion is thus the density contrast between the gravity reduction density of 2,670 kg/m^3 and the density of the Santa Fe Group; this density varies in a step-wise fashion with depth, as shown in figure 10. Thus, the lower Tertiary and Mesozoic units that have densities much lower than 2,670 kg/m^3 at depths less than 3,000 m (9,840 ft) should produce low values in the bedrock gravity after inversion. This outcome is discussed in the section on interpretations regarding the pre-rift sedimentary section. Volcanic cover consisting primarily of basalts no more than about 250 m (820 ft) thick, such as in the Cerros del Rio volcanic fields (Rodriguez and others, 2006), are considered volumetrically unimportant compared with the mass of sediments contained in the basins (Cordell, 1976; Birch, 1982). The higher density volcanic rocks influence details, but not gross features, of the inversion results. Thus, the thickness model should be considered as an overall model of the combined sedimentary and volcanic portions of the basin fill.

Third, lithologic and stratigraphic picks from wells, seismic-reflection depth picks, and model results from MT soundings (appendixes 1 and 4) were used to help constrain the inversion (fig. 9). Useful well information is particularly abundant in the southeast part of the basin, where many wells penetrate the base of the Santa Fe Group. The seismic and MT information, in particular, provide critical constraints in some of the deeper parts of the basin and extend outside the study area.

The isostatic residual gravity data were regridded from a 250 m (820 ft) to a 1 km (0.6 mi) interval for the gravity inversion. The coarser grid interval minimizes excursions associated with data problems or local variations. After inversion, the resulting thickness model was subtracted from a regional terrain surface and displayed as an elevation surface (fig. 11). The companion product, bedrock gravity, is also shown as a gravity map (fig. 12). This map contains information about density variations and structural relief on pre-rift bedrock, discussed in a following section. Because areas where volcanic rocks are thick (>250 m (820 ft)) are not properly accounted for in the density-depth function used in the inversion process, the results surrounding the Valles and Toledo calderas should not be considered valid.

The model results should be considered in a regional sense owing to several problems inherent in gravity inversion. First, data problems and lack of coverage produce inaccurate results because these artifacts are incorporated as valid data. Second, the thickness model becomes erroneous where the assumed density-depth function of the basin fill misrepresents the actual average densities. If the assumed density contrast (density of basin fill minus that of bedrock) is higher than the actual contrast, the resulting thickness will be too great; if the assumed density contrast is lower, the resulting thickness will be too small. Third, the large grid-interval size and inherent difficulties in separating gravity effects at gravity stations near the basin margins result in local excursions of the model at the basin-bedrock margin (not apparent at regional

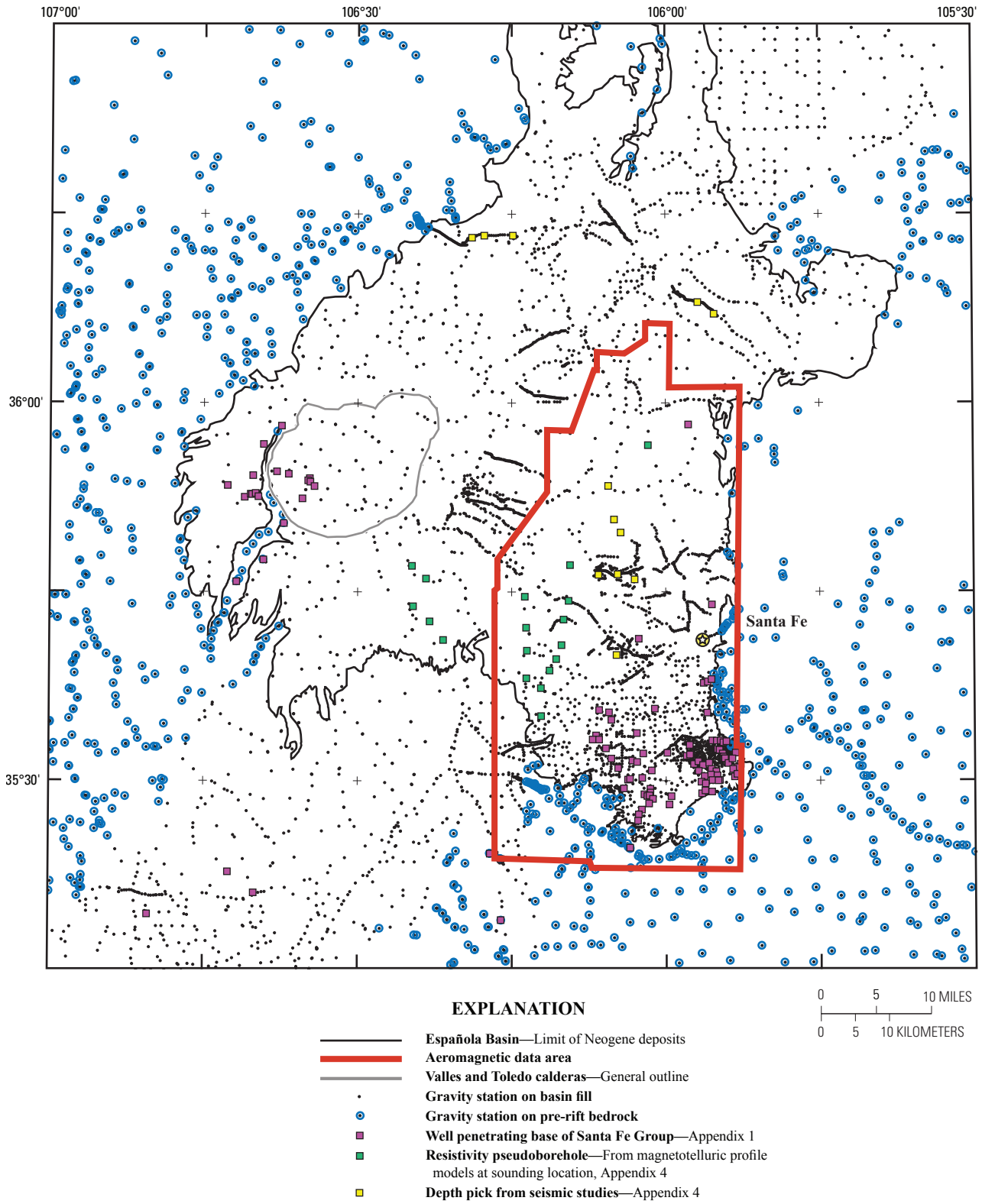

Figure 9. Data coverage and types of independent constraining data used in the gravity inversion (appendixes 1 and 2). Some gravity stations are coded as basin fill as defined by the extent of Neogene units shown in figure 1; others are considered to lie on pre-rift bedrock.

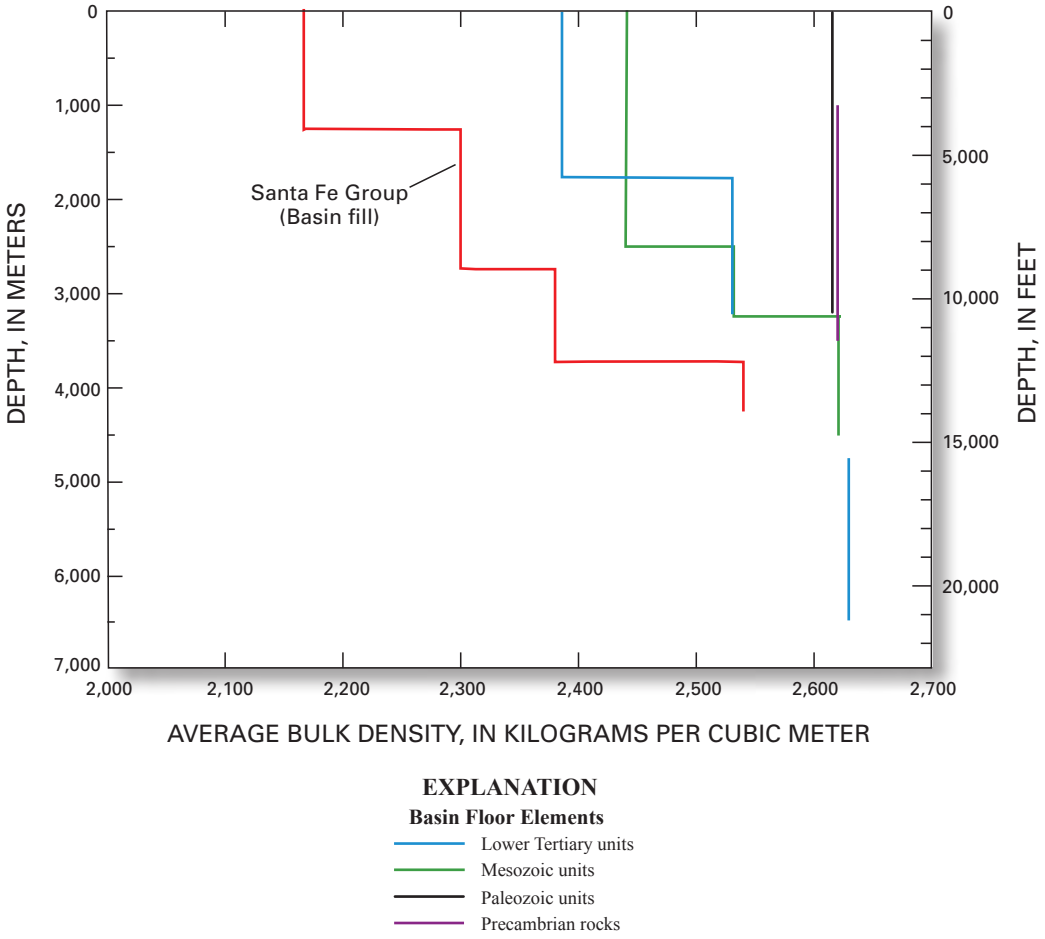

Figure 10. Simplified density-depth functions (step functions) developed from examination of borehole density logs in geologic units of different ages in the Albuquerque and Española Basins (table 2). The function shown for the Santa Fe Group was used in the gravity inversion and two-dimensional geophysical models.

scale). Finally, gridding techniques used in constructing both the regional gravity field and the thickness of basin fill do not properly account for abrupt density variations, such as those that may be caused by faults. Thus, faults affecting the basin-fill thickness may appear as smooth gradients and faults in the under-lying pre-rift rocks may result in unreasonable local excursions (either too low or too high) of the base of the thickness model.

Profile Models

We developed several 2D gravity and magnetic models (fig. 13) to better understand the sources of aeromagnetic anomalies and help constrain the 3D integrated model. The 2D models follow profiles used as input to the 3D model; several coincide with and are modified from Grauch and Bankey (2003). A few partial models were also constructed to resolve specific uncertainties near the mountain front. The data used for the profile models were extracted from the isostatic residual gravity (fig. 6) and the reduced-to-pole aeromagnetic data (fig. 5). The profiles cross the central parts of aeromagnetic anomalies of interest and lie in the vicinity of as many gravity stations as possible. Gridded data were extracted rather than gravity-station or flight-line data to ensure that gravity gradients were represented consistently and that aeromagnetic data did not contain unnecessary detail.

The 2D models employ polygonal bodies with discrete vertices and infinite strike in the direction perpendicular to the profile, following a standard 2D forward-modeling procedure (Talwani, 1965, as implemented by GM-SYS software of Geosoft®). With this approach, the vertices, magnetic properties, and densities are varied by the modeler until the computed magnetic and gravity fields of the model sufficiently match the observed data. To minimize ambiguities during this process, we placed fairly rigid constraints on initial model construction on the basis of independent information, concepts developed previously (Biehler and others, 1991; Baldridge and others,

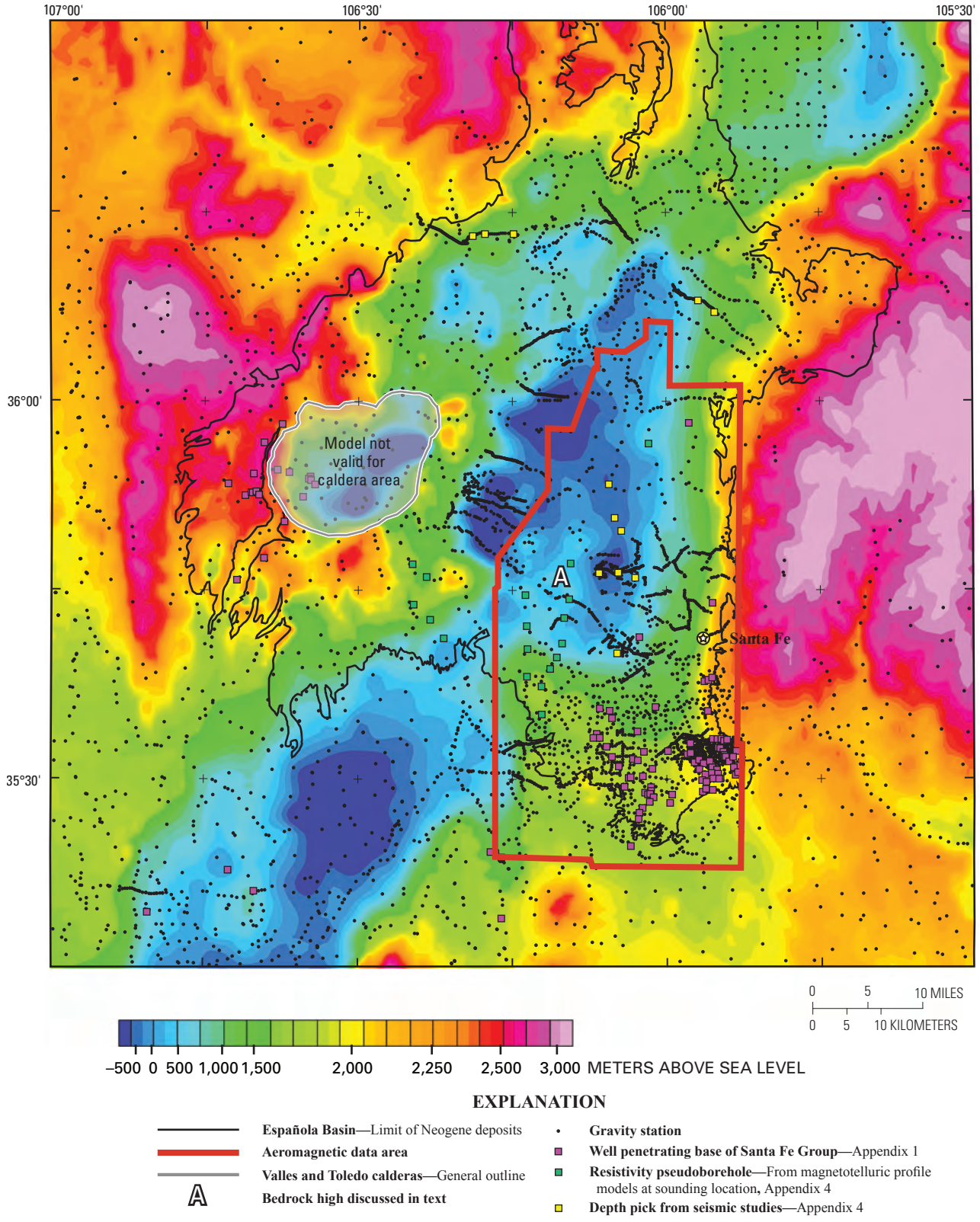

Figure 11. Elevation of the base of basin fill derived from gravity inversion. The surface was constructed by subtracting the thickness model derived from the gravity inversion (not shown) from a smooth topographic surface. Artifacts related to topography may be introduced by this subtraction because the modeled surface tends to be smoother than the regional topographic surface. Note that the deepest part of the basin is just outside the northwest part of the aeromagnetic data area. As discussed in the text, ignore results in vicinity of Valles and Toledo calderas.

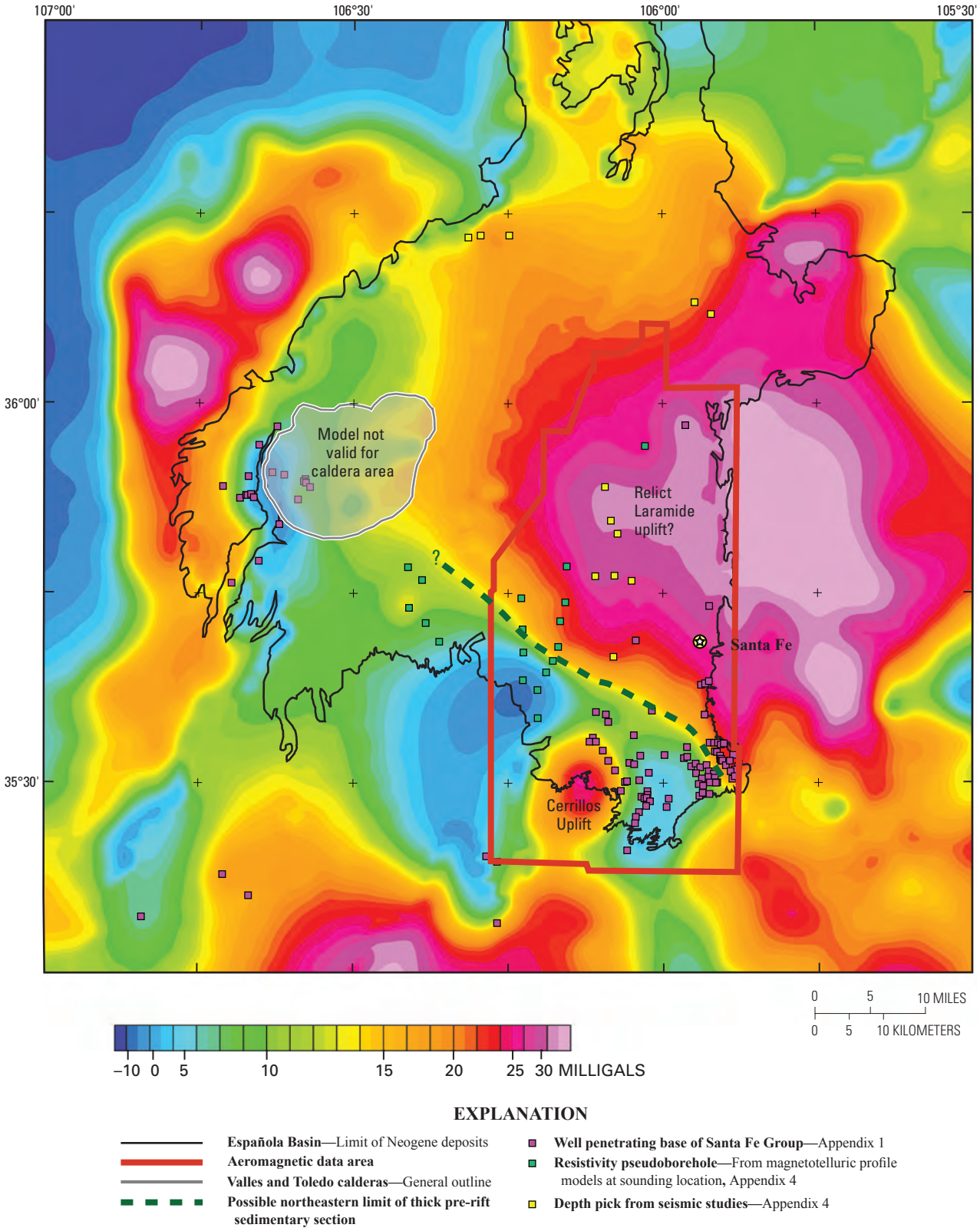

Figure 12. Bedrock gravity derived from gravity inversion. The final regional field resulting from the gravity inversion is shown; it is a companion of the thickness model discussed in figure 11. The map approximates the gravity effects of pre-rift bedrock as observed from the ground surface. Ignore results in vicinity of the Valles and Toledo calderas. Forward calculations of the three-dimensional model suggest that gravity values might be much lower in the northeastern part of the study area. If so, the thickness of pre-rift section may be greater in that area than is indicated on this map.

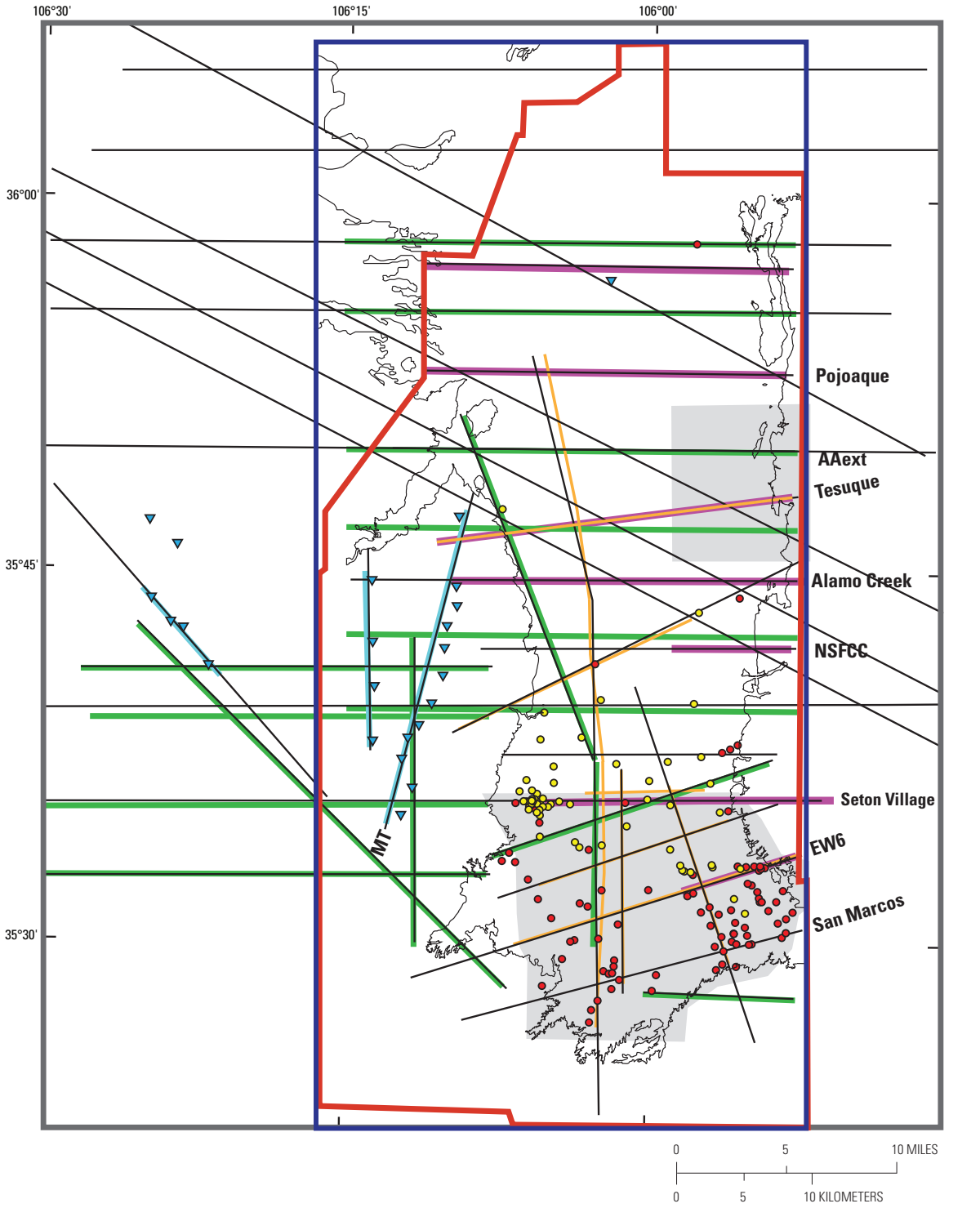

EXPLANATION

3D Model Control

- **Area of detailed analysis**—Additional closely spaced lines not shown
- **Section line used for digitized input**—Labeled if discussed in text

Point-Source Input

- Well that penetrates through the Santa Fe Group
- Well that bottoms within the Santa Fe Group
- Magnetotelluric sounding location where resistivity pseudoborehole was constructed

Profile-Based Input

- Magnetotelluric profile model used to construct resistivity pseudoboreholes
- Seismic-reflection time section or depth picks
- Geologic cross section
- 2D gravity and magnetic model

Miscellaneous

- 3D model area
- Study area
- Aeromagnetic data area
- Mapped contact of Santa Fe Group sediments

2001; Grauch and Bankey, 2003), expected physical properties of geophysical interpretative packages, and the results of our data analyses. Geologic mapping helped constrain several of the geophysical models near the basin margins on the eastern and southwestern sides of the study area (fig. 1). Geologic cross sections in these areas are from Sawyer and others (2006) and coauthor Daniel Koning, who updated cross sections from Read and others (2005) and developed new cross sections north of the Tesuque profile. Although these geologic cross sections span much of the basin (fig. 13), the deeper parts of the sections were based in large part on geophysical modeling, thus illustrating the iterative nature of the geophysical and geologic interpretations developed for this report. Other constraints on the geophysical profile models included limited well data, MT models, and seismic depth picks, as coded and located on figure 13.

Grid points representing the base of the thickness model from the gravity inversion were used as a general guide to locate the base of the modeled Santa Fe Group. Limitations in the gravity inversion results were apparent near the mountain front where the method could not resolve detail, in areas of poor station coverage, and on the west side of the study area where large excursions in the thickness model suggest major density contrasts (such as faults) in the underlying pre-rift bedrock. Magnetic depth solutions from the multisource Werner method were used to guide the modeling in the top 2,000 m (6,560 ft), especially where solutions cluster. In addition, the grid-based local wavenumber solutions guided definition of dip on magnetic interfaces.

After initial model setup, vertices of the polygonal bodies were varied by hand to best match computed model curves to both the observed gravity and the magnetic curves and to fit all the constraints as best as possible. Model bodies are based mainly on general differences in lithology. Table 3 lists the physical properties assigned to the model bodies and the geologic units they are designed to represent. The corresponding ages and geologic unit names are given to help put the model into its geologic context and are subject to reinterpretation. The magnetic properties of the bodies representing Precambrian basement are not well constrained and yet strongly influence the computed magnetic curve. To minimize the ambiguities, we varied the physical properties of these bodies as little as possible between profiles. There are also discrepancies in the representation of the Santa Fe Group and Paleozoic limestones that are required by their physical properties. Where Precambrian rocks have very low magnetic susceptibilities, they cannot be distinguished by density or magnetic properties from Paleozoic limestones (fig. 4 and table 2) that directly overlie them. Moreover, even where the Precambrian basement rocks are magnetic at depth, the limestones are too thin to discriminate on the basis of gravity and magnetic modeling. Therefore, the Paleozoic limestones are not separated from the modeled bodies of Precambrian basement. Where the Santa Fe Group is thick, the section cannot be represented as one model layer owing to expected increases in density with depth caused by compaction (table 2). Therefore, we divided the Santa Fe Group into a lower density shallow layer (density of 2,170 kg/m^3) and higher density deeper layer (density of 2,300 kg/m^3); the depth cutoff is 1,250 m (4,100 ft). This division of the Santa Fe Group sediments into two layers represents a density boundary, not a geologic interface.

The geophysical models are designed to focus on the main features of the data and are inherently somewhat ambiguous. Grauch and Bankey (2003) describe in detail the limitations of 2D geophysical modls for the area. In this study, the 3D model helped resolve some of these ambiguities, because it incorporates additional information off section and tracks variations in all directions. The 2D geophysical models provide general guides for the depths to basement, the configuration of magnetic units, and the thickness of the Santa Fe Group aquifer—a goal of this study. They also guide the construction of the 3D model and aid the understanding of the sources of aeromagnetic anomalies. Detailed discussion is reserved for following sections on interpreted subsurface geology.

Integrated Three-Dimensional Model

The primary goal in constructing a 3D model was to develop a surface representing the base of the basin-fill aquifers (Santa Fe Group) that integrated the many sources of information available. However, we expanded the efforts to incorporate also several concepts about the configuration of the Precambrian basement and the Tertiary older volcanic rocks that developed from the aeromagnetic interpretations. Unlike the geophysical interpretations discussed in the sections on interpreted subsurface geology, the 3D model ignores basalts of the Cerros del Rio volcanic field and intrusions related to the Cerrillos Hills and Espinaso Formation, and it attempts to distinguish Paleozoic limestones from Precambrian basement. Thus, the 3D model defines only three surfaces below the topography: the base of the Santa Fe Group, the base of the Tertiary older volcanic rocks, and the top of Precambrian basement. However, owing to the original goal of the 3D model and uncertainties in the lower two surfaces throughout most of the study area, the output for this report is limited to a digital grid of the base of the Santa Fe Group. The other two 3D surfaces are shown in subsequent figures only for illustration of key concepts.

The software package 3D GeoModeller™ was used to develop the 3D model. Surfaces representing geologic contacts are interpolated between points defined in three-dimensional space using orientation data, then stored as equations that define the surfaces. The surfaces can be easily recomputed using new information or modified data. The primary inputs to

Figure 13 (facing page). Locations of section lines and data used to construct three-dimensional integrated model. Labeled section lines and geophysical profile models are referred to in text or subsequent figures. Magnetic-depth-estimate locations not included because of their dense coverage.

Table 3. Bodies used in two-dimensional geophysical profile models.

[Model body codes and physical properties assigned to polygonal bodies of the two-dimensional geophysical profile models (figs. 17, 20, 22, 30), the geologic units (fig. 3), and basin element (table 1) that they are intended to represent. Assigned magnetic susceptibilities are mathematical representations that incorporate both magnetic susceptibility and a remanent component, if applicable. Thus, negative values represent dominant reverse-polarity magnetization. A value of 51,715 nanoteslas was assumed for the Earth's field. ft, feet; kg/m^3, kilograms per cubic meter; m, meter; SI, Système International]

Model body code	Equivalent geologic unit	Basin element	Body representation	Assigned density (kg/m^3)	Assigned magnetic susceptibility (SI)
			Elements of basin fill		
QTv	Qbt, QTv	Tertiary younger volcanic rocks.	Quaternary-Tertiary rift-related volcanic rocks, mainly basalts of Cerros del Rio volcanic field. The negative magnetic susceptibility is used to represent strong, reverse-polarity remanent magnetization.	2,670	–0.015
SFG	QTsf, Tsf	Santa Fe Group sediments	Santa Fe Group sediments, shallower than 1,250 m (4,100 ft), following the density-depth function used in gravity inversion.	2,170	0.001
SFGdeep	Tsf	Santa Fe Group sediments	Santa Fe Group sediments, deeper than 1,250 m (4,100 ft), following the density-depth function used in gravity inversion.	2,300	0.001
mag	?	Unknown basin fill	Magnetic sediments(?) within the basin fill. Magnetic susceptibility estimated on basis of magnetic portions of Santa Fe Group.	2,170	0.010
			Elements of basin floor		
Tov	Tmov, Te	Tertiary older volcanic rocks	Tertiary older volcanics, mainly the Espinaso Formation. Possible reverse-polarity component not represented.	2,450	0.013
pre-rift	Tgd, MzPzu, IPap.	Pre-rift sedimentary section (incomplete).	Pre-rift clastic sedimentary section, variably eroded. Includes Eocene through Paleozoic formations, except for limestones of the Paleozoic Alamitos and La Pasada Formations.	2,530	0.000
p€/Pz	p€, IPap	Precambrian basement; base of pre-rift sedimentary section.	Precambrian basement rocks that have negligible magnetization and overlying Pennsylvanian limestones. These rock types are indistinguishable from each other.	2,670	0.000
p€-weak1	p€	Precambrian basement	Precambrian basement rocks that have weak magnetization, less than p€-weak2.	2,670	0.001
p€-weak2	p€	Precambrian basement	Precambrian basement rocks that have weak magnetization, but more than p€-weak1.	2,670	0.005
p€-mod1	p€	Precambrian basement	Precambrian basement rocks that have moderate magnetization and are somewhat denser than p€-weak.	2,680	0.016
p€-mod2	p€	Precambrian basement	Precambrian basement rocks that have moderate magnetization and are moderately dense.	2,700	0.016
p€-mag	p€	Precambrian basement	Precambrian basement that is highly magnetic	2,670	0.040

3D GeoModeller are points representing geologic contacts digitized along section lines and in map view, strike-and-dip points, and contacts defined by the well data. Where the interpreter places digitized points along a particular section is guided by georegistered images or points projected onto the plane of the section. For this study, images included geologic cross sections and 2D geophysical models. Projected points included magnetic depth solutions, thickness-model grid points, and seismic depth picks. Magnetic depth estimates resulting from the grid-based local wavenumber method and the two-step extended Euler method both represented tens of thousands of points, so solutions were most usefully viewed as clusters of points rather than as single points. Profile-based magnetic depth estimates were incorporated into the 2D geophysical models, which then could be used as an added guide when we digitized from the 2D models. In addition, wells that do penetrate the base of the Santa Fe Group and the resistivity pseudoboreholes derived from the MT models, which both give imprecise information on geologic contacts, were used as guides for digitizing. The model sections along which points were digitized for the 3D model (section lines) and the types of information provided along or near the sections are shown in figure 13. The approach and data that constrain the interpretation of the three principal surfaces (base of the Santa Fe Group, the base of the older volcanic rocks, and the top of Precambrian basement) are described in table 1.

Several modeling strategies developed during construction of the 3D model. First, we expanded the model area outside the immediate study area (fig. 1). This expansion allowed us to smoothly merge our model with subsurface models already published for the Santo Domingo Basin (Minor, 2006) and to fully characterize gravity anomalies that extend northwest and east of the study area (fig. 6). On the other hand, because many geologic complexities in the extended areas were deemed unimportant for understanding the study area, the model is not adequate for presentation in these areas.

Second, two areas (gray areas on fig. 13) required more detail to define the surfaces. In these areas, many closely spaced sections were constructed and examined one by one. These detail areas are located primarily in the southeastern part of the study area, where well information is more abundant, and along the eastern mountain front, where we questioned gravity model results.

Third, a strategy was developed for use of the magnetic depth estimates, depending on the magnetic interface represented. A need for such a strategy became apparent when we realized that the magnetic depth estimates were commonly locating magnetic interfaces internal to the Tertiary older volcanic rocks and Precambrian basement rocks. Examples of the former situation are shown in two sections (fig. 14) from the southeastern detail area (fig. 13). In these examples, the picks in wells and the thickness model obtained from the gravity inversion closely constrain the contact between the base of the Santa Fe Group and the underlying Espinaso Formation (representing the package of Tertiary older volcanic rocks in this area). This interface is projected from the 3D model onto the sections (brown lines on fig. 14). Magnetic depth estimate solutions from both the local wavenumber and the two-step extended Euler methods both cluster at this interface in some places and in other places indicate magnetic sources that are much deeper. If the magnetic depth estimate solutions are used to represent the contact of the Santa Fe Group and Espinaso Formation, as was done previously (Phillips and Grauch, 2004), then the magnetic results suggest surface irregularities with more than 100 m (330 ft) of relief. Although irregularities in the top of the Espinaso Formation surface are apparent from closely spaced drill holes elsewhere (Koning and Hallett, 2001), relief does not appear to exceed 45 m (150 ft). Instead, we now consider that the magnetic depth solutions provide information on the internal structure of the Tertiary older volcanic rocks, which was used as a general guide for developing the shape of the base of the older volcanic rocks.

Where magnetic rocks appear absent on the basis of lack of aeromagnetic anomalies, the local wavenumber depth solutions commonly showed a characteristic pattern of deepening scatter into the area with no magnetic sources (fig. 14*B*). This pattern may be due to median filtering that incorporates information from neighboring depth solutions as the window passes across the boundary between magnetic and nonmagnetic rocks. In some cases, the local wavenumber depth solutions appear more clustered within the Precambrian basement, generally following the dip of the basement surface but at greater depths, consistent with hypotheses of nonmagnetic Precambrian rock types overlying magnetic ones, as discussed in a following section. Other magnetic depth estimates show good clustering within the pre-rift section, but the sources are enigmatic.

Finally, to simplify the modeling, only three faults were defined in the model: (1) a west-down normal fault representing the La Bajada fault system and its connection to the Cochiti Cone fault on the north (figs. 2 and 3); (2) an east-down normal fault representing the Pajarito-Embudo fault system that bounds the west-dipping half-graben of the Española Basin on the northwest (fig. 2); and (3) an east-down normal fault representing the west limit of zones of intense deformation (the Agua Fria and Barrancos fault systems) that extend northerly across the central part of the study area (fig. 2). Because major gravity gradients are generally associated with both the La Bajada and Pajarito-Embudo fault systems, these gradients were used to determine the exact locations of the model faults. All other faults were represented by steep slopes on the surfaces.

Despite the advantages of integrated multiple inputs, the 3D model is still subject to alternative scenarios, subjective judgment, lack of information in certain areas, and artifacts of mathematical interpolation. The best-constrained surface throughout the area is the base of the Santa Fe Group. The base of Tertiary older volcanic rocks is fairly well constrained within most parts of the southeastern part of the area, but it is poorly constrained farther north owing to its greater depth. Because of the variability of magnetic properties of the Precambrian basement, this surface was constrained primarily

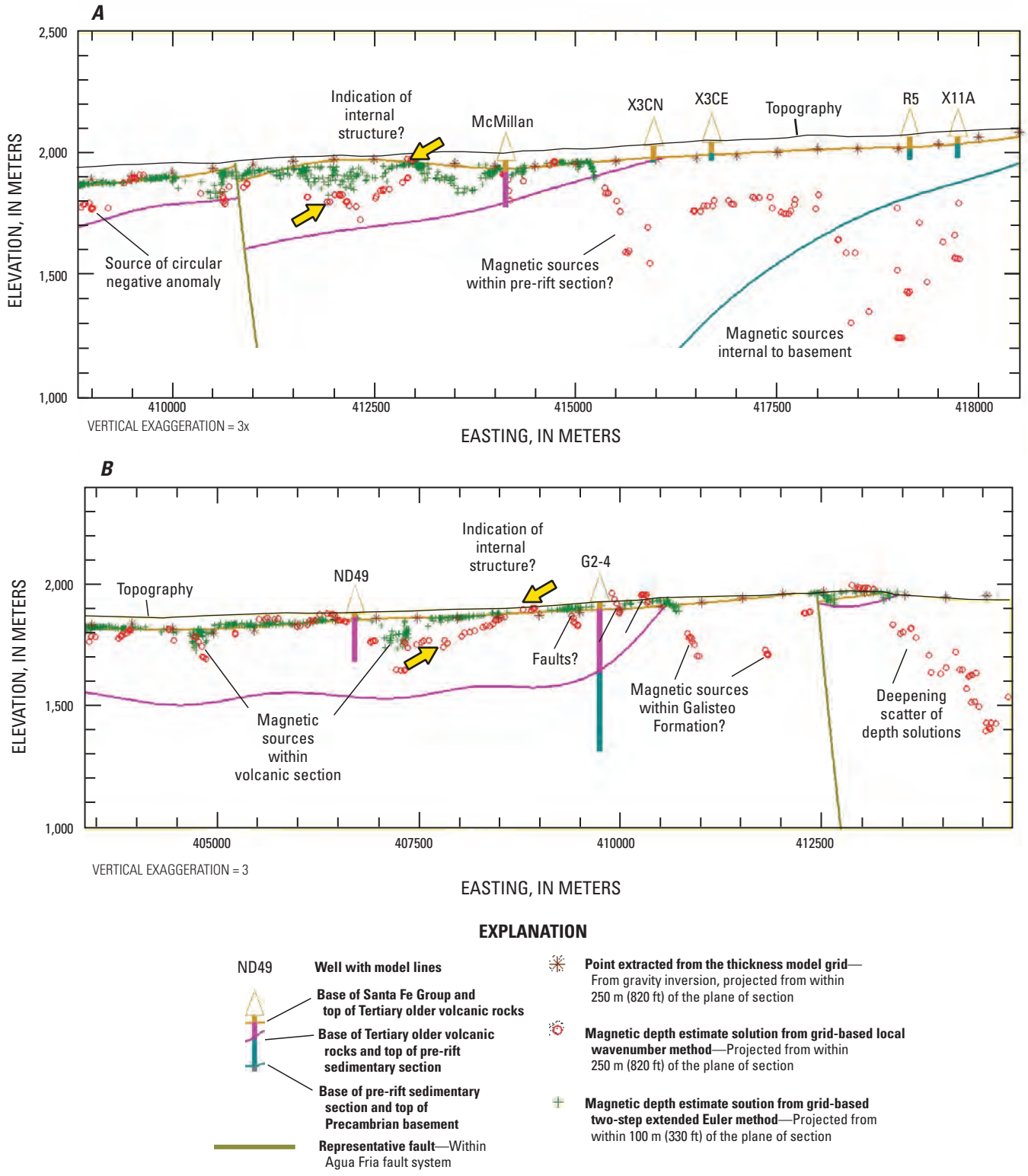

Figure 14. Examples of two short east-west sections from the area of detailed analysis in the southeastern part of the study area. The three-dimensional model surfaces are projected onto the sections and show detail that is constrained by neighboring, as well as by these, sections. Digitized points used as model input not shown. Scatter and clustering is typical of magnetic depth estimates. The Euler solutions that closely follow a flatter surface have been forced to the surface as a consequence of the two-step method. *A*, Section follows northing 3930000 m; *B*, Section follows northing 3925500 m; Universal Transverse Mercator Zone 13, North American datum of 1927.

by the seismic interpretation and gravity-derived thickness-model base, both of which have limited coverage throughout large areas. The model smoothes faulted surfaces and is insensitive to other local variations that may be recognized from closely spaced wells. Thus, none of the models in this study should be used to answer local subsurface questions.

Interpreted Elements of the Basin Floor

The dominant features of the aeromagnetic map are associated with Precambrian basement rocks, intrusive rocks in the Cerrillos Hills, and Miocene-Pliocene basalts in the Cerros del Rio volcanic field (fig. 15). More subdued features are related to pre-rift volcanic and volcaniclastic rocks in the southern part of the data area, magnetic sediments contained in the Puye Formation of the Santa Fe Group in the northwestern part of the data area, and linear features related to faulting. Very small but prominent anomalies that look like circular or elongate raised areas are caused by anthropogenic structures, such as buildings, bridges, and landfills.

Information about the overall structure of the basin is contained in the aeromagnetic data but is not readily apparent on the map. In contrast, the isostatic residual gravity map is dominated by the expression of basin geometry; the highest gravity values represent uplifted, relatively dense Precambrian basement, and the lowest values represent areas of the deepest parts of the basin (fig. 16).

The following sections discuss interpretations of geologic features primarily from the aeromagnetic data and draw from the results of the data analysis and modeling. The features are generally discussed from oldest to youngest.

Precambrian Basement

Some of the most prominent anomalies on the aeromagnetic map are caused by Precambrian basement rocks. These anomalies include the broad, roughly vase-shaped magnetic high in the center of the area; north- and northwest-trending, strong magnetic highs along the mountain front from Santa Fe south to Eldorado at Santa Fe; and the subtle, broad anomaly just northwest of Española (fig. 15). The anomalies are prominent in the lowpass-filtered map (fig. 8), suggesting that the underlying magnetic rocks are massive and extend to great depths. Several of these large magnetic highs are truncated along linear trends, such as the southern termination of the broad magnetic anomaly north of Santa Fe and the western terminations of large anomalies along the mountain front (bold blue dashed lines on fig. 15). The terminations are interpreted as a primary contrast in rock type between magnetic and weakly magnetic Precambrian basement that has only minor structural relief. This interpretation is based on comparisons with the gravity data, which show only minor gradients in association with these boundaries (fig. 16). The major differences in the magnetic properties are demonstrated by the model for the Tesuque profile (fig. 17), which requires within the Precambrian basement a massive, highly magnetic body bounded by a steep contact on the east and a gently dipping one on the west. The steep boundary suggests an origin as an intrusive contact or a major fault that formed before erosion of the Precambrian surface.

Basement rocks are also associated with both magnetic highs and lows where they are exposed along the entire mountain front. The heterogeneity is not surprising, considering that Precambrian basement rocks in this area include a wide range of compositions (Read and others, 2003, 2004). Heterogeneity of magnetic properties is evident from reconnaissance magnetic-susceptibility measurements at outcrops, which show that basement rocks range from weakly magnetic to strongly magnetic (fig. 4). However, a simple correlation between magnetic susceptibility and mapped rock unit is not apparent.

A characteristic pattern of linear alternating high and low anomalies is noticeable in the magnetic map for areas mapped as Precambrian rock (figs. 18 and 19). Many of these linear anomalies are designated as undetermined magnetic lineaments on plate 1. In the southeastern part of the study, this pattern is evident from Eldorado at Santa Fe to north of Seton Village (for example, A on fig. 18). The linear pattern is well defined in the first vertical derivative map (fig. 7). These patterns trend northwest to north-northwest and appear to terminate along a north-northeast-striking line at the mountain front just north of Seton Village. The second area is in the northeast part of the study area, from latitudes 35°45' to 35°50' (for example, A on fig. 19). In contrast to patterns in the southeastern area, these patterns trend north-south. In both areas, similar linear patterns lie just west of the basin margin, where the source of these linear anomalies appears deeper than its neighboring sources because the anomalies are broader and more subdued (B on figs. 18 and 19). Some contribution to the linear anomalies northeast of Santa Fe may be due to the contact between Paleozoic limestone and Bishops Lodge member of the Tesuque Formation (between B and C north of Santa Fe on fig. 18). A significant contrast in magnetic susceptibility between these two units is suggested by reconnaissance measurements (fig. 4).

In the southeastern part of the study area, both topography and geologic trends in the Precambrian rocks parallel the orientation of the linear anomaly pattern. However, the topography does not correspond directly, suggesting that the sources of the linear anomalies are primarily below the surface. For example, five ridge-like magnetic anomalies parallel Interstate 25 southeast of Seton Village (between A and the basin margin, fig. 18). In contrast, the topography in the same area consists of one wide valley surrounding Interstate 25 and one wide zone of hills aligned northwest at the mountain front. There is also no definitive correlation between elongate trends of differing Precambrian lithology that are partially exposed in the same area (pl. 4 of Spiegel and Baldwin, 1963; Read and others, 2004). However, the anomalies may relate to alternating lithologic layers and

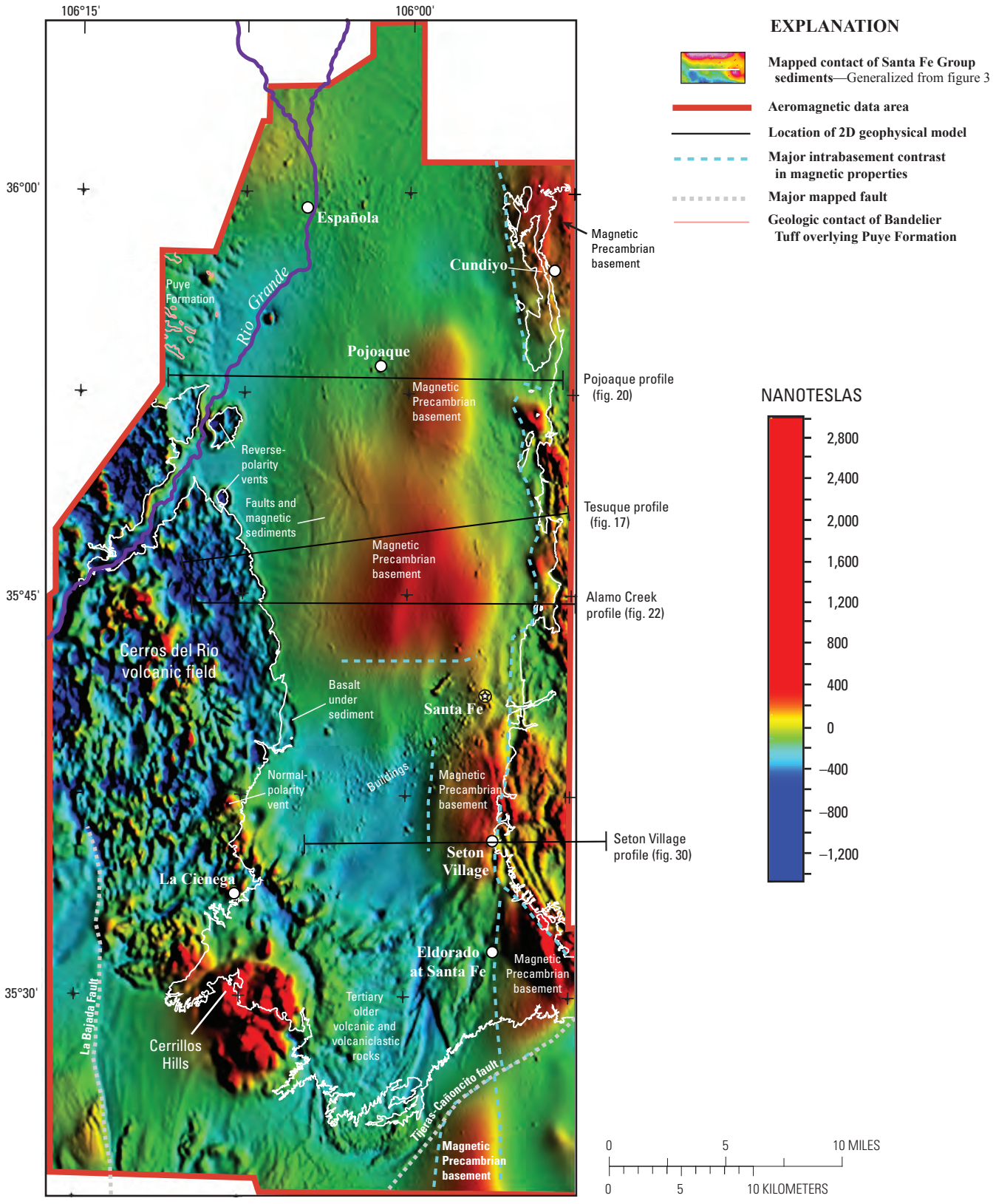

Figure 15. Selected features of aeromagnetic map (fig. 5) and their interpreted sources, as discussed in the text. Marked terminations of basement-related anomalies represent large contrasts in magnetic properties (light blue dashed lines) that are interpreted as major contacts between different rock types within the basement. Locations of two-dimensional geophysical profile models (figs. 17, 20, 22, and 30) are indicated. Image is color-shaded relief with illumination from the east.

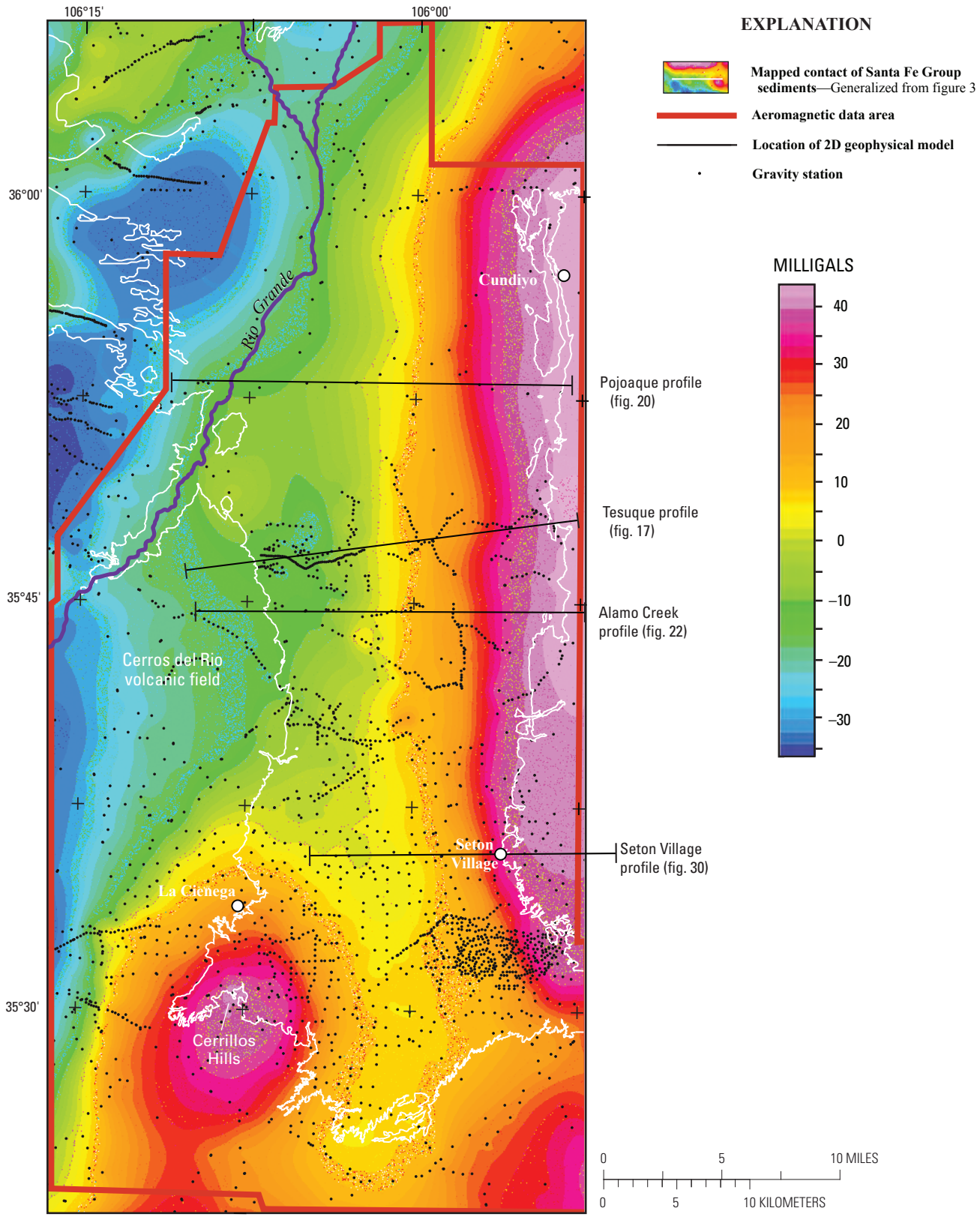

Figure 16. Isostatic residual gravity extracted for the study area from figure 6. Contours generally show basin form. The magnetic lithology boundaries of figure 15 are not apparent, suggesting that the magnetic boundaries do not correspond with major structural relief on the basement. The locations of two-dimensional geophysical profile models (figs. 17, 20, 22, and 30) are indicated.

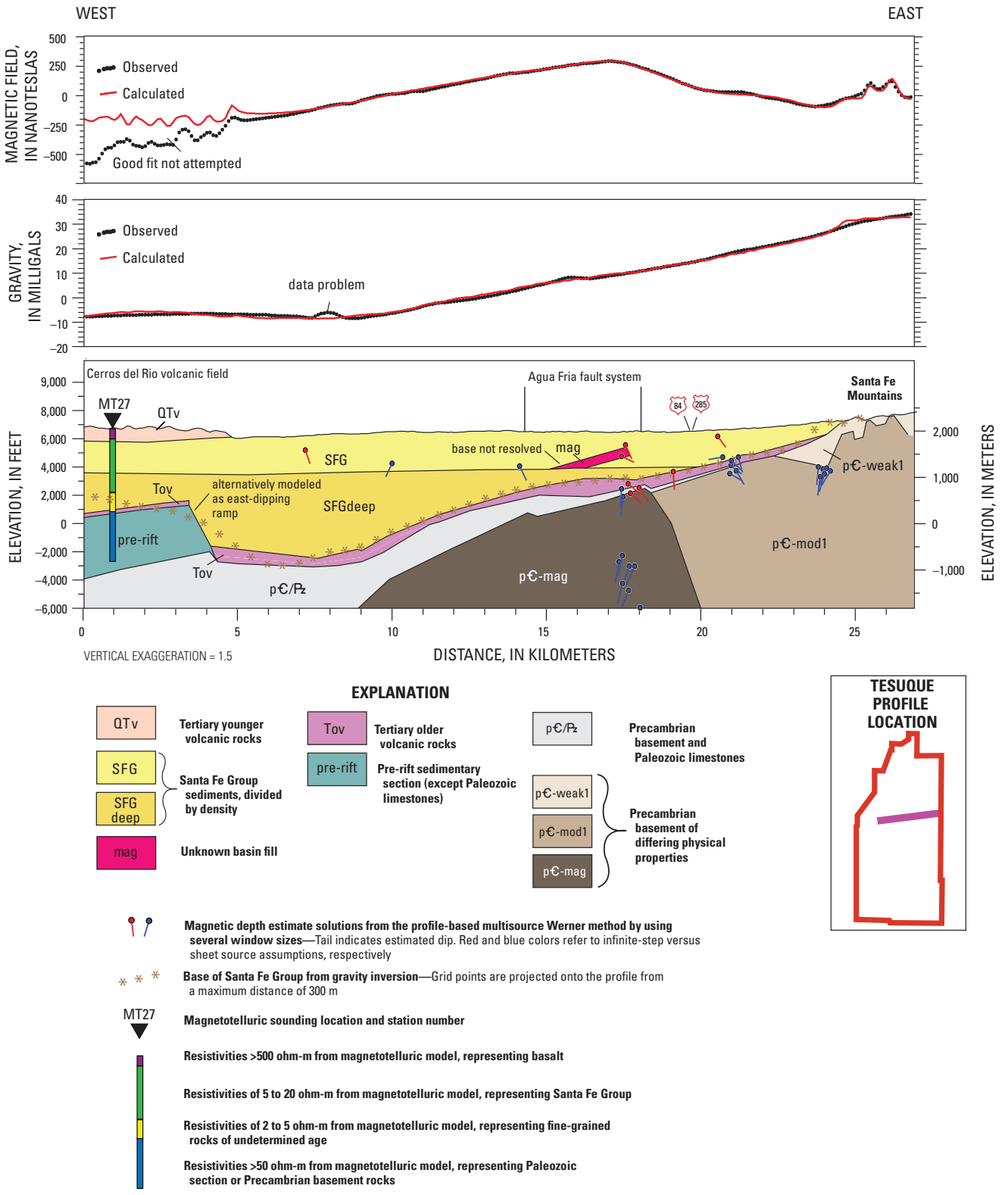

Figure 17. Two-dimensional gravity and magnetic model for Tesuque profile. Model bodies are described in table 3. The profile is also located on the inset and on figures 13, 15, and 16. The model demonstrates variable magnetic properties of the Precambrian basement, both at large scale and as small-scale folding where exposed on the east. The Agua Fria fault system is manifested in both shallow and deep basement disruptions. The bedrock high on the west can be alternatively modeled in this location as an east-dipping ramp. The profile is also constrained by seismic data (not shown). Note that the horizontal division between unit SFG and unit SFGdeep is a density boundary, not a geologic contact.

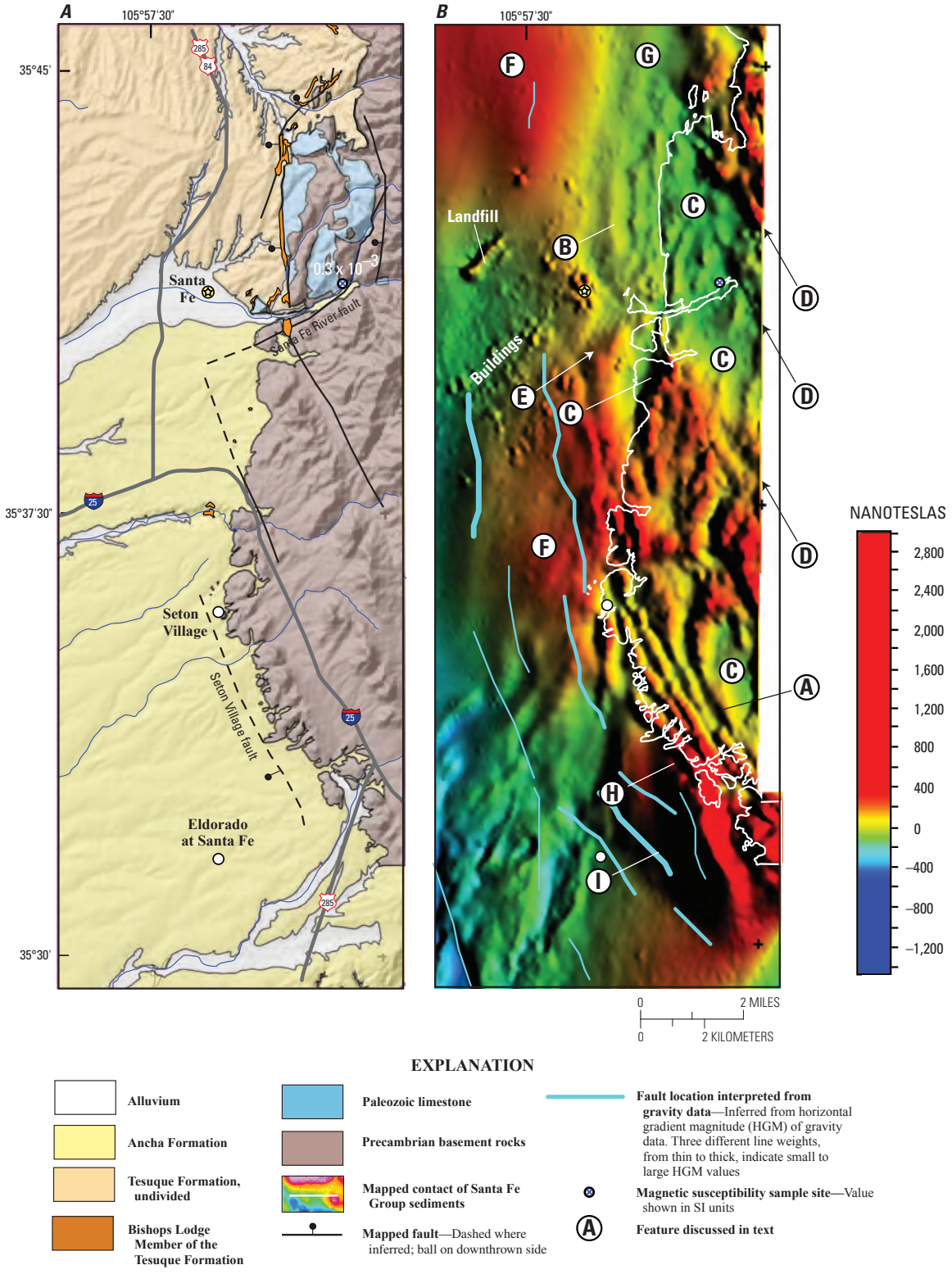

Figure 18. Closeup of the mountain front in the southeastern part of the study area. *A*, General geology underlain by a shaded digital elevation model. Geologic contacts from figure 3; additional information on the Bishops Lodge Member from Read and others (2004). Location and average value at one measured magnetic-susceptibility traverse is shown along the Santa Fe River canyon east of Santa Fe (information collected by Mark Hudson and V.J.S. Grauch (unpub. data, 2007)). *B*, Shaded-relief aeromagnetic image from figure 5. Higher gradient magnitudes indicated by thicker lines may indicate steeper basement slope or, more likely, faults with greater displacement than is indicated by lesser gradient magnitudes (thinner lines).

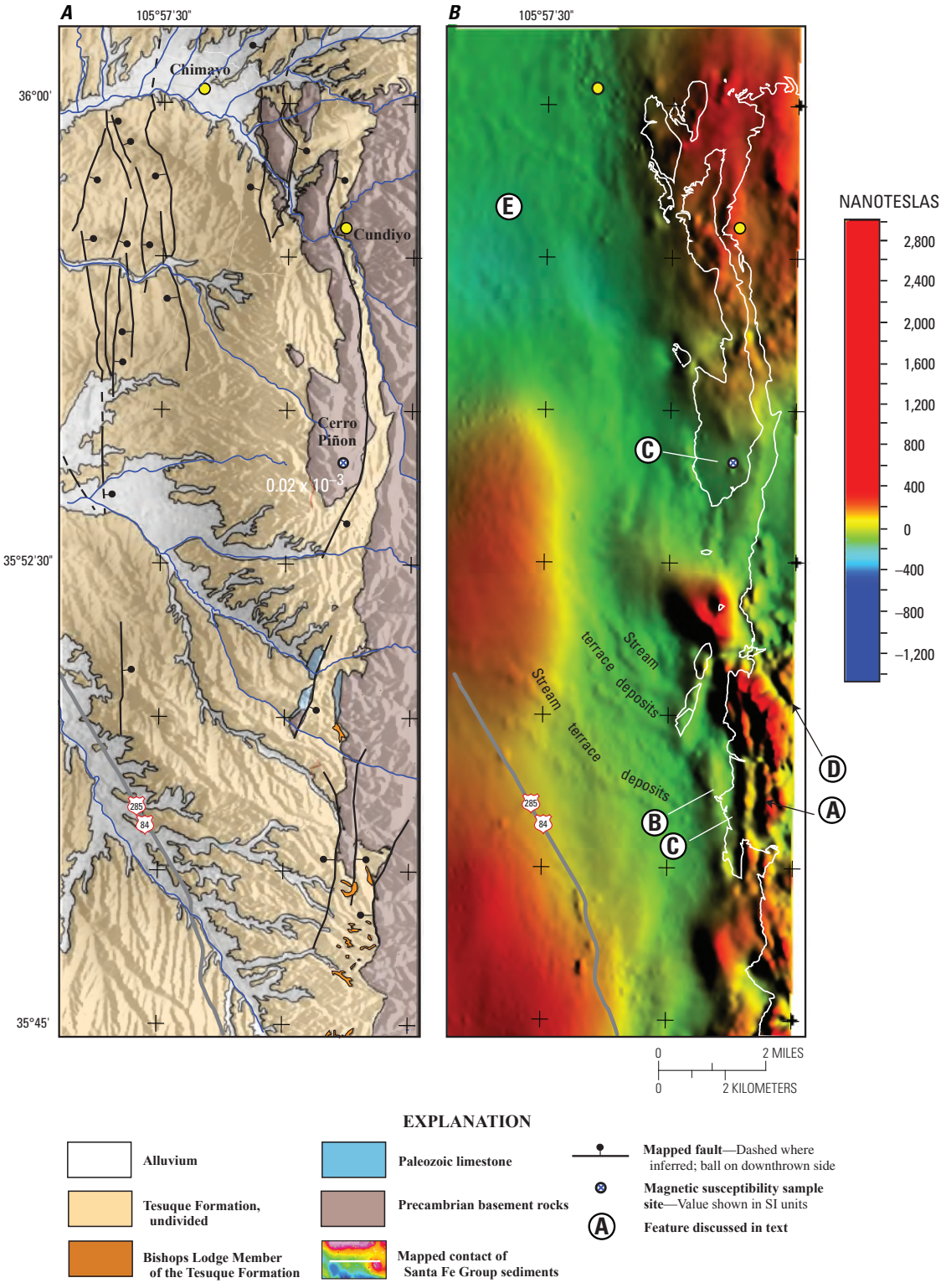

Figure 19. Closeup of the mountain front in northeastern part of study area. *A*, General geology underlain by a shaded digital elevation model. Geologic contacts are from figure 3, with additional information on Bishops Lodge Member from Read and others (2004). The location and average value at one measured magnetic susceptibility traverse is shown at Cerro Piñon (information collected by Mark Hudson and V.J.S. Grauch (unpub. data, 2007)). *B*, Shaded-relief aeromagnetic image from figure 5. Stream terrace deposits are expressed as subtle aeromagnetic anomalies that correlate well with topography.

tight folds that were later injected with magma preferentially along layering in Precambrian time (Spiegel and Baldwin, 1963; Read and others, 2005; Evans and Lindline, 2004). Experiments with modeling the basement mountain front at the easternmost end of the 2D geophysical model for the Tesuque profile (fig. 17) confirm that buried folds rather than multiple dikes provide a better fit to the anomaly patterns. A better understanding may come from re-examination of Precambrian lithologic contacts, more magnetic susceptibility measurements, and consideration of remanent magnetization, all of which are beyond the scope of this study.

Weakly magnetic rocks are evident in local areas of the exposed Precambrian basement at several places along the mountain front (C on figs. 18 and 19). In these areas, generally low magnetic anomaly values and little correlation between the anomalies and the shapes of topographic features are evidence that the exposed rocks have low magnetic susceptibilities. This interpretation is corroborated by measured low magnetic susceptibilities averaging 0.0003 (SI) for gneiss that crops out along the Santa Fe River (fig. 18) and averaging 0.00002 (SI) for muscovite granite at Cerro Piñon (fig. 19).

The character of aeromagnetic patterns associated with exposed Precambrian rocks changes abruptly at several linear trends, which may indicate terrane boundaries within the basement or more recent faulting. Only a few of the most prominent trends are annotated (D on figs. 18 and 19; pl. 1). East of Santa Fe, these northwesterly trends appear to cross the head of the Santa Fe River canyon with only minor disruption, suggesting that any lateral displacement along the Santa Fe River fault is minor. On the other hand, northerly trending linear anomalies are disrupted along an east-northeast trend that connects to the mouth of Santa Fe River Canyon (E on fig. 18).

All along the basin margin, the basement rocks associated with detailed aeromagnetic patterns can be traced by their aeromagnetic expression and by the magnetic depth estimates no more than 1–2 km (0.6–1.3 mi) basinward into the subsurface, to depths of 150–300 m (500–990 ft). West of this zone, the aeromagnetic expression of basement rocks changes abruptly to very broad magnetic highs (F near Seton Village on fig. 18) or to broad areas of low values onto which more subtle anomalies are superimposed owing to the overlying sediments (E on fig. 19). This change in character is marked by bright blue dashed lines on figure 15 and plate 1. In some places, the detailed and broad anomalies seem to be superimposed, which is evident by comparing the lowpass and first-vertical-derivative maps, especially for the area extending 4 km (2.5 mi) south of Cundiyo (figs. 7, 8, and 19*A*). The change from detailed to broad character is especially evident near the basin margin south of Seton Village (H on fig. 18). This difference in aeromagnetic character is not likely caused by a large-displacement rift fault, because modeling of the 2D geophysical profiles and gradients in the gravity data suggest mostly regional dip on the top of the basement in this area. Perhaps the basement terrane associated with detailed anomaly patterns forms a fairly thin top layer overlying the basement terrane represented by broader anomalies, and the top layer is absent just west of the basin margin. If so, the strikingly linear character of the western termination of this top layer suggests that it is related to structure developed during a pre-rift tectonic event.

North of Santa Fe, the buried basement surface undulates from moderate westward dip (~20°) at the mountain front to shallow dip (~5°) and back to moderate dip 10–12 km (16–19.2 mi) west of the front; these changes are especially evident in the Tesuque and Pojoaque 2D geophysical profile models (figs. 17 and 20). South of Santa Fe, the basement slopes more steeply to the west and southwest, and it rises on the west side of the study area, as demonstrated by sections through the 3D model (fig. 21). In the vicinity of Eldorado at Santa Fe, wells indicate that the basement and overlying Paleozoic section are quite variable in elevation along trends parallel to the mountain front, but this variation cannot be resolved by the modeling. Moreover, the geophysical models do not show the individual basement faults; rather, they depict only the general form of the basement as a dipping surface. This general form shows that the greatest slope (or drop) of the basement surface occurs about 1.6 km (1 mi) southwest of the mountain front, coincident with a gravity-interpreted fault (I on fig. 18) rather than the change in aeromagnetic character (H on fig. 18).

Broad magnetic anomalies related to Precambrian basement rocks that are elongate north-south in the southeastern part of the study area appear to be offset across the Tijeras-Cañoncito strike-slip fault system (fig. 15). Preliminary magnetic depth-estimate analysis indicates that the sources on both sides of the fault are about 1,000 m (3,280 ft) deep. If these depths represent similar stratigraphic levels in the Precambrian rocks, then the offset suggests about 5 km (3 mi) of net right lateral displacement on this fault.

Pre-Rift Sedimentary Section

The pre-rift sedimentary section includes strata deposited during Paleozoic through Eocene time. They rest unconformably on the Precambrian basement surface, are variably eroded across the Española Basin, are intruded by the Cerrillos Hills intrusive complex, and are overlain by Tertiary older volcanic rocks. The best information on the pre-rift sedimentary section is contained in proprietary seismic-reflection data (Baldridge and others, 2001; Ferguson and others, 2007), which are yet to be fully analyzed. Only limited information from the seismic data on the total thickness of this package (provided by John Ferguson, University of Texas at Dallas, written commun., 2007) has been incorporated into the 3D model of this study. The seismic data show that the pre-rift section is thickest (almost 3,000 m (9,840 ft)) in the southern part of the study area, as depicted by sections through the 3D model (fig. 21). In this area, it forms a syncline with a north-south axis (Ferguson and others, 2007). To the north, the Paleozoic-Mesozoic sedimentary section underlies

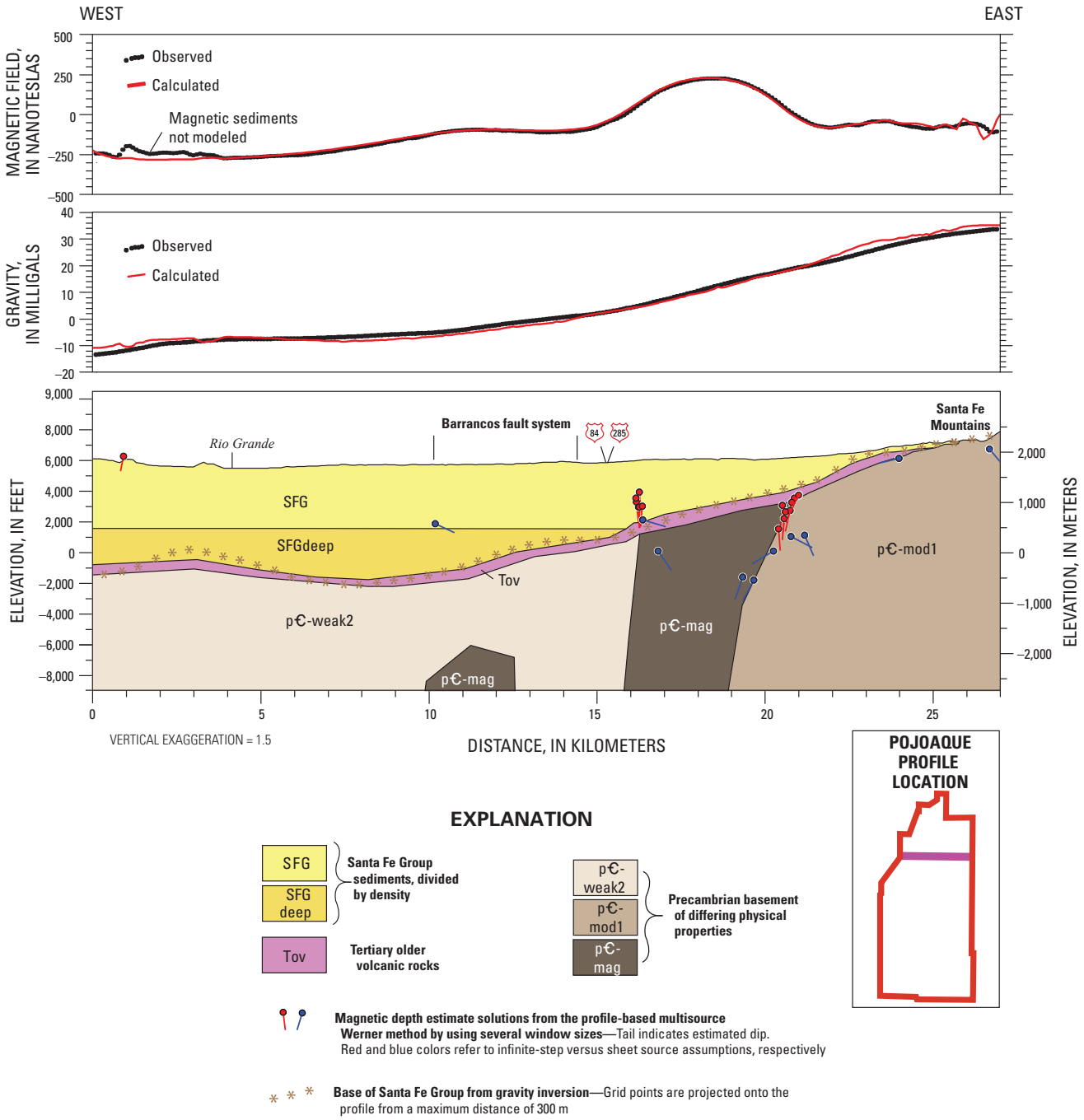

Figure 20. Two-dimensional gravity and magnetic model for Pojoaque profile. Model bodies are described in table 3. Profile is located on the inset and on figures 13, 15, and 16. This model demonstrates the faulted Barrancos monocline, which dips to the west. In the geophysical model, individual faults are not distinguished. Although the Agua Fria fault system is not defined in this area, the magnetic depth estimates and their relation to the edges of the magnetic Precambrian body (unit p€-mag) suggest the presence of faulting east of the Barrancos fault system.

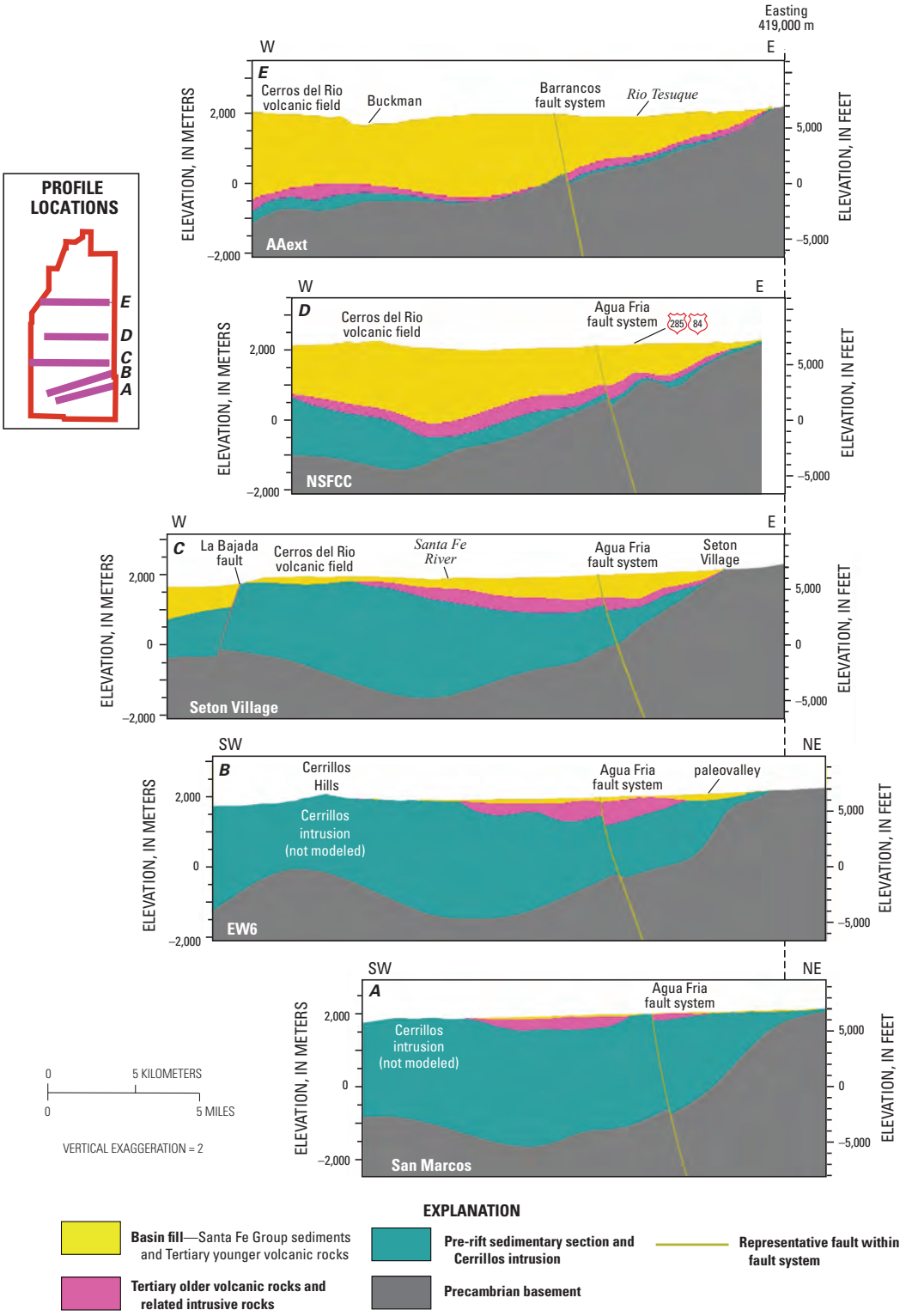

Figure 21. Sections through three-dimensional model showing general relations between the three modeled surfaces across the basin from south (A) to north (E). The sections, labeled in the lower left, are located on figure 13. (Only portions of model sections C, D, and E are shown.) Only one fault was used in the model to represent the Agua Fria and Barrancos fault systems. It generally follows the west sides of the zones of faulting. Fault blocks and numerous other faults are depicted only by change in slope of the surface. The lack of detail in these sections compared with standard geologic cross sections demonstrates the regional scale for which the model was intended. Universal Transverse Mercator Zone 13, North American Datum of 1927.

a north-dipping angular unconformity defining the base of pre-rift Tertiary units. The seismic data indicate that the Galisteo or Diamond Tail Formations (or both) represent greater than 700 m (2,300 ft) of the maximum thickness of the pre-rift section (Ferguson and others, 2007). A thickness of 2,380 m (7,810 ft) thus remains for Paleozoic-Mesozoic units (Baldridge and others, 2001), a value considerably larger than the ~1,700 m (~5,580 ft) median Paleozoic-Mesozoic thickness measured in the surrounding areas (Sawyer and Minor, 2006).

Constraints provided by the seismic-reflection data help explain the strong northwest-trending gradient apparent in the pre-rift bedrock gravity results from the gravity inversion (fig. 12). The gradient implies a substantial density contrast within the basin floor below the Santa Fe Group; a greater volume of lower density bedrock lies on the southwest side. This scenario is consistent with the interpretations of the seismic data southwest of Santa Fe showing a lower density, pre-rift sedimentary section that is substantially thicker on the south compared with the north. On the north, the section is much thinner over higher density Precambrian basement. Moreover, the location and trend of this gravity gradient generally follow where the Paleozoic-Mesozoic units appear truncated in the seismic data within the Santa Fe embayment. Thus, we extrapolate the interpretation to suggest that the truncations of the Paleozoic-Mesozoic section extend the whole length of the remarkably linear, nearly 40-km (25-mile)-long gravity gradient trend. If this interpretation is correct, the trend may mark the southernmost limit of the Laramide uplift that has been hypothesized to underlie the Española Basin (Cather, 1992; Myer and Smith, 2006). A strong gravity high associated with the Cerrillos uplift interrupts the gravity low associated with inferred thick, pre-rift sedimentary section (fig. 12). This scenario is consistent with previous studies that concluded that the Cerrillos uplift is a structurally high block formed in response to footwall uplift of the La Bajada fault during rifting (Baldridge and others, 1991; Minor, 2006).

Synthesis of results from the thickness model obtained by gravity inversion, the MT profile models, and seismic constraints indicates the presence of a previously unreported bedrock high under the Cerros del Rio volcanic field. This high is best displayed in the thickness model as a north-northeast trending triangle-shaped area with about 500–1,000 m (1,640–3,280 ft) of relief (A on fig. 11). The best constraints for this high come from an unpublished north-northwest trending 2D MT model developed by Brian Rodriguez and Jackie Williams (U.S. Geological Survey, written commun., 2007) on the basis of 12 soundings across the middle of the volcanic field (profile MT on fig. 13). Their model consistently shows a basal resistive layer (>50 ohm-m) overlain by a thin conductive layer (2–5 ohm-m) and a thick layer of less conductive crust (5–20 ohm-m), as depicted for station MT27 on the Tesuque (fig. 17) and station MT9 on the Alamo Creek (fig. 22) 2D geophysical profiles. Although the geologic affinity of the conductive layer is ambiguous, as discussed in the section "Other Data," the base of the Santa Fe Group can be no deeper than the top of basal resistive layer, interpreted as Paleozoic rocks. Using this reasoning, the base of the Santa Fe Group lies no lower than 170 m (560 ft) below sea level (depths of 1,500–1,750 m (5,000–5,750 ft)) for the northern two stations on the profile, MT9 and MT27 (appendix 4). Depth picks from a seismic line that comes as close as 3 km (2 mi) east of these MT stations constrain the base of the Santa Fe Group to elevations of about 800 m (2,624 ft) below sea level (a depth of 2,652 m (8,702 ft) for location EW_005 (appendix 4), for example). These constraints suggest that the bedrock high has about 600 m (1,970 ft) of relief in this area. Initial gravity inversion runs, independent of the MT data, also indicated a bedrock high in the area. Subsequently, MT model results at selected stations were used to constrain the gravity model (fig. 9), which gave somewhat better definition to the shape of the high in map view. The shape is still poorly defined owing to poor gravity station coverage (fig. 11). Although the shape of this gravity-derived bedrock high is suspiciously coincident with the Cerros del Rio volcanic field, the MT results are sufficiently compelling to conclude that the underlying cause is in the pre-rift section. This hypothesis is also permissible from the 2D geophysical models of the Tesuque and Alamo Creek profiles (figs. 17 and 22). The geologic configuration of this geophysical feature is interpreted as a west-tilted fault block of pre-rift sedimentary rocks in the 2D geophysical models. Although conjectural, it is consistent with regional geologic considerations. An alternative geologic model, which also fits the geophysical data, consists of an east-tilted block whose fault-bounded face coincides with the west side of the geophysically defined bedrock high.

Although the pre-rift sedimentary rocks are generally invisible to the aeromagnetic data of this study, some parts of the Galisteo Formation may be magnetic. North-south curvilinear magnetic anomalies in the southern part of the area near the Tijeras-Cañoncito fault ("Beds of Galisteo Fm?" on fig. 23*A*) parallel interpreted erosional contacts of the Espinaso Formation (discussed in a later section) and correspond with mapped Galisteo Formation (fig. 23*B*; Lisenbee, 1999). Similar northeast-trending anomalies parallel the Espinaso-Galisteo contact just east of the fault labeled "East-down fault" in figure 23*A*. These anomalies are also evident in the first vertical derivative map (fig. 24*A*). Magnetic depth estimates show clustered solutions (fig. 14*B*) that fall within a depth range that has been interpreted as Galisteo Formation in cross-section (Lisenbee, 1999).

Intrusions

Both positive and negative aeromagnetic anomalies are associated with intrusions and volcanic vents of Tertiary age (fig. 23). The most prominent of these is an area of strong positive anomalies associated with mapped Eocene and Oligocene intrusive rocks in the Cerrillos Hills, which coalesces into one broad positive anomaly on the lowpass-filtered map (fig. 8).

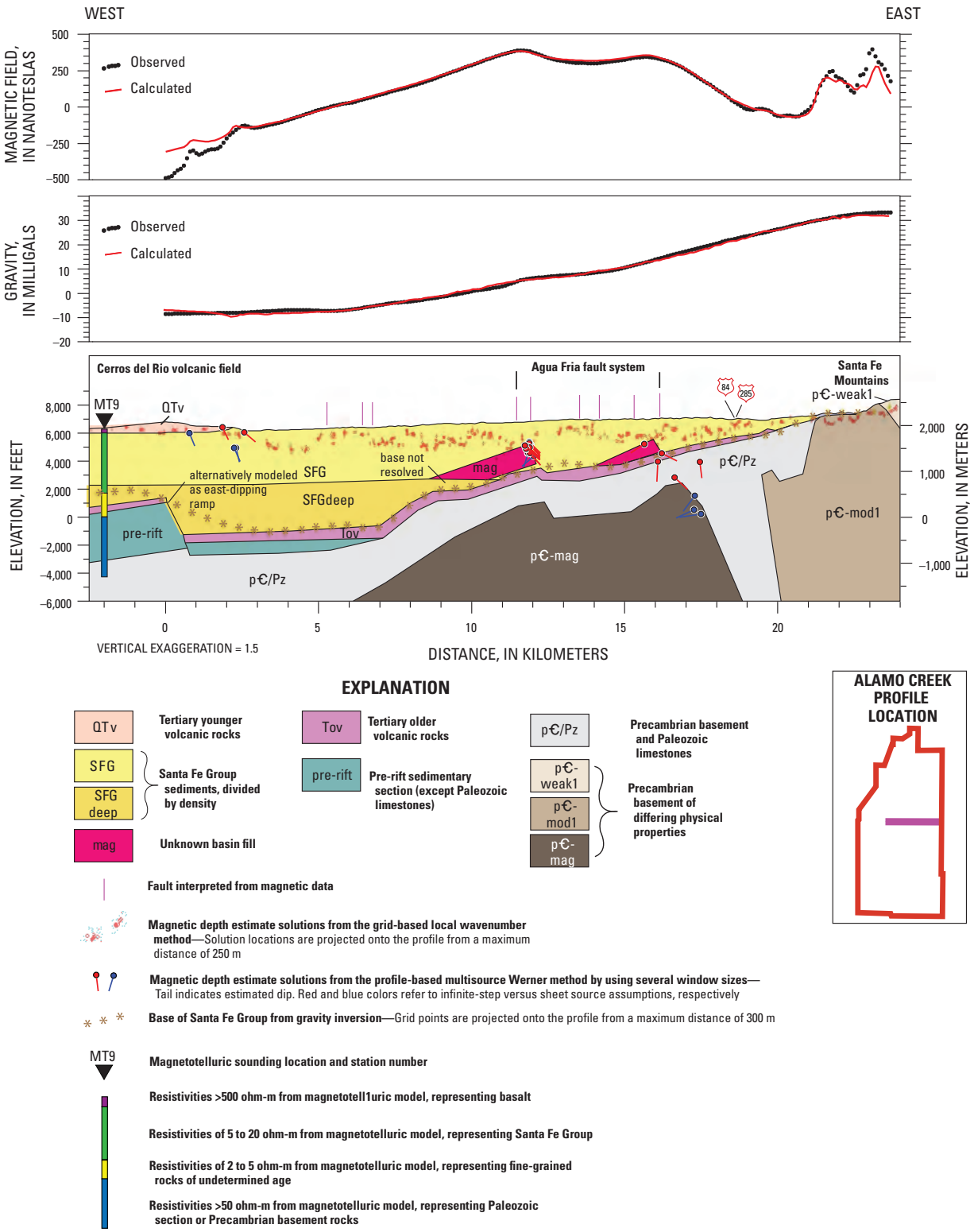

Figure 22. Two-dimensional gravity and magnetic model of the Alamo Creek profile. Model bodies are described in table 3. Profile is located on the inset and on figures 13, 15, and 16. This model demonstrates well-clustered magnetic depth estimates (from profile and grid-based methods) and modeling that requires magnetic material at shallow depths related to the Agua Fria fault system. Using other geophysical constraints, the magnetic sources must be within the basin fill. The grid-based magnetic depth solutions (small red points) locate multiple magnetic sources within the Santa Fe Group. Faults interpreted from the aeromagnetic map correspond with abrupt level shifts. The bedrock high on the west can be alternatively modeled as an east-dipping ramp. The horizontal division between unit SFG and unit SFGdeep is a density boundary, not a geologic contact.

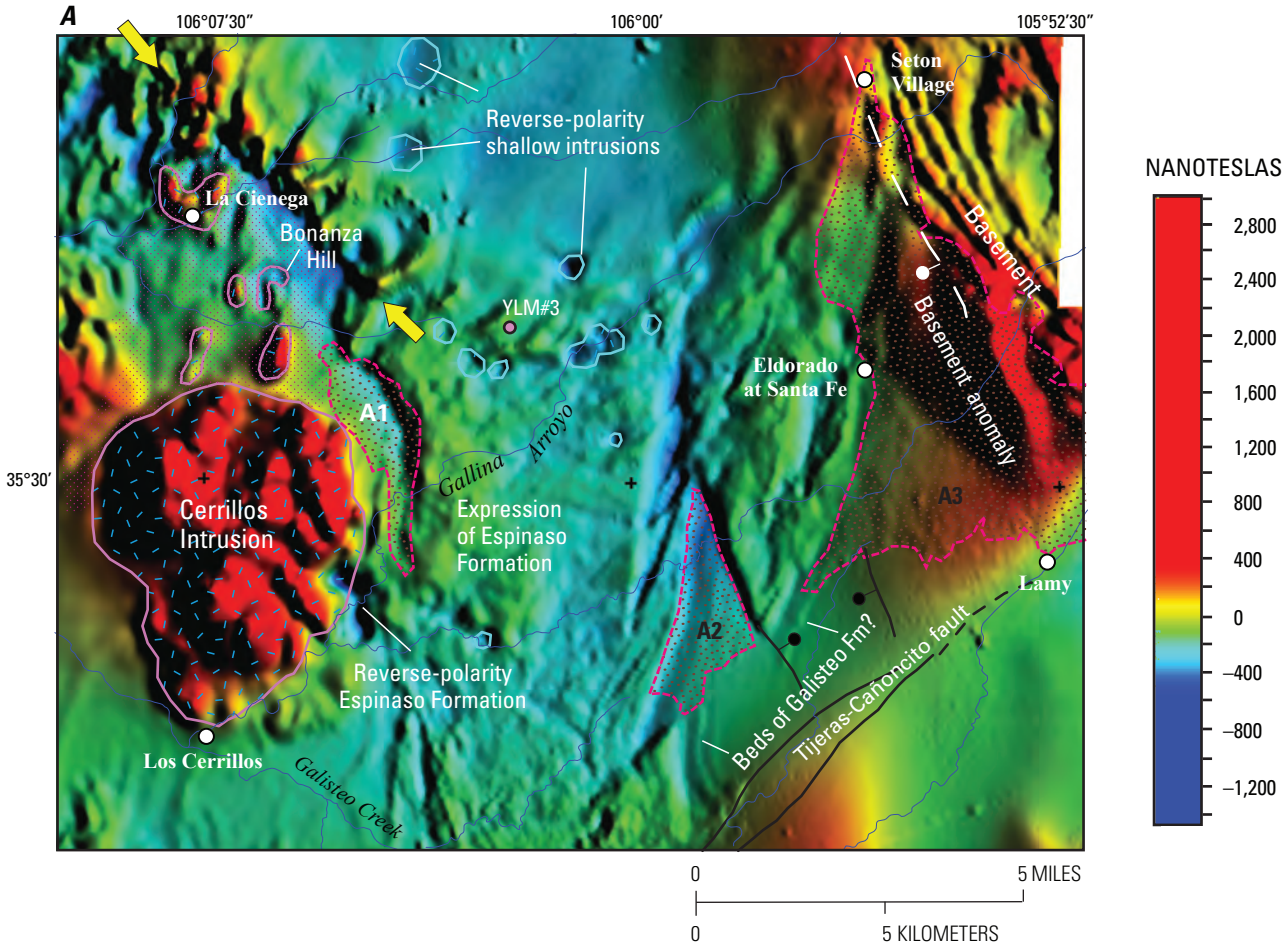

EXPLANATION

- Interpreted intrusive body associated with Cerrillos intrusion
- Interpreted volcanic vent associated with Espinaso Formation
- A2 — Absence of Tertiary older volcanic rocks interpreted from aeromagnetic data. Labels refer to discussion in text
- Area difficult to interpret because both intrusive and volcanic rocks are present
- Qal — Quaternary valley-fill alluvium and landslides
- QTsf — Plio-Pleistocene Santa Fe Group sediments (Ancha Formation, Tuerto Gravel)
- QTv — Plio-Pleistocene basalts and andesites of the Cerros del Rio Volcanic field
- Tomv — Early Tertiary mafic volcanic rocks (Cieneguilla volcanic complex and undivided)
- Te — Late Eocene-Oligocene Espinaso Formation
- Ti — Late Eocene and Oligocene intrusive rocks
- Tgd — Late Paleocene and Eocene clastic rocks of the Galisteo and Diamond Tail Formations
- MzPzu — Mesozoic-Paleozoic clastic sedimentary rocks, undivided
- p€ — Precambrian basement rocks, undivided
- Representative fault within Agua Fria fault system—Used in three-dimensional model
- Magnetic unit inferred within Galisteo Formation
- —1000— Isopach of modeled thickness of Tertiary older volcanic rocks—Contour interval = 100 feet
- Arrow indicating aeromagnetic ridge
- Fault mapped from surface geology—Ball on downthrown side
- Fault inferred from geophysics (Speigel and Baldwin, 1963)—Ball on downthrown side
- Espinaso Formation or Cieneguilla volcanic rocks present in well below Santa Fe Group
- Espinaso Formation absent in well—Santa Fe Group overlies pre-rift rocks (see plate 2)
- Town

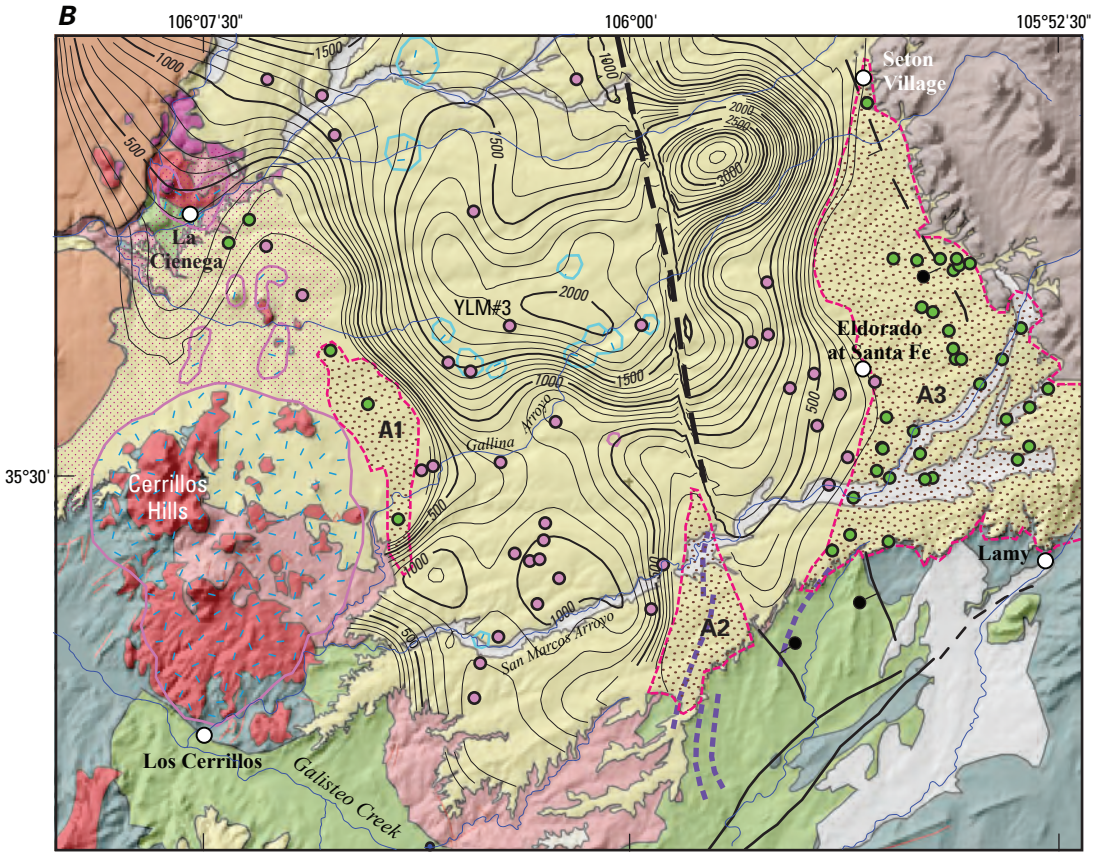

Figure 23 (facing page and above). Closeup of southern part of study area showing interpretations of intrusions and older volcanic rocks. *A*, Aeromagnetic data (from fig. 5) with interpreted intrusions and areas lacking Espinaso Formation superimposed. *B*, Geology from figure 3 underlain by shaded digital elevation model. Interpreted intrusions and isopach contours of Tertiary older volcanic rocks from three-dimensional model are also shown. Areas of missing Espinaso Formation are indicated in three main areas from west to east (A1, A2, A3). Lithologic information provided after interpretation from wells drilled in the A1 and A3 areas correspond well with interpretations.

Geophysical modeling suggests that there are several sources on the basis of their densities and magnetic properties (Grauch and others, 2006). The physical-property differences may arise from the variable composition and petrology of intrusive rocks of various ages, which have been documented by geologic mapping (Maynard and others, 2002). Steep magnetic gradients on all but the western side of the area of positive anomalies suggest that the bulk of the intrusive complex is contained within a volume having nearly vertical sides for most of its perimeter. The maxima of the horizontal-gradient magnitude of both the reduced-to-pole magnetic data and pseudogravity form the basis for the interpreted outline (figs. 23 and 24). The roots of the intrusion extend to great depths, inferred from its prominent expression in both of the anomaly-separation maps (figs. 7 and 8). Steep sides indicated by the geophysical data pose an apparent conflict with the laccolithic nature of the intrusion indicated by geologic mapping and boreholes (Grant, 1999; Maynard and others, 2002). However, the discrepancy can be explained by one or more of several factors that do not preclude the presence of sills: (1) sills are generally thin and do not have sufficient volume to produce magnetic anomalies; (2) sills are uniformly horizontal and thin gradually so that they do not produce lateral magnetic contrasts; and (3) sill rocks may not be magnetic enough to produce pronounced aeromagnetic anomalies, especially where they underlie the magnetic Espinaso Formation. Separation of anomalies by geologic unit is ambiguous in the area between La Cienega and the Cerrillos Hills owing to geologic complexity, the possibility that magnetic volcanic and intrusive rocks are superposed, and the presence of Espinaso Formation that is weakly magnetic (Phillips and Grauch, 2004).

Despite difficulties in interpretation in this area, most strong positive anomalies surrounding the Cerrillos Hills appear to be related to the intrusive complex. An exception is

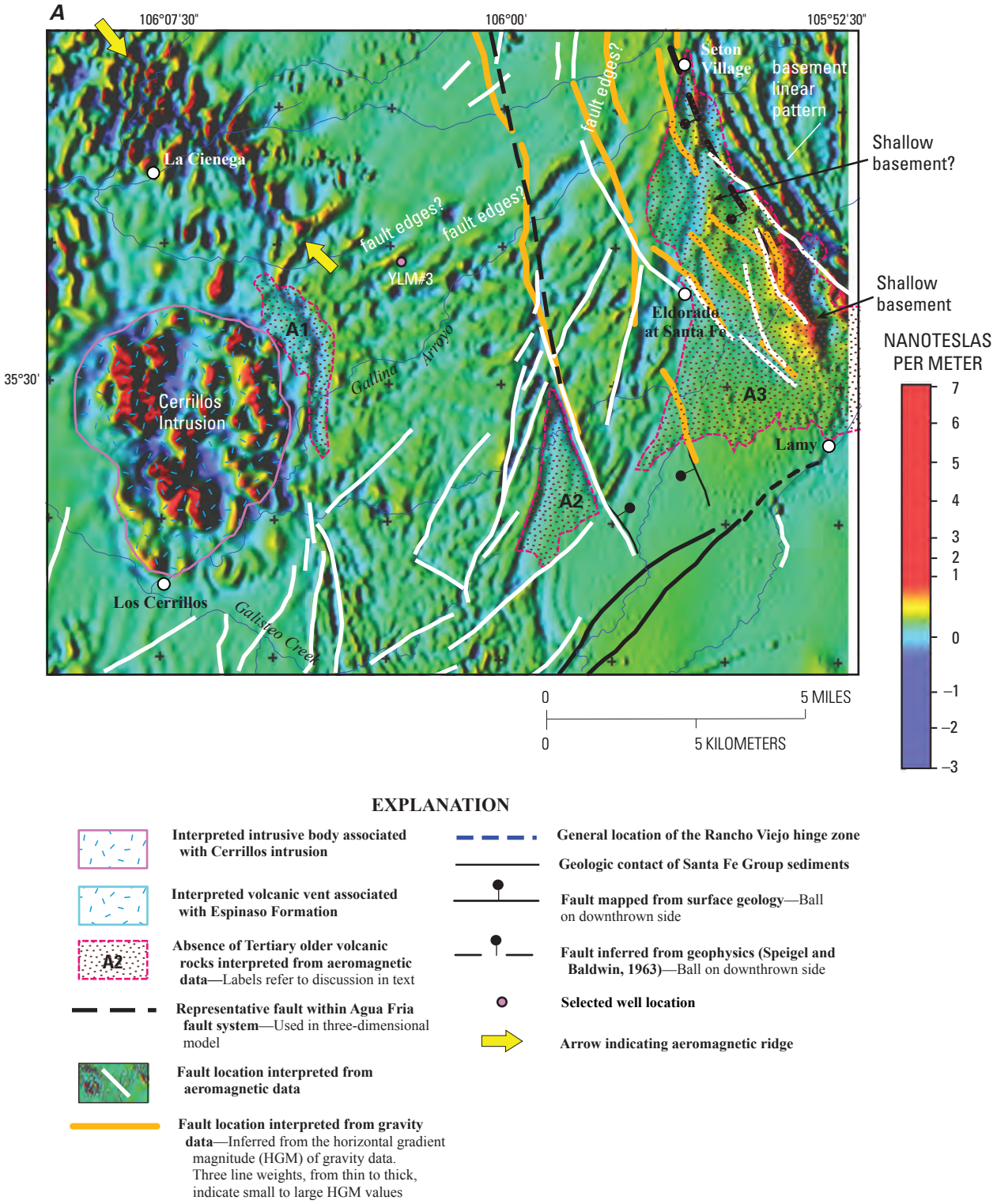

Figure 24 (above and facing page). Closeup of southern part of study area showing faults, detailed anomalies, and thickness of fill on the Santa Fe platform. *A*, First vertical derivative (a different display than in fig. 7) showing linear patterns and interpreted faults (from horizontal-gradient magnitude maps). Image is color shaded-relief illuminated from the west. *B*, Isopach map of thickness of Santa Fe Group from three-dimensional model, with superimposed interpreted faults and intrusions (fig. 23), and shaded digital elevation model in areas where the three-dimensional model is not applicable.

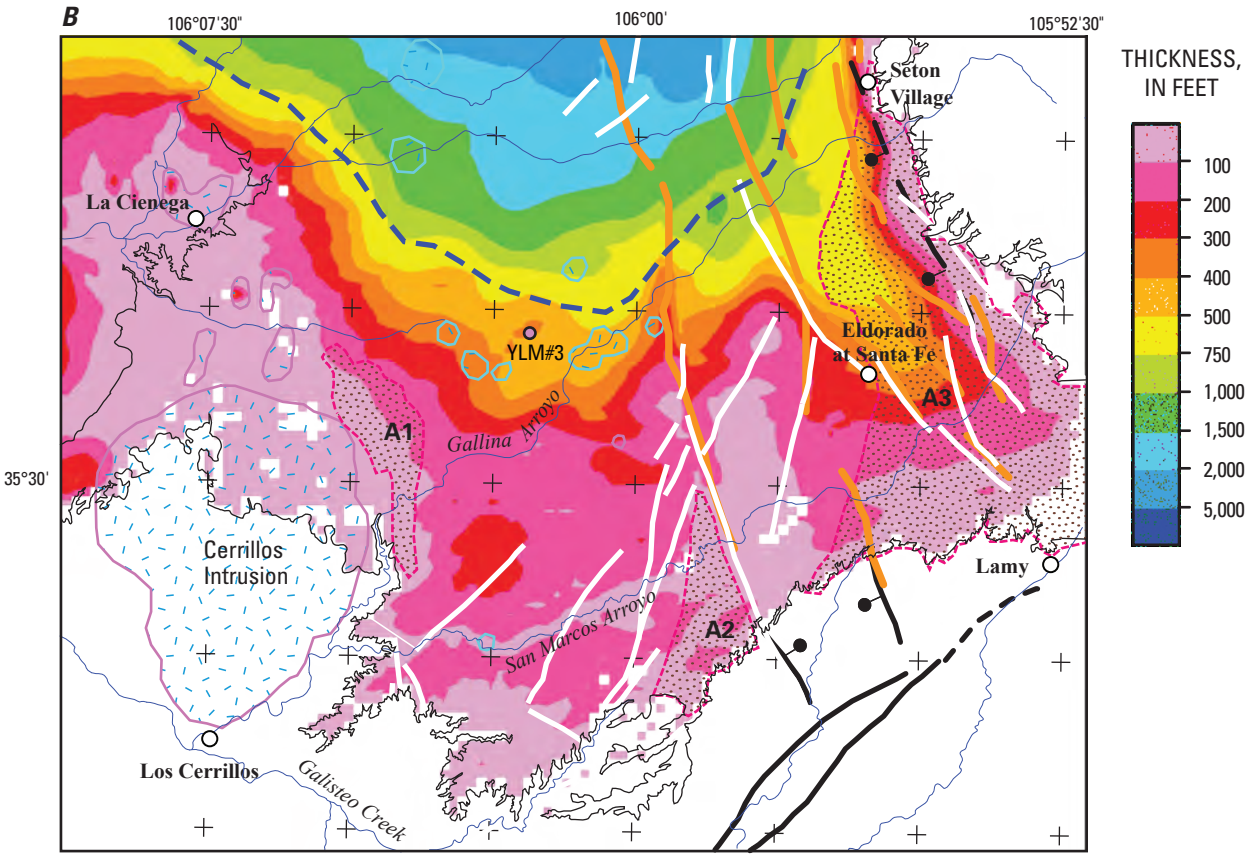

the negative anomaly that corresponds in part with Bonanza Hill (fig. 23*A*), where Oligocene hornblende monzonite is mapped (Koning and Hallett, 2001). This rock unit may have been emplaced during a reversal of Earth's magnetic field. Observation of both positive and negative aeromagnetic anomalies associated with the Cerrillos Hills intrusive complex is consistent with paleomagnetic measurements, which record both normal and reverse polarities (Stephen Harlan, George Mason University, written commun., 2008).

Smaller intrusions that served as vents for volcanoes or cinder cones are commonly associated with local, circular, high-amplitude magnetic anomalies, generally less than 1.6 km (1 mi) in diameter, that can be can be either positive or negative. Examples of these circular magnetic anomalies are abundant in the Plio-Pleistocene Cerros del Rio volcanic field where vents are exposed (Grauch and others, 2006). The positive or negative character of the anomalies indicate strong normal- or reverse-polarity remanent magnetization, respectively, that can be tied generally to different eruption episodes (Thompson and others, 2006; fig. 4). Examples of negative anomalies associated with exposed middle- or late-phase vents, inferred as having reverse-polarity remanent magnetization, are located at the northeastern end of the Cerros del Rio field (fig. 15; pl. 1). An exposed vent associated with a positive anomaly 6.4 km (4 mi) north of La Cienega formed during the early eruptive phase (fig. 15; anomaly E8 of Grauch and others, 2006). The number of anomalies in the Cerros del Rio that are caused by volcanic vents are too numerous to distinguish for this study. Therefore, they are indicated collectively except for several isolated ones near the margin of the volcanic field, such as the ones just mentioned.

Many negative circular anomalies, similar in character to the ones associated with exposed volcanic vents, have sources that are buried under mapped Santa Fe Group in the southern part of the study area (fig. 23). Some of the anomalies appear broader and more diffuse than those observed over exposed vents because of their greater depth (Grauch and Bankey, 2003). We interpret the sources of these anomalies as volcanic vents on the basis of the nature of the circular anomalies. We infer that they are associated with Eocene-Oligocene magmatic activity because magnetic depth estimation indicates that the sources of the inferred vents are located within the more-or-less horizontally layered Eocene-Oligocene Espinaso Formation, discussed in the following section.

Part of the elliptical negative magnetic anomaly in Gallina Arroyo, located about 2 km east of the Yates La Mesa #3 well (fig. 23*A*), was interpreted previously as an intrusion that coincides with a ground-water high (Spiegel and Baldwin, 1963).

Older Volcanic Rocks

Older volcanic rocks are considered as a package; they contain the Espinaso Formation, overlying Cieneguilla volcanic complex, and any intervening sediments, as described in the section Geologic Setting. They are considered a package because the volcanic units closely overlie one another and are expected to have similar densities on the basis of their rock type. This similarity makes them difficult to distinguish by using aeromagnetic or gravity data.

Where exposed southeast of the Cerrillos intrusion, the Espinaso Formation corresponds with a distinctive mottled pattern on the aeromagnetic map interrupted by negative circular anomalies, mentioned previously ("Expression of Espinaso Formation" on fig. 23*A*). The mottled pattern can be followed throughout an extensive area between the Cerrillos Hills and Eldorado at Santa Fe, implying that the Espinaso Formation extends into this area underneath mapped Santa Fe Group (fig 23*B*). Measurements of magnetic susceptibility on a few typical hand samples and outcrops of Espinaso Formation give high values (0.01–0.03 (SI), fig. 4), which result in induced magnetizations of about 0.4–1.2 A/m (assuming an inducing Earth field of 51,715 nanoteslas (nT)). In a recent paleomagnetic study of breccias in the Espinaso Formation (Stephen Harlan, George Mason University, written commun., 2008), reverse-polarity remanent directions were established for a few sites, and a wide range of natural remanent magnetizations were measured overall (0.027–7.21 A/m). Comparing these ranges of remanent and induced magnetizations suggests that a reverse-polarity remanent component may dominate the induced component in some areas and that the opposite may be the case in other areas. Thus, an amalgamation of these sources would produce highly variable anomalies consistent with the observed aeromagnetic pattern, which ranges from strongly negative (dominant remanent magnetization) to moderately positive (dominant induced magnetization). One irregularly shaped local negative anomaly is located in the area of exposed Espinaso Formation on the southeast side of the Cerrillos intrusion (fig. 23*A*). This anomaly may indicate a local area of the Espinaso Formation where the reverse-polarity remanent component exceeds the magnitude of the induced component. If the entire thickness of the Espinaso Formation is considered, detailed examination of the magnetic depth estimates suggests that magnetic-property differences may locally occur at subhorizontal interfaces (fig. 14), perhaps related to layering of the deposits. Recognition of this internal layering helped resolve problems with interpreting the magnetic depth estimates, as discussed in a previous section.

None of the circular negative anomalies within the area of the mottled anomaly pattern mentioned in the previous section occur where the Espinaso Formation is exposed. However, the few sites in the paleomagnetic study yielding well-grouped remanent magnetizations were collected from small-volume, near-vent pyroclastic flows. This association supports the interpretation that the circular negative magnetic anomalies are associated with vents.

In contrast to the Espinaso Formation, Cieneguilla volcanic rocks are associated with strong local positive anomalies where they are exposed 1 km (0.625 mi) north of La Cienega (Grauch and Bankey, 2003; fig. 23), which suggests that they will produce positive anomalies elsewhere. Similar strong positive anomalies extend southeast from the area of exposed rocks towards the Yates La Mesa #3 well as patterns of northeast-directed linear anomalies that are truncated along a northwest-southeast aeromagnetic ridge (fig. 23*A*). The truncation is interpreted as a concealed contact between Tertiary older volcanic rocks on the northeast against an area of mixed rock types on the southwest (pl. 2). Additional northeast-directed linear anomalies, parallel to each other and more subdued in amplitude, are apparent in an east-west swath including the Yates La Mesa #3 well (labeled "fault edges?" on fig. 24*A*). Grauch and Bankey (2003) interpreted these anomalies to be caused by paleochannels filled with basalt. An alternate hypothesis is that they represent upturned edges of fault blocks of the older volcanic rocks. Examination of the seismic data supports the latter interpretation. Upturned fault blocks of Espinaso Formation with strong, reverse-polarity remanent magnetization may also be the source of linear negative anomalies farther east near Eldorado at Santa Fe.

The unique aeromagnetic patterns associated with the Tertiary older volcanic rocks provided guides for outlining their lateral extents in the integrated 3D model. In the southern part of the study area, most of the lateral limits of the older volcanic rocks were determined from the termination of aeromagnetic patterns (fig. 23). Magnetic depth solutions were used as far as 4 km (6.4 mi) north of Yates La Mesa #3 well to trace the top of the volcanic package as it plunges to the north. North of this, modeling of the volcanic rocks relied on extrapolation of widely separated information from wells and seismic-reflection depth picks (John Ferguson, University of Texas at Dallas, written commun., 2007). The volcanic surface forms a shallow but irregular platform in the area of mottled aeromagnetic pattern (fig. 23*A*), consistent with erosion before deposition of the Ancha Formation. This surface is discussed in more detail in the following section because it also represents the base of the Santa Fe Group in this area.

In contrast to the top surface, the modeled base of the Tertiary older volcanic section is folded (fig 21*A, B*). The modeled top and base of the Tertiary older volcanic rocks were subtracted to construct an isopach map of modeled thickness (fig. 23*B*). The folding of the base of the older volcanic rocks is well reflected in the patterns of thinning and thickening of the isopach map, such as the two areas of >300 m (1,000 ft) thickness between San Marcos and Gallina Arroyos. The isopach map is consistent with maximum thicknesses in the range of 250–580 m (820–1,900 ft), which have been determined

in various areas from geologic mapping and the Yates La Mesa wells (Lisenbee, 1999; Myer and Smith, 2006; David Sawyer, U.S. Geological Survey, and Daniel Koning, New Mexico Bureau of Geology and Mineral Resources, written commun., 2008).

In the southern part of the study area, where the mottled aeromagnetic pattern is associated with the Espinaso Formation, both the isopach map and aeromagnetic patterns indicate that the Espinaso Formation is notably absent in three large areas (A1–A3, fig. 23), first recognized by Grauch and Bankey (2003). In these areas, Santa Fe Group sediments likely rest directly on pre-rift sedimentary rocks. Interpretations of the geologic units that directly underlie the Santa Fe Group throughout the study area are depicted in plate 2 (CD in pocket and downloadable from the U.S. Geological Survey Web site) and are discussed next.

In the western area (A1) on the northeast side of the Cerrillos intrusion, Santa Fe Group sediments likely overlie Galisteo Formation, on the basis of data from three wells located in the area of A1 (fig. 23*B*; pl. 2). Northwest of area A1, the underlying geologic unit is unclear. In the area surrounding Bonanza Hill (fig. 23*A*), wells intersect shallow Espinaso Formation but aeromagnetic anomalies lack the characteristic patterns of this formation. Where anomalies exist, the preponderance of Cerrillos intrusive rocks makes interpretation ambiguous.

In the second area (A2), which is recessed into the region of volcanic rocks just southeast of 35°30' N., 106° W., Ancha Formation likely overlies west-dipping Galisteo Formation, on the basis of geologic map relations exposed to the south (Lisenbee, 1999; pl. 1). The east side of this area is defined by an east-down fault on the basis of its alignment with a mapped fault that juxtaposes Espinaso Formation against Galisteo and various strata within the Galisteo Formation (fig. 23; Lisenbee, 1999). This fault and its northern extension defined by the aeromagnetic data form the west side of the Agua Fria fault system, discussed in a following section. The western side of the area (A2) is interpreted as an erosionally truncated contact between the Espinaso and underlying Galisteo Formations, which was buried subsequently by the Ancha Formation, on the basis of comparisons with geologic map relations of Lisenbee (1999). Thus, the area of missing Espinaso Formation appears to be the result of relative footwall uplift along the east-down fault, followed by erosion that locally removed the cap of Espinaso Formation volcaniclastic and volcanic rocks on the footwall. These relations are well developed in the 3D model, which are apparent in cross section (fig. 21*A*) and in the isopach map of the modeled thickness of the volcanic section (fig. 23*B*).

The third and largest area devoid of Espinaso Formation on the east (A3) extends as an irregular triangle covering much of the community of Eldorado at Santa Fe (fig. 23). Grauch and Bankey (2003) recognized most of this area previously but were hindered on the eastern side by the limit of the earlier aeromagnetic coverage. Subsequent to that study, information compiled from local water wells confirmed the absence of the Espinaso Formation (fig. 23*B*). With the addition of the Santa Fe East survey in 2005 (fig. 5), the full area of missing Espinaso Formation is now apparent. It is shaped as an irregular triangle with the apex near Seton Village (fig. 23). Aeromagnetic interpretations combined with strike and dip measurements from isolated exposures of the Espinaso Formation (Lisenbee, 1999; pl. 1) suggest that the western edge of area A3 is the eastern limit of the Tertiary older volcanic rocks. The limit is represented primarily by the erosional edge of dipping Espinaso Formation, analogous to the western side of the triangular area A2. The western edge of A3 bulges to the west just north of latitude 35°32'30", which aligns with the prominent ridge of a strong basement-related anomaly ("basement anomaly" on fig. 23*A*). The southwestern side of this basement anomaly corresponds with aeromagnetic and gravity gradients that are interpreted as a major down-to-the-west fault, on the basis of examination of seismic-reflection data to the south. The northwestward continuation of this fault likely accounts for the southwestern side of the bulge.

Near the northern apex of the triangular area (A3), linear anomalies characteristic of Tertiary older volcanic rocks come together with the linear anomalies caused by basement rocks, leading to some ambiguities in interpretation. North of Seton Village and the northern apex of area A3, these two rock types are nearly superposed; the older volcanic rocks rest only on a thin layer of Galisteo Formation that directly overlies basement rocks in Arroyo Hondo, about 2.4 km (1.5 miles) north of Seton Village (just off figure 23*A*) (Read and others, 2005). Despite this ambiguity, the strong linear anomaly that extends 2 km (1.25 mi) southward from Seton Village is interpreted as a basement related-anomaly. Even though its north-south trend differs from the northwesterly trends of the linear basement-related anomalies in the neighboring mountain front to the east, its strong amplitude is more similar to amplitudes of basement-related anomalies than to amplitudes of older volcanic rocks to the west. Another isolated linear anomaly within area A3 is more enigmatic. It has a north-south trend, is located about 5 km (3.1 mi) south of Seton Village, and is mostly evident in the first vertical derivative map ("shallow basement?" on fig. 24*A*). Magnetic depth estimates in this area show sources that are clearly within the pre-rift section (fig. 14*A*).

The older volcanic rocks thicken markedly near Yates La Mesa #3 well; the thickening is constrained by this and other wells in the area and is evident in the isopach map (fig. 23*B*). The bulk of the thickened section is due to increased thickness of the Espinaso Formation, which is 575 m (1,890 ft) thick in the Yates La Mesa #3 well and underlies 23 m (77 ft) of Cieneguilla volcanic rocks (David Sawyer, U.S. Geological Survey, and Daniel Koning, New Mexico Bureau of Geology and Mineral Resources, written commun., 2008). The Cieneguilla volcanic rocks thicken to the north and northwest, where they have a maximum thickness of 200 m (660 ft) in a limited area of exposure just north of La Cienega (fig. 23*B*; Sawyer and others, 2002). They are about 300 m (1,000 ft)

thick above a similar thickness of Espinaso Formation in the Yates La Mesa #2 well (Myer and Smith, 2006). Several of the negative circular anomalies discussed in the previous section are generally located in the thicker sections of the older volcanic rocks (fig. 23*B*). They are interpreted as volcanic vents synchronous with the Espinaso Formation, as argued in the section on intrusions. Implications of these associations are discussed in the Interpreted Structure section.

Interpreted Elements of Basin Fill

Santa Fe Group Sediments

Santa Fe Group sediments in the Albuquerque and Española Basins produce weak to moderate aeromagnetic anomalies where units of contrasting magnetic susceptibilities are juxtaposed at faults and where they directly underlie irregular topographic surfaces (Grauch and Bankey, 2003; Grauch and Hudson, 2007). Results of detailed magnetic property studies in the northern Albuquerque Basin (Hudson and others, 2008) show that the sediments have magnetic susceptibilities that generally fall between 0.0002 and 0.0050 (SI), and that means are on the order of 0.001–0.003 (SI). The higher values generally correspond with fractions of coarser grain size, especially for stream-deposited sediments. Reconnaissance magnetic susceptibility measurements of Santa Fe Group sediments in the Española Basin suggest they have similar or even higher magnetic susceptibilities (fig. 4). The highest averages (about 0.010 SI) were measured from the Bishops Lodge member of the Tesuque Formation (fig. 18) and the Puye Formation (fig. 15), where both contained considerable volcanic detritus. The moderately high values of lithosome E of the Tesuque Formation (fig. 4) may also be related to its high volcanic content, because it is derived primarily from erosion of the Espinaso Formation and Cieneguilla basanite. However, sediment containing 5–7 percent volcanic lithic grains (basin-floor strata of lithosome B of Cavazza (1986)) has relatively low magnetic susceptibility values that average 0.001 (SI). In comparison, alluvial slope (piedmont slope) sediment of lithosome A of the Tesuque Formation (Cavazza, 1986; Kuhle and Smith, 2001) also averaged on the order of 0.001 (SI), even though lithosome B contains 10 times as much volcanic detritus as lithosome A (as calculated from data presented in Cavazza (1986)). The lack of correlation between volcanic-lithic content and magnetic susceptibility in lithosome B may be explained by volcanic source rocks that are low in magnetic susceptibility. The presumed source area for lithosome B volcanic detritus is the Latir volcanic field, about 25 km (16 mi) north of Taos (fig. 1) and outside the region of study. This volcanic field is associated with moderate- to low-amplitude aeromagnetic anomalies (Grauch and Keller, 2004), consistent with moderate to low magnetizations.

A tentative correlation between grain size and magnetic susceptibility in the Tesuque Formation is suggested by the higher magnetic susceptibility values of the coarse-grained Cuarteles Member compared with those of its finer grained and older lithologic equivalent, lithosome A (fig. 4). However, reconnaissance magnetic-susceptibility measurements of sand- and clay-rich fractions of lithosomes A and B in the northeastern part of the study area showed little correlation with grain size (V.J.S. Grauch, U.S. Geological Survey, and Daniel Koning, New Mexico Bureau of Geology and Mineral Resources, unpub. data, 2007).

Regions where the Santa Fe Group tends toward higher magnetic susceptibilities can be interpreted from the aeromagnetic data where aeromagnetic anomalies correlate with topography, indicating that the material that forms the hills is magnetic (Grauch and others, 2006). An excellent example is located in the northwest part of the aeromagnetic data area, where the aeromagnetic expression looks very similar to topography ("Puye Formation" on fig. 15). The aeromagnetic anomalies correlate better with hills composed of Puye Formation (Kelley, 1978) than with local exposures of overlying Bandelier tuff, indicating that the Puye Formation is the source of the anomalies. Correlation of subtle aeromagnetic anomalies with topography is also evident southwest of Pojoaque (labeled "Faults and magnetic sediments" on fig. 15) in an area generally underlain by Cuarteles Member of the Tesuque Formation (Koning and Maldonado, 2003). The most prominent linear anomalies in this area are interpreted as faults, whereas the more subtle ones correlate with drainages and ridges. Although magnetic-susceptibility has not been measured in this area, analysis of the topographic-magnetic correlation suggests that magnetic susceptibilities may be on the order of 0.010 (SI) in parts of the area.

Two other areas underlain by especially magnetic sediment, as indicated by anomalies that correlate with topography, are located northeast of Highway 84 and 285 where it parallels the Rio Tesuque (pl. 1; "Stream terrace deposits" on fig. 19*B*), and along and north of the Santa Cruz River (pl. 1). The magnetic sediments northeast of the highway may be related to thick Quaternary-Tertiary stream-terrace gravels derived from granitic terrane (Read and others, 2005; Borchert and others, 2003). The magnetic sediment north of the Santa Cruz River, along the northern study area boundary, is probably due to a combined effect of the coarse-grained Cuarteles and Cejita Members of the upper Tesuque Formation and thick Quaternary stream gravels derived from granitic terrane in the Sangre de Cristo Mountains (Koning, 2005a; Koning, Connell, and others, 2005). A third area possibly underlain by magnetic sediments lies within the area devoid of Espinaso Formation near Eldorado at Santa Fe (area A3 on fig. 23*A*). The very subtle mottled pattern in the southern part of the A3 area may be caused by variations in the Ancha Formation, which can be quite magnetic (fig. 4). In contrast, the high-amplitude circular anomalies are caused by buildings and bridges.

The overall thickness of Santa Fe Group sediments was determined by integrating information from all sources during development of the 3D integrated model, as described in the section on model construction. A map showing the elevation

of the base of the Santa Fe Group from the 3D model is shown in figure 25 and plate 1. An isopach map of the thickness, constructed by subtracting the base elevation surface from a regional topographic surface, is shown in figure 26 and plate 2. The overall form of the basin is that of a platform on the south and a west-dipping half-graben on the north. The base of the Santa Fe Group descends precipitously across a faulted, generally curvilinear, hinge zone, which we propose to call the Rancho Viejo hinge zone (fig. 24*B*). This hinge zone wraps to the southeast from 4 km (6.4 mi) north of La Cienega to the area around the Yates La Mesa #3 well, then northeast toward Seton Village. Santa Fe Group sediments thicken markedly northward across the hinge zone at about 130–150 meters per kilometer (m/km) (700–800 feet per mile (ft/mi)). This zone is discussed in more detail in the section Interpreted Structure. The disruptions in the generally north-south contours on the base of the Santa Fe Group (fig. 25), which continue between Eldorado at Santa Fe and Española, are also discussed in the Interpreted Structure section. They are the model depiction of the combined Agua Fria and Barrancos fault systems.

From Santa Fe to the north, the base of the Santa Fe Group dips relatively steeply westward (7°–20°) within 5–10 km (3–6.3 mi) west of the present-day foot of the mountain front (fig. 25), following the geologic map data of Koning, Nyman, and others (2005), Read and others (2005), and Borchert and others (2003). The deepest part of the basin (>3,000 m (10,000 ft)) is in the west-dipping half-graben underneath the Pajarito Plateau west of the Rio Grande. The 3D model depicts this area only in general form owing to poor constraints at depth. The bedrock high under the Cerros del Rio, as discussed in the section on the pre-rift sedimentary section, forms an added north-south complexity to the overall basin picture. Finally, the model predicts thinner Santa Fe Group on the footwall (northwest side) of the Pajarito-Embudo fault system (fig. 26), consistent with interpretations of geophysical data by Baldridge and others (1994) regarding thickness of basin fill near Abiquiu (fig. 1).

The base of the Santa Fe Group on the Santa Fe platform generally appears to undulate from southwest to northeast (figs. 24*B* and 27*B*). In detail the surface is irregular, on the basis of exposures to the south (Maynard and others, 2002) and correlations between neighboring water wells (Koning and Hallett, 2001). The lower parts of the surface appear as elongated connections to the deep basin to the north, suggesting paleovalleys that drained in that direction in the past. Relatively small paleovalleys previously have been interpreted on the basis of water-well lithologic logs (Koning and Hallett, 2001). These small paleovalleys preserve relatively thin (<70 m (230 ft)) Tesuque Formation strata. However, thicker fill modeled in the vicinity of Eldorado at Santa Fe resembles a paleovalley containing about 90–150 m (300–500 ft) of Santa Fe Group sediments (fig. 24*B*). This thicker low-density material is required by the gravity inversion, which is well constrained by the gravity and well data coverage in this area (fig. 9).

To assess the relative thickness of Tesuque Formation and overlying Ancha Formation in the areas modeled as thick Santa Fe Group, we used preliminary lithologic picks from the well data (Peggy Johnson and Daniel Koning, New Mexico Bureau of Geology and Mineral Resources, unpub. data, 2008) in the vicinity of the Rancho Viejo hinge zone (fig. 27). We compared elevation contours for the base of the Ancha Formation constructed from the well data with those of the modeled base of Santa Fe Group (fig. 27). The base of the Ancha Formation generally slopes gently to west-southwest (fig. 27*A*). The gentle slope contrasts with 3D model surface of the base of the Santa Fe Group (fig. 27*B*), which shows much more irregularity, greater relief, and an overall slope to the north. Because the interval between these surfaces is inferred to be Tesuque Formation, the differences suggest that (1) the Tesuque rather than the Ancha Formation accounts for much of the additional thickness of Santa Fe Group within paleovalleys and irregularities on the Santa Fe platform; and (2) considerable tectonic deformation occurred in Miocene to early Pliocene time, the time interval between the deposition of these two formations.

A considerable thickness of Tesuque Formation is thus inferred for the large paleovalley modeled in the vicinity of Eldorado at Santa Fe (fig. 24*B*). This buried paleovalley, identified here for the first time, is located within one of the areas devoid of Espinaso Formation (area A3 on fig. 23*A*) and appears to be bounded by faults inferred from both the aeromagnetic and gravity data (fig. 24*B*). The faults are all interpreted as down-to-the-west on the basis of independent information (pl. 1), which is unexpected for a paleovalley within a fault-bounded graben. An alternative explanation is that the block between the west-down faults was eroded of its cap of Espinaso Formation after faulting and that the softer pre-rift sedimentary section was exposed. Further erosion created the paleovalley, which was then backfilled by the Tesuque Formation. If this scenario is correct, the faulting, erosion, and backfilling must have occurred largely in Miocene time, to account for events that postdate the deposition of the Espinaso Formation and predate the termination of aggradation of the Tesuque Formation. Afterwards, the Ancha Formation was deposited over the erosional unconformity in Pliocene to early Pleistocene time.

The 3D modeled base of the Santa Fe Group surface was also used to investigate stratigraphic and structural relations just north of the Rancho Viejo hinge zone. Stratigraphic correlations of marker beds within the lower Tesuque Formation between three neighboring wells (fig. 27) give an estimated strike and dip of N. 95° E. and 8° N., respectively (Koning, Read, and others, 2006). This orientation is similar to that of the modeled base of Santa Fe Group, if one allows for discrepancies caused by local differences in the strike of the modeled surface in the vicinity of the wells (fig. 27*B*). Because the modeled surface in this area represents the top of the basin floor that is likely composed of Cieneguilla volcanic rocks, the similar dips imply that (1) little deformation occurred between the time that the Cieneguilla rocks and the lower Tesuque Formation

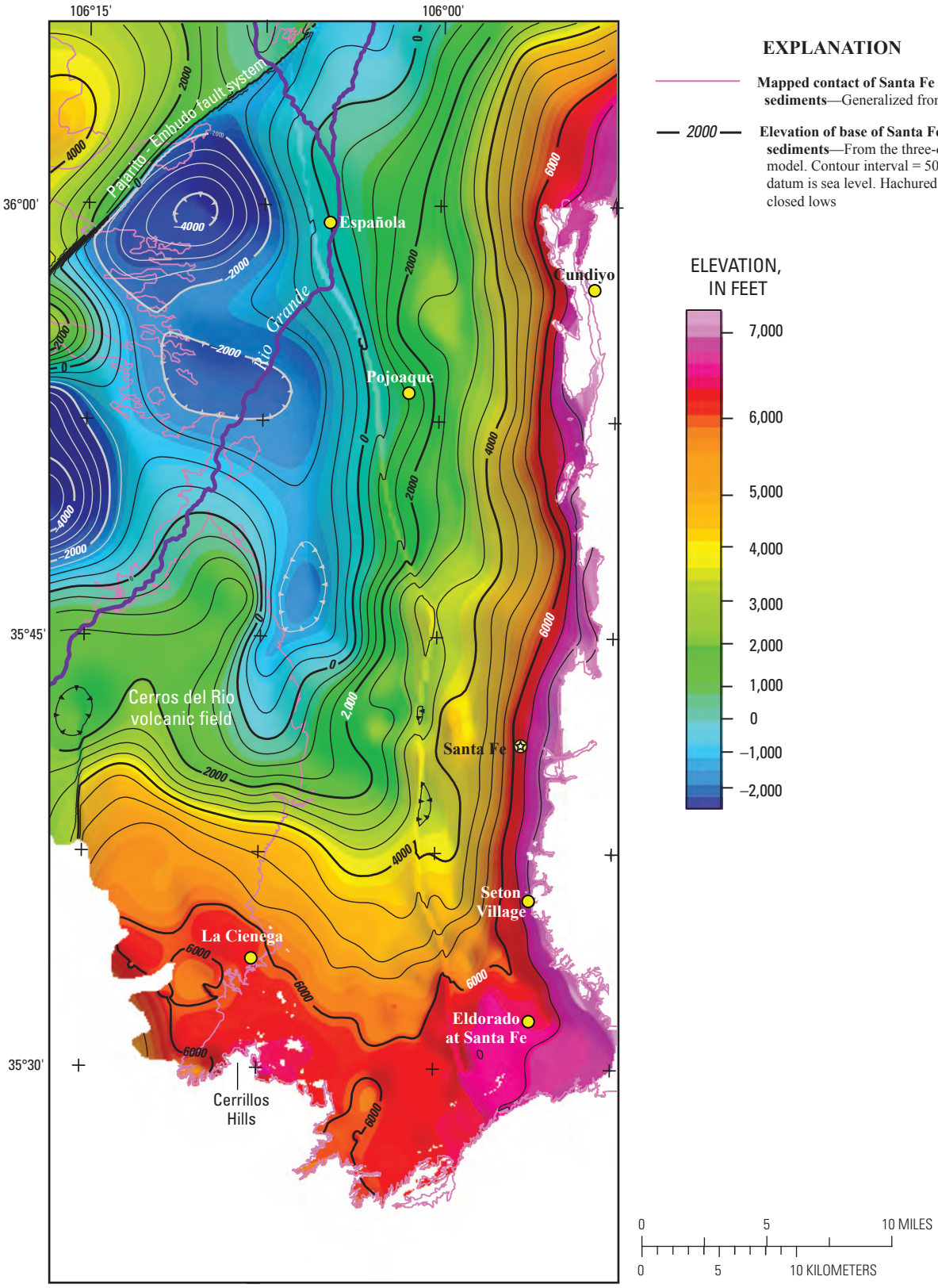

Figure 25. Elevation of base of the Santa Fe Group from three-dimensional model. The surface is displayed by contours (fixed interval of 500 ft), colors (stretched display), and shading (illumination from the northeast) in order to capture details of the shallow section as well as regional trends.

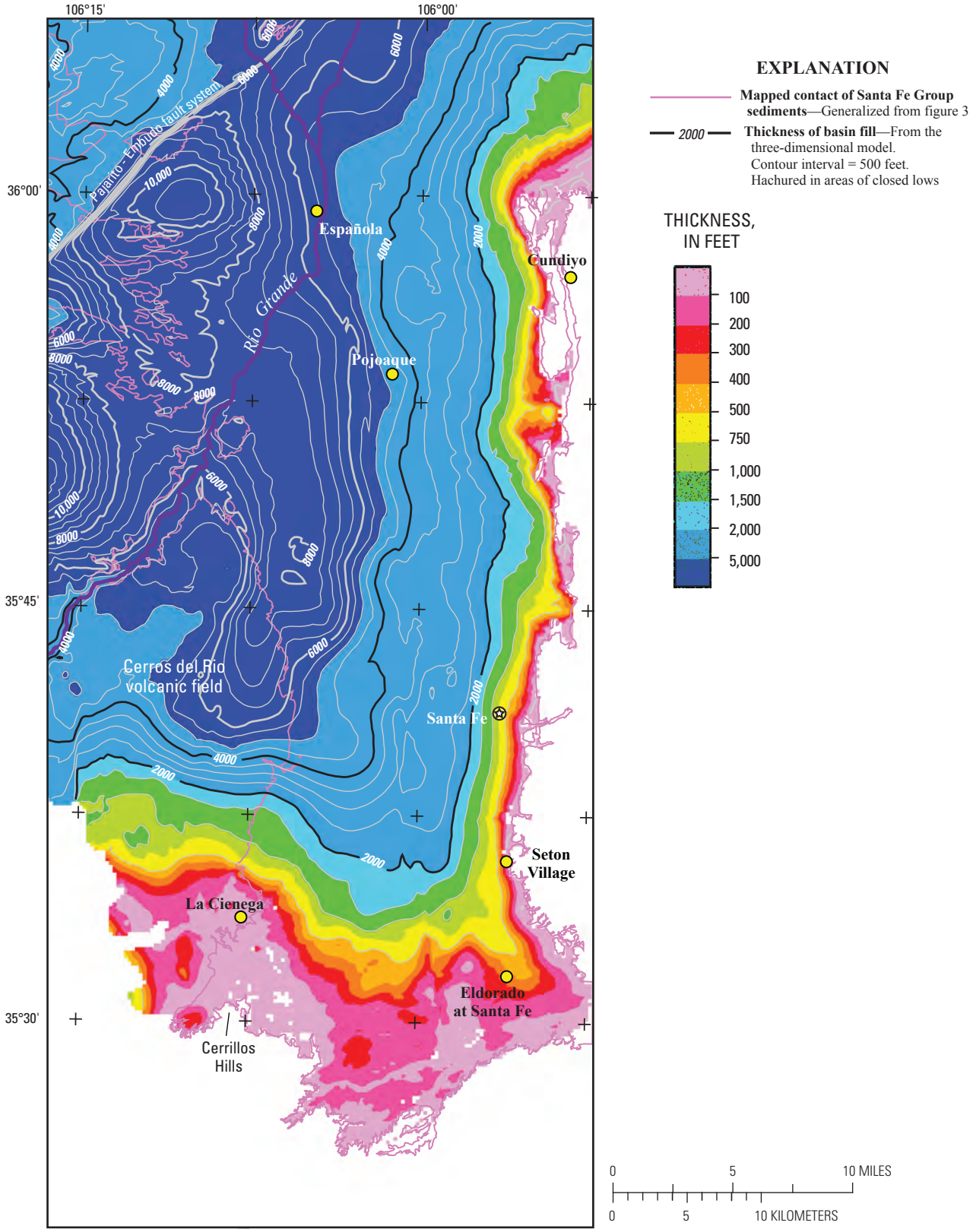

Figure 26. Isopach map of thickness of Santa Fe Group from three-dimensional model. Detailed irregularities in the thickness map likely due to variations in the topographic surface and may not be important. The surface is displayed by contours (fixed interval of 500 ft), and colors (stretched display) to capture details of the shallow section as well as regional trends.

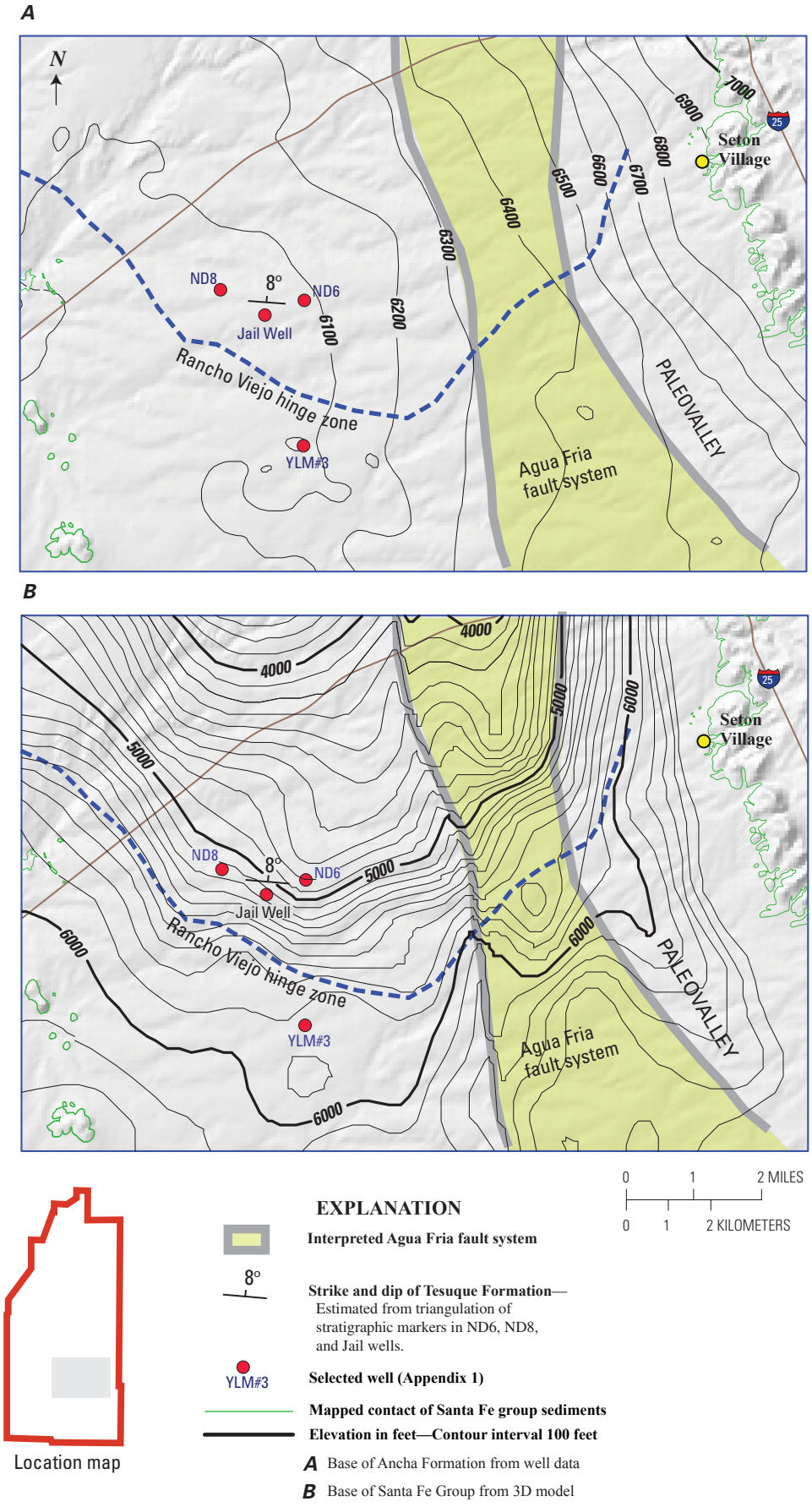
A
N
7000
6900
6800
6700
6600
6500
6400
6300
6200
6100
Seton Village
25
ND8
8°
ND6
Jail Well
Rancho Viejo hinge zone
YLM#3
Agua Fria fault system
PALEOVALLEY
B
4000
5000
6000
Seton Village
25
ND8
8°
ND6
Jail Well
Rancho Viejo hinge zone
YLM#3
Agua Fria fault system
PALEOVALLEY
0 1 2 MILES
0 1 2 KILOMETERS
EXPLANATION
Interpreted Agua Fria fault system
8°
Strike and dip of Tesuque Formation—Estimated from triangulation of stratigraphic markers in ND6, ND8, and Jail wells.
YLM#3
Selected well (Appendix 1)
Mapped contact of Santa Fe group sediments
Elevation in feet—Contour interval 100 feet
A Base of Ancha Formation from well data
B Base of Santa Fe Group from 3D model
Location map

were deposited, and (2) the basin floor to the north was tilted after deposition of the lower Tesuque Formation. Moreover, the base of the Ancha Formation dips gently to the southwest above the steeper northward dip of the lower Tesuque Formation in the vicinity of the three wells (fig. 27*A*). This contrast implies that northward tilting had ceased before deposition of the Ancha Formation in Pliocene time.

Younger Volcanic Rocks

Where exposed, the Cerros del Rio basaltic rocks are very magnetic, as shown by the high-amplitude magnetic anomalies that correlate with topographic contours and mapped flow contacts (Grauch and others, 2006). Paleomagnetic and rock-property measurements indicate that the magnetizations of these rocks are generally dominated by strong remanent magnetization having both normal and reverse orientations with respect to the present Earth's magnetic field, depending on the age of formation (Thompson and others, 2006). The normal and reverse orientations of the strong remanent magnetizations give rise to the positive and negative anomalies, respectively.

Because of the associated strong magnetic anomalies, the lateral extent of the Cerros del Rio volcanic field can be readily distinguished from Santa Fe Group sediments. This distinction is important for recognizing areas where Plio-Pleistocene Ancha Formation of the Santa Fe Group locally covers basalts in the southern part of the study area (fig. 3; Read and others, 2005). The eastern and southwestern limits of the volcanic field, as interpreted from aeromagnetic data, are shown on plate 1. The interpreted limits were determined from visual inspection of the aeromagnetic patterns and the local maxima of horizontal-gradient magnitudes to determine the edges (Grauch and Bankey, 2003). The interpretation is approximate between La Cienega and the Cerrillos Hills, owing to ambiguities caused by older igneous rocks that are also magnetic, as discussed previously. The aeromagnetically determined lateral extent of the Cerros del Rio volcanic field closely approximates geologically mapped contacts (pl. 1) except along the eastern margin of the field near the center of the study area, directly west of downtown Santa Fe. Here the busy aeromagnetic pattern extends about 1 km (0.625 mi) east of the mapped contact on the west side of the Agua Fria quadrangle (Shroba and others, 2005) at about 35°42'30" ("basalt under sediment" on fig. 15). The aeromagnetic pattern and mapped geology indicate that Ancha Formation overlies basalt in this area.

Figure 27 (facing page). Base of Ancha Formation compared with base of underlying Tesuque Formation in southern part of study area. *A*, Elevation contours on the base of Ancha Formation derived from numerous wells in the area (Peggy Johnson, unpub. data, 2008). *B*, Elevation contours on the base of the Tesuque Formation from three-dimensional model surface. Strike and dip from well data are from Koning, Read, and others (2006).

The aeromagnetic data can also be used to estimate general areas of thin basalt (estimated at less than about 50 m (160 ft)). These areas (pl. 1) are derived from previous interpretations (Grauch and Bankey, 2003). These authors used two analytic methods to locate magnetic sources that are mathematically best represented as sheets (structural index N=1): the profile-based local wavenumber method (Thurston and Smith, 1997) and the grid-based horizontal-gradient method applied to both reduced-to-pole magnetic data and pseudogravity (Phillips, 2000). A predominance of sheet sources suggests that the basalts are much thinner than the observation height of 100 m (330 ft). Thin basalt determined in this way surrounds the intrusion north of Buckman (pl. 1), consistent with mapping by Dethier (1997).

In contrast to the areas of thin basalt, a large area of the volcanic field contains many exposed vents and intrusions (pl. 1; Thompson and others, 2006), which are too numerous to distinguish within the scope of this report. MT soundings inside this area indicate that the total basalt thickness is typically about 200–225 m (660–740 ft; Rodriguez and others, 2006). Thus, areas of the volcanic field on plate 1 that are not designated as either vent area or as thin basalt presumably contain basalts that are 50–200 m (160–660 ft) thick.

The Bandelier Tuff represents exposures of Jemez volcanic rocks in the study area, located northwest of the Cerros del Rio volcanic field and west of the Rio Grande (fig. 3). These exposures do not produce prominent aeromagnetic anomalies, implying the Bandelier Tuff is only weakly magnetic in this area. The lack of anomalies is evident where the aeromagnetic pattern associated with the magnetic sediments of the Puye Formation appears uninterrupted (fig. 15), even though exposures of overlying Bandelier Tuff are present. However, the Bandelier Tuff is inferred to cause strong negative anomalies where it lies within the Valles caldera (Grauch and others, 2006).

Interpreted Structure

Faults that juxtapose Santa Fe Group units of differing magnetic properties in the Española Basin are generally expressed as linear aeromagnetic anomalies, with considerable variation in detail (Grauch and Hudson, 2007). Associated anomaly amplitudes typically range from 2 to 5 nT, so they can be difficult to distinguish from solely topographic effects such as the somewhat linear edges of arroyos. Faults within more magnetic units, such as the Tertiary older volcanic rocks, have much more prominent expression on the aeromagnetic map because they produce anomalies with much higher amplitudes.

Faults interpreted from the aeromagnetic data for this study are from Grauch and Hudson (2007), who primarily used the horizontal-gradient magnitude (HGM) of the reduced-to-pole aeromagnetic data to locate faults. They also discuss the methods used, limitations, and utility of their approach. An

example of this approach from the middle of the study area shows the HGM of the reduced-to-pole aeromagnetic data first without (fig. 28*A*) and then with (fig. 28*B*) interpreted and mapped faults. The figure demonstrates how the HGM map can be used to guide fault interpretation and how the interpretation must take into account other linear sources, and the relations of the aeromagnetically interpreted faults to the mapped faults. The mapped faults show better detail; the aeromagnetically interpreted faults, which reflect major contrasts in bulk magnetic properties at depth, depict the structure at a more regional scale. Moreover, guides provided by Grauch and Hudson (2007) suggest that the faults in this area must have at least 30 m (100 ft) of throw to produce these anomalies.

Interpreted faults generally strike north to northeast where they offset Santa Fe Group sediments in the central and northern parts of the study area (fig. 29). As in the example area (fig. 28), aeromagnetically interpreted faults generally correspond with mapped faults in much of the area. In particular, the dense fault patterns in the northern part of the area are apparent in both the geology and the aeromagnetic data. In this area, Kelley (1978) and Koning (2005b) recognized the Barrancos monocline and faults offsetting the monocline, called the Barrancos fault system. The Barrancos monocline is evident as a basement feature on the 2D geophysical model along the Pojoaque profile (fig. 20). In many areas, aeromagnetically inferred faults are corroborated by breaks in the patterns of magnetic depth estimates observed in profile form, as demonstrated for the Alamo Creek profile (fig. 22).

A newly defined structure in the southern part of the study area, called the Agua Fria fault system, is recognized by a combination of geologic mapping and multiple geophysical data sets (fig. 29). It extends from the center of the study area, where faults are exposed and offset Miocene Tesuque Formation, to the area near Eldorado at Santa Fe on the south, where normal faults terminate against the Tijeras-Cañoncito strike-slip fault system (fig. 3). In between the northern and southern extents, the fault system underlies a large tract of relatively undeformed Plio-Pleistocene Ancha Formation, which constrains the minimum age of the faulting.

In the aeromagnetic data, the Agua Fria fault system is best recognized by parallel sets of inferred north-south, sinuous faults that cross the Santa Fe River and by a strong north-northwest aeromagnetic lineament on the Santa Fe platform. Some of the parallel inferred faults generally coincide with the mapped San Isidro Crossing fault (fig. 3), named for the road that crosses the river there. This fault is important because it coincides with a drop in the water table (Mourant, 1980; Johnson and Frost, 2004). At shallow levels, the electrical resistivity character changes across the fault; a layer of high resistivity lies on the west side (Spiegel and Baldwin, 1963). The aeromagnetic expression of the San Isidro Crossing fault is lost amid anomalies caused by buildings south of the river. However, the fault is imaged in seismic-reflection data from just north of the Santa Fe River to the southern part of the study area, and it corresponds with the aeromagnetic expression and exposures of the fault zone at the Santa Fe River and the north-northwest aeromagnetic lineament on the Santa Fe platform. As discussed previously, the aeromagnetic lineament also bounds the east side of the triangular area devoid of Espinaso Formation (area A2 on fig. 23) and connects with a mapped, east-down fault outside the area of the basin on the south. The seismic images show the San Isidro Crossing fault as a major down-to-the-east fault that bounds the western side of a pervasive fault zone (Ferguson and others, 2007). The fault zone is characterized by west-tilted and chaotic fault blocks across a 3–5 km (2–3 mi)-wide zone, as shown in the 2D geophysical model for the Seton Village profile (fig. 30). Faults interpreted from the gravity data provide additional evidence for the Agua Fria fault system, especially south of 35°37'30" N. (fig. 29), where its aeromagnetic expression is unclear.

Part of the expression of the Agua Fria fault system in the aeromagnetic data coincides with several north-south trending, elongated aeromagnetic anomalies northwest of Santa Fe. Grauch and Bankey (2003) tentatively interpreted these anomalies as narrow structural highs underlain by Precambrian through Oligocene rocks. On the basis of 2D geophysical profile models and magnetic depth estimates, they concluded that magnetic rocks (presumably bedrock) were detected about 600 m (2,000 ft) below the surface. On the basis of integration of gravity, well, and seismic information (John Ferguson, University of Texas at Dallas, written commun., 2007), this depth must be too shallow. However, the magnetic depth estimates and modeling results still require magnetic sources at this depth. These sources are depicted as layers with magnetic susceptibility of 0.01 (SI) (table 2) that follow the inferred dip of beds in fault blocks in the Tesuque and Alamo Creek profile models (figs. 17 and 22). These magnetic sources must be contained within the overlying Santa Fe Group sediments and have been upturned owing to tilting of fault-bounded blocks within the Agua Fria fault system. Perhaps the sources are upturned layers of magnetic sediment, such as lithosome E of the Tesuque Formation (fig. 4). Alternatively, there could be previously unrecognized basalt interbedded with the Tesuque Formation, but no plausible source has been recognized. In any case, the 2D and 3D models and seismic data all indicate that the Santa Fe Group, Tertiary older volcanic rocks, and Precambrian basement (and pre-rift strata where present) are all involved in the tilted fault blocks. These structural highs at the modeled base of the Santa Fe Group surface are shown by the disrupted elevation contours on both sides of the modeled east-down fault (fig. 25).

Faults that can be recognized by use of aeromagnetic data are important because the magnetic expression indicates a substantial difference in bulk lithology on either side of the fault, such as differences in grain size or lithic type. The juxtaposition of such different materials identifies places where average aquifer properties may differ across the fault. Conversely, the absence of aeromagnetic expression associated with mapped faults known to offset magnetic sediments suggests that the sediment type, when considered in bulk, does not differ significantly across these faults. Such a case

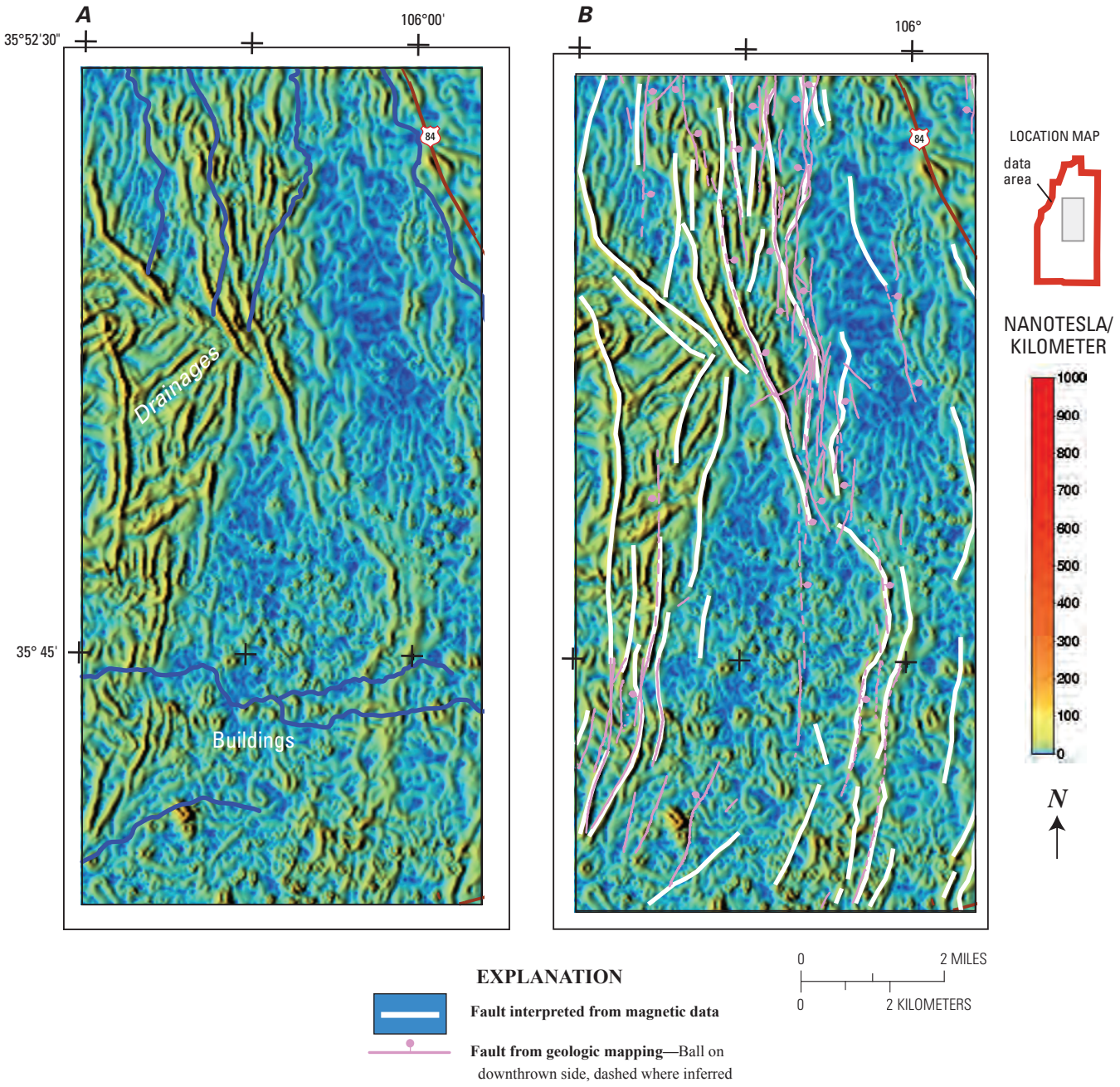

Figure 28. Demonstration of horizontal-gradient magnitude of reduced-to-pole aeromagnetic data used to interpret faults geophysically and to see relations to faults mapped geologically. Color shaded-relief images illuminated from the west. *A*, horizontal-gradient magnitude of reduced-to-pole aeromagnetic map. Most linear ridges on the map are related to faults; others are related to drainages, as labeled. *B*, The horizontal-gradient-magnitude map overlain with interpreted faults following ridges (white lines) and mapped faults (pink lines) from Koning and Maldonado (2003). Relations are discussed in text. (Modified from Grauch and Hudson, 2007).

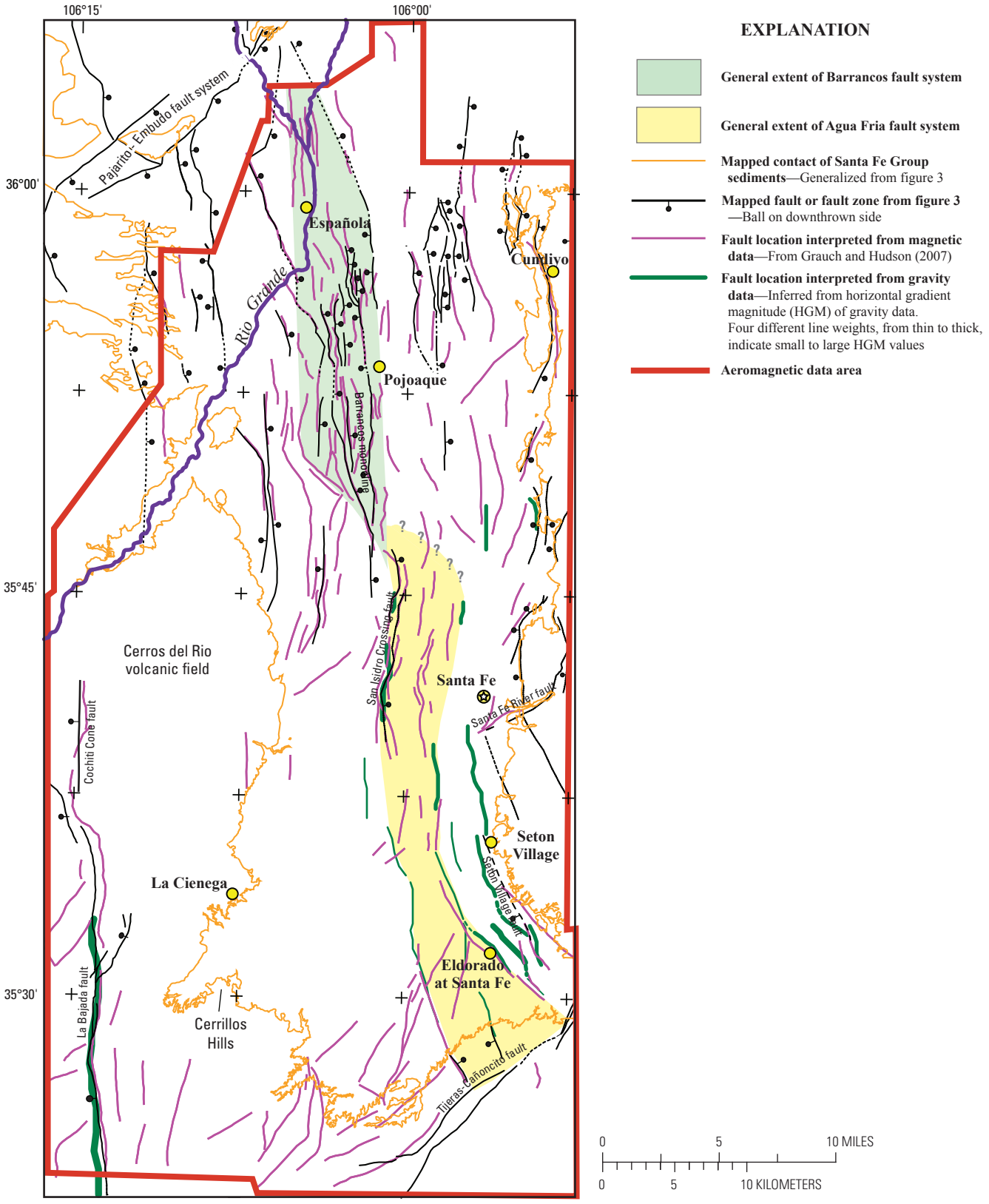

Figure 29. Mapped and geophysically interpreted faults. Faults interpreted from aeromagnetic data (magenta lines) are from Grauch and Hudson (2007). Faults interpreted from gravity data (green lines) are from the horizontal-gradient magnitude of the isostatic residual gravity. Mapped faults are from figure 3. Agua Fria and Barrancos fault systems are discussed in text.

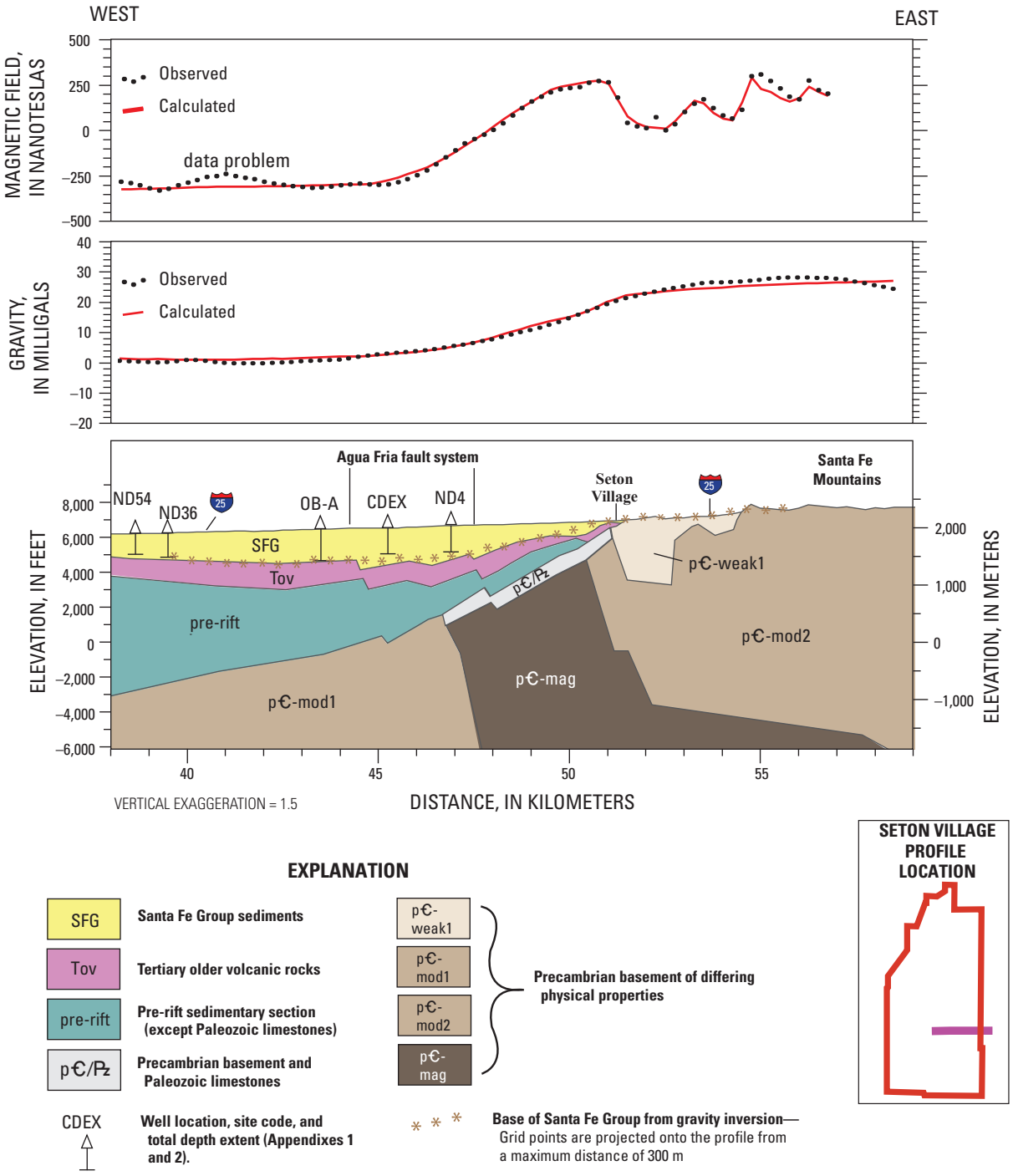

Figure 30. Two-dimensional gravity and magnetic model for Seton Village profile. Profile is located on inset and on figures 13, 15, and 16. Model demonstrates the Agua Fria fault system and a fundamental difference in the configuration of Precambrian basement in the southern part of study area. The disrupted surface over the Agua Fria fault system shows a series of east-down faults, the details of which are defined primarily by seismic information (John Ferguson, University of Texas at Dallas, written commun., 2007). Note the east-dipping sides of the shallow part of the magnetic Precambrian body.

occurs south of Chimayó in the northeastern part of the study area, where many more mapped faults are present than are apparent in the aeromagnetic map (E on fig. 19*B*; Koning, Nyman, and others, 2005). Reconnaissance magnetic susceptibility measurements suggest that most sediment types in the area are fairly magnetic (on the order of 0.001 (SI)), so the lack of aeromagnetic expression implies that these magnetic sediments are juxtaposed against similar magnetic sediments at depth. Moreover, coarse gravels with low magnetic susceptibilities (<0.0005 (SI), V.J.S. Grauch, unpub. data, 2007) measured close to the Precambrian basement contact about 2 km (1.25 mi) west of Cundiyo may not be extensive at shallow depths to the west. If they were, their juxtaposition with magnetic sediments at the mapped faults would produce linear anomalies.

A comparison of mapped and geophysically inferred faults with the modeled base of Santa Fe Group (fig. 31) shows a relation between the two. The Agua Fria fault system forms the faulted and irregular form of the basin floor along the southern mountain front. The Barrancos monocline, dissected by the Barrancos fault system, is apparent as a steep slope in the basin floor as it dips westward toward the deepest parts of the basin.

Overall basin structure is depicted by the modeled base of the Santa Fe Group (fig. 25 and pl. 1) and the corresponding isopach map (fig. 26 and pl. 2). As an additional visualization tool, figure 32 shows a 3D perspective view looking east; the topographic surface is positioned above for comparison. The isopach map shows that the southern Española Basin transitions northward from an extensive platform structure in the southern Santa Fe embayment to a west-tilted half graben where basin-fill thickness increases to 2,000–3,000 m (8,000–10,000 ft). The basin deepens northward relatively abruptly at a north-facing, curvilinear, north-down flexure called the Rancho Viejo hinge zone and is superimposed on an asymmetric, north-plunging syncline developed in the pre-rift rocks. We define the hinge zone primarily by examining the modeled thickness of the Santa Fe Group and secondarily on noted differences in aeromagnetic patterns (fig. 24). It differs in detail from the "Santa Fe embayment hinge line" of Phillips and Grauch (2004), which was defined on the basis of the aeromagnetic data alone. The abrupt deepening is most evident in the southernmost extent of the hinge zone; it generally follows the 600-ft isopach contour on plate 2. Rate of increase in thickness to the north across this part of the hinge zone is about 130–150 m/km (700–800 ft/mi). The eastern and western limbs of the hinge zone generally track between the 500 and 1,000-foot isopach contours (pl. 2).

North of the hinge zone, the basin floor slopes fairly steeply westward from the mountain front, flattens slightly, then steepens again into the deepest parts of the basin, as discussed in the section on Precambrian basement. A subsurface bedrock high bounds the western side of the deep part of the basin on the south, generally located underneath the Cerros del Rio volcanic field. On the far northwestern part of the study area, irregular displacements along the Pajarito fault system are evident from large undulations of the basal surface.

The Rancho Viejo hinge zone generally coincides with thickened Espinaso Formation underlying the Santa Fe Group, northeast-trending linear aeromagnetic anomalies (interpreted as upturned fault blocks of older volcanic rocks or paleochannels filled by Cieneguilla basalt flows), and circular negative aeromagnetic anomalies of about 1.6 km (1 mi) diameter interpreted as volcanic vents associated with the Espinaso Formation (figs. 23 and 24). These coincidences suggest that volcanism and possible faulting may have been associated with the formation of the hinge. The Rancho Viejo hinge zone may represent a long-lived crustal weakness that underwent a reversal of motion from Laramide time (north side up) to Rio Grande rift time (north side down). As the motion reversed, volcanic eruptive centers may have localized near the hinge zone along dilational fractures. Roughly similar dips between the lower Tesuque Formation and the top of the older volcanic rocks just north of the hinge zone suggest that pronounced tilting did not occur until after deposition of the Tesuque Formation. This tilting may have preserved Espinaso Formation to the north and facilitated erosion of Espinaso Formation in the uplifted area to the south. Lack of deformation in the overlying Ancha Formation suggests that the tilting had ceased before Pliocene time.

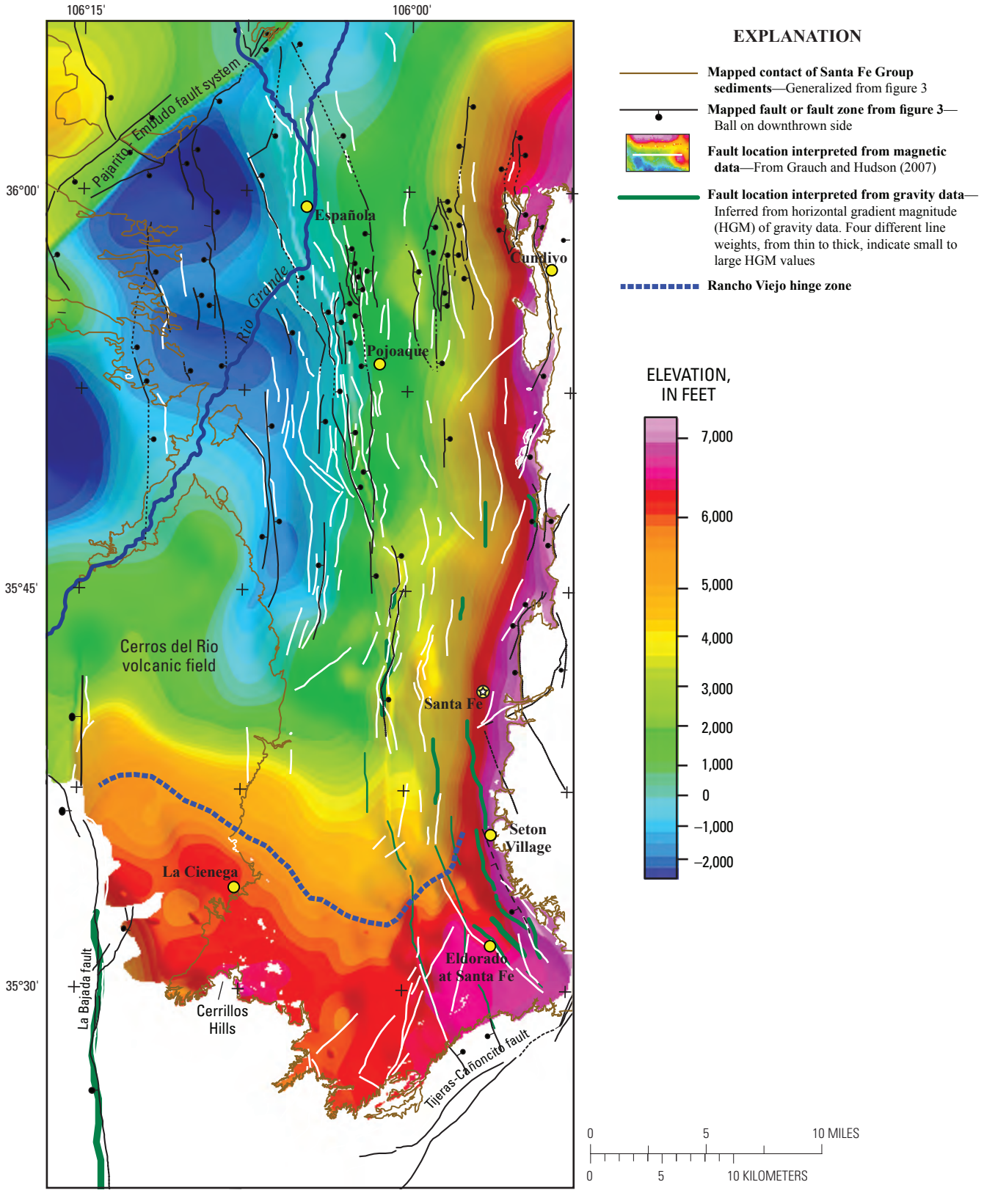

Figure 31. Geologically mapped and geophysically interpreted faults on the base of Santa Fe Group surface (shown without contour lines). Faults from figure 29 are overlain on the three-dimensional model surface that represents the elevation of base of the Santa Fe Group from figure 25. Labeled faults are from figure 3.

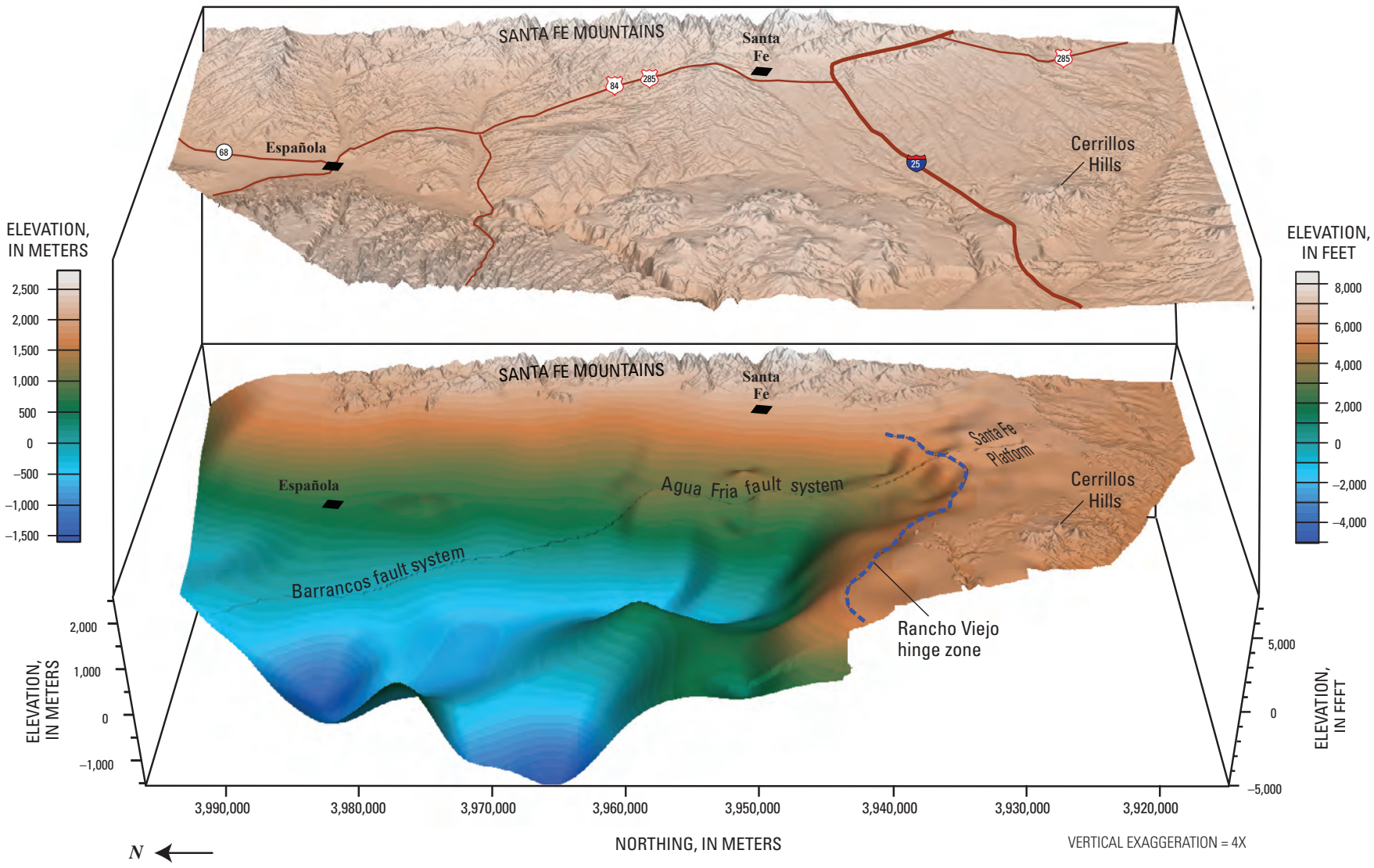

Figure 32. Perspective view of the modeled elevation of the base of the Santa Fe Group in relation to topography, looking east. Topographic surface is raised above the base.

Summary

The Española Basin is situated between the right-stepping, en echelon Santo Domingo and San Luis Basins of the Rio Grande rift in north-central New Mexico. Located between the Santa Fe Mountains on the east and the Jemez Mountains on the west, the southern Española Basin consists of a westward-thickening wedge of rift sediment that serves as an important aquifer for the city of Santa Fe and surrounding areas. Regional gravity data show that the deepest parts (>3,000 m (10,000 ft)) of the Española Basin are west of the Rio Grande under the Pajarito Plateau.

To better understand the hydrogeologic framework in this semiarid region, detailed aeromagnetic surveys were flown over the southern Española basin, including the area commonly known as the Santa Fe embayment. This report presents a synthesis of these data with gravity data and other constraints. The interpretations were accomplished using qualitative interpretation, quantitative data analysis, and 2D and 3D modeling. The results depict the presence of and depth to many geologic features that have hydrogeologic significance, such as shallow faults, various types of igneous units, and basement rocks. A composite of selected map interpretations is presented in plate 1. In addition, a digital surface was constructed that depicts the base of Santa Fe Group sediments, which constitutes the primary aquifer system for residents of Santa Fe, Española, and six Pueblo nations. The surface is shown as a contour map on plate 1 and is available in geo-registered digital format on the CD. From this basal surface, an isopach of the thickness of Santa Fe Group sediments was computed; it estimates the maximum potential aquifer thickness across the basin (pl. 2).

The modeled base of the Santa Fe Group shows that the southern Española Basin transitions from a platform on the south to a deep, west-tilted half graben on the north. The Santa Fe platform is generally composed of eroded late Eocene and Oligocene volcanic and volcaniclastic rocks overlain by rift sediments of the Santa Fe Group that are typically less than 75 m (250 ft) thick. The sediments thicken over local irregularities and paleovalleys incised into the platform. Models that are constrained primarily by the gravity data imply that one paleovalley in the vicinity of Eldorado at Santa Fe is filled with 90–150 m (300–500 ft) of Santa Fe Group sediments. In this and two other areas on the platform, aeromagnetic analysis implies that volcanic and volcaniclastic rocks are absent underneath the Santa Fe Group. In these areas we infer a direct hydrologic connection between Santa Fe Group sediments and underlying early Tertiary to Paleozoic sedimentary rocks.

The basin transitions abruptly from the platform to the deeper basin across a curvilinear zone west and southwest of Santa Fe, called the Rancho Viejo hinge zone. The Rancho Viejo hinge zone is of particular importance to the hydrogeologic framework as well as to rift-related and pre-rift structural interpretations. Santa Fe Group sediments thicken substantially across the hinge zone at about 130–150 m/km (700–800 ft/mi). North of the hinge zone, the basin deepens less markedly but ultimately reaches depths greater than 3,000 m (10,000 ft) under the Pajarito Plateau west of Española. Thus, the hinge zone defines the southern extent of a relatively thick Santa Fe Group aquifer. Below the area of the hinge zone, seismic interpretations by other workers indicate that most of the deeper Paleozoic and Mesozoic sedimentary section is unconformably truncated. The truncation results in a thin section of mostly basal limestones preserved below the deep basin on the north and a thick section of mostly clastic rocks preserved below the shallow basin on the south. Gravity modeling suggests that the erosional truncation of this pre-rift sedimentary section follows a northwest trend, possibly marking the southernmost limit of a Laramide uplift.

The Rancho Viejo hinge zone may represent a long-lived crustal weakness that underwent a reversal of motion from Laramide time (north side up) to Rio Grande rift time (north side down). Magmatism may have been associated with the beginning of the reversal in Eocene time, on the basis of interpretations that thick Tertiary older volcanic rocks and associated vents underlie the Santa Fe Group in the vicinity of the hinge zone. Inferences from well data combined with the modeled surfaces suggest that the volcanic rocks tilted to the north after the deposition of the Miocene lower Tesuque Formation and before deposition of the Plio-Pleistocene Ancha Formation.

Basin models show a west-tilted, narrow half graben north and west of Santa Fe; it is bounded on its west side by a north-northeast-elongated bedrock high underneath the Cerros del Rio volcanic field. This bedrock high is constrained by MT and gravity models considered together. Its eastern side may be represented by east-down faults or an east-dipping monocline. The eastern side of the half graben lies with variable dip parallel to the north-trending mountain front of the Santa Fe Mountains. The buried basement surface there undulates from moderate westward dip (7°–20°) at the mountain front, to shallow dip (~5°), and back to moderate dip 10–12 km (6.25–7.5 mi) west of the front.

At several places along the front of the Santa Fe Mountains, northerly elongated, alternating narrow highs and lows in the aeromagnetic data suggest that Precambrian basement has a regional linear fabric. This fabric may influence groundwater flow within the mountain block. However, the regional fabric is not apparent more than 1–5 km (0.6–3 mi) west of the mountain front. Thus, the Precambrian basement in the subsurface likely has lithologic or structural characteristics that are much different at regional scale than the characteristics observed in exposed basement rocks. The marked difference in basement character along the western side of the mountain front probably originated from tectonic events that preceded rifting.

Using the geophysical data, we recognize numerous north- to northeast-striking faults throughout the basin that likely offset strata by at least 30 m (100 ft). In the southern part of the study area the faults do not penetrate the overlying

Plio-Pleistocene Ancha Formation of the Santa Fe Group. Combined with detailed geologic mapping, the geophysical data suggest that faults are more abundant than previously thought in the southern Española Basin. This abundance increases the potential for partial ground-water barriers or aquifer compartmentalization within the Santa Fe Group aquifer because (1) other workers have found that clay is common in the cores of fault zones in the basin, which reduces permeability at fault zones, and (2) fault-related aeromagnetic anomalies are likely caused by major contrasts in bulk lithologic characteristics, which may indicate permeability differences on either side of faults.

We categorize many of the numerous faults into two major fault systems, the Agua Fria and Barrancos fault systems. Interpretations based on several types of geophysical data show that the Agua Fria fault system is a zone 3–5 km (2–3 mi) wide consisting of generally east-down faults that bound west-tilted and chaotic fault blocks. It can be traced from the Tijeras-Cañoncito strike-slip system on the far south to the latitude of 35°47'30" on the north, where its northern termination is unclear. The western side of the Agua Fria fault system includes the mapped San Isidro Crossing fault, which is associated with a drop in water table. Near its farthest southern extent, the east side of the fault system marks the western side of an extensive paleovalley inferred to lie in the vicinity of Eldorado at Santa Fe. North of Santa Fe near latitude 35°45', magnetic modeling and analysis indicate that magnetic beds apparently within the basin fill are disrupted by the Agua Fria fault system at depths of about 610 m (2,000 ft). Their geologic affinity has not been determined.

The Barrancos fault system is best defined in exposures north of latitude 35°47'30" to the vicinity of Española. It is characterized by a zone ~5 km (3 mi) wide consisting of east- and west-down faults across a large-scale, west-dipping monocline. Structural relief on the monocline is 450–1,800 m (1,500–6,000 ft). The southern and northern extents of the Barrancos fault system are poorly defined.

Finally, the high-amplitude aeromagnetic anomalies associated with the volcanic rocks of the Cerros del Rio volcanic field and the Cerrillos intrusion can be used to determine their lateral extents under cover. Examination of aeromagnetic patterns suggests that basalts from the volcanic field generally do not extend beyond the limits of exposure except in one local place about 9 km (5.6 mi) west of Santa Fe, where the Ancha Formation of the Santa Fe Group covers the basalt. Aeromagnetic anomalies associated with the late Eocene and Oligocene Cerrillos intrusion show that it is a large intrusive complex that encompasses the Cerrillos Hills and areas to the east and southeast. Aeromagnetic data suggest that the bulk of the intrusion has fairly steep sides except on the west. This interpretation suggests that laccolithic sills known to be present must be volumetrically insignificant, occur only on the west side, or cannot be distinguished magnetically from overlying Tertiary older volcanic rocks.

Description of Digital Products

Table 4 presents short descriptions of digital files related to this study that can be downloaded from the CD in the pocket or from directories in the U.S. Geological Survey Web site. They contain grids and vector files that can be used in standard geographic information systems and in geophysical software packages.

Acknowledgments

This work was funded by the U.S. Geological Survey National Cooperative Geologic Mapping Program and the New Mexico Office of the State Engineer (OSE). Dan Koning and Peggy Johnson collaborated under the auspices of the New Mexico Bureau of Geology and Mineral Resources. We are grateful to John Ferguson (University of Texas at Dallas and Summer of Applied Geophysical Experience (SAGE)), to Shawn Biehler (University of California, Riverside and SAGE), and to Mark Hudson, David Sawyer, and Brian Rodriguez (U.S. Geological Survey) for generously sharing their unpublished work. We greatly appreciate reviews of earlier drafts by Alan Cuddy (OSE), Jack Frost (OSE), Darcy McPhee (U.S. Geological Survey and SAGE), Mike Sully (OSE), and Don Sweetkind (U.S. Geological Survey), which led to significant improvements.

J.D. Phillips designed and modified magnetic depth estimation techniques specifically for this study (section "Magnetic Depth Estimation" and appendix 3). He also supplied computer programs and collaborated on general data analysis and magnetic interpretation. D.J. Koning provided extensive guidance on geologic information, much of which is derived from his own mapping (sections "Geologic Setting" and "Other Data"). P.S. Johnson provided locations, data, and assistance on interpreted lithology in wells that she and D.J. Koning compiled (section "Other Data" and appendixes 1 and 2). Viki Bankey compiled and rectified inconsistencies in gravity data available as of 2006 (section "Gravity Data") and helped construct two-dimensional geophysical models (section "Profile Models"). Additional independent constraints are in large part from unpublished sources (most recently from 2008) that are described in the text; they include physical-property measurements (section "Physical Properties," table 2, and fig. 4) and other types of geophysical interpretations and well data (section "Other Data" and appendix 4). V.J.S. Grauch digitally merged high-resolution aeromagnetic data from surveys flown during 1997–2005 (section "Aeromagnetic Data"). She is also responsible for analysis, interpretation, and modeling that is not otherwise attributed.

Table 4. Digital georegistered files.

[Coordinates in meters based on Universal Transverse Mercator Projection, zone 13, North American Datum of 1927. XYZ points are extracted from grids at intervals as indicated. Lines and polygons for import in shapefile format are represented by several files with the same prefix and different suffixes, represented below by an asterisk]

File type	FileName	Description
XYZ ASCII points	seb_sfgbasem.xyz	Base of Santa Fe Group sediments from three-dimensional model. Elevation in meters; datum is sea level. Original grid interval 100 meters (330 feet).
	seb_sfgbaseft.xyz	Base of Santa Fe Group sediments from three-dimensional model. Elevation in feet; datum is sea level. Original grid interval 100 meters (330 feet).
	seb_sfgthickm.xyz	Isopach of Santa Fe Group sediments from three-dimensional model. Thickness in meters. Original grid interval 250 meters (820 feet).
	seb_sfgthickft.xyz	Isopach of Santa Fe Group sediments from three-dimensional model. Thickness in feet. Original grid interval 250 meters (820 feet).
Shapefile format	seb_mag_flts.*	Lines representing faults interpreted from magnetic data. Extracted for the study area from digital files (crgrmag_faults1.0.*) of Grauch and Hudson (2007).
	seb_no_tov.*	Lines outlining areas interpreted to be devoid of Tertiary older volcanic rocks underneath Santa Fe Group sediments.
	rv_hinge.*	Line following general location of interpreted Rancho Viejo hinge zone.
	seb_cdr_extent.*	Lines representing magnetically inferred extent of Cerros del Rio volcanic field and related flows within study area.
	seb_grv_flts.*	Lines representing faults interpreted from gravity data.
	seb_intrusions.*	Lines outlining interpreted extents of Tertiary older volcanic vents and intrusions. Includes bodies inferred to be associated with the Cerrillos intrusion and the Espinaso Formation.
Metadata text files	sfg_model_metadata.txt	Metadata describing the grid surfaces related to the three-dimensional model of Santa Fe Group sediments.
	seb_interp_metadata.txt	Metadata describing the interpretations represented by lines and polygons.

References Cited

Baldridge, W.S., Cole, G.L., Robinson, B.A., and Jiracek, G.R., 2007, Application of time-domain airborne electromagnetic induction to hydrogeologic investigations on the Pajarito Plateau, New Mexico, USA: Geophysics, v. 72, no. 2, p. B31–B45, doi:10.1190/1.2347701.

Baldridge, W.S., Damon, P.E., Shafiqullah, M., and Bridwell, R.J., 1980, Evolution of the central Rio Grande rift, New Mexico—New potassium-argon ages: Earth and Planetary Science Letters, v. 51, p. 309–321.

Baldridge, W.S., Ferguson, J.F., Braile, L.W., Biehler, S., Jiracek, G.R., Gilpin, B.E., Alumbaugh, D.L., Gratwick, D.S., Richards, T.L., and Hasterok, D.P., 2001, Architecture of the southern Española Basin (Rio Grande rift) and flank uplift adjacent to the La Bajada fault [abs.]: Geological Society of America Abstracts with Programs, v. 33, no. 5, p. 61.

Baldridge, W.S., Ferguson, J.F., Braile, L.W., Wang, B., Eckhardt, K., Evans, D., Schultz, C., Gilpin, B., Jiracek, G.R., and Biehler, S., 1994, The western margin of the Rio Grande rift in northern New Mexico—An aborted boundary?: Geological Society of America Bulletin, v. 105, p. 1538–1551.

Baltz, E.H., 1978, Resume of Rio Grande depression in north-central New Mexico, *in* Hawley, J.W., ed., Guidebook to Rio Grande rift in New Mexico and Colorado: New Mexico Bureau of Geology and Mineral Resources Circular 163, p. 210–228.

Bankey, Viki, Grauch, V.J.S., Drenth, B.J., and Geophex, Inc., 2006, Digital data from the Santa Fe East and Questa–San Luis helicopter magnetic surveys in Santa Fe and Taos Counties, New Mexico, and Costilla County, Colorado: U.S. Geological Survey Open-File Report 2006–1170, 6 p. *http://pubs.usgs.gov/of/2006/1170/*.

Bartolino, J.R., and Cole, J.C., 2002, Ground-water resources of the Middle Rio Grande Basin, New Mexico: U.S. Geological Survey Circular 1222, 132 p.

Bates, R.L., and Jackson, J.A., 1984, Dictionary of Geological Terms: New York, Bantam Doubleday Dell Publishing Group, Inc., 571 p.

Bath, G.D., 1968, Aeromagnetic anomalies related to remanent magnetism in volcanic rock, Nevada Test Site: Geological Society of America Memoir 110, p. 135–146.

Biehler, Shawn, Ferguson, J.F., Baldridge, W.S., Jiracek, G.R., Aldern, J.L., Martinez, M., Fernandez, R., Romo, J., Gilpin, B., Braile, L.W., Hersey, D.R., Luyendyk, B.P., and Aiken, C.L., 1991, A geophysical model of the Española Basin, Rio Grande rift, New Mexico: Geophysics, v. 56, p. 340–353.

Birch, F.S., 1982, Gravity models of the Albuquerque Basin, Rio Grande rift, New Mexico: Geophysics, v. 47, no. 8, p. 1185–1197.

Black, B.A., 1984, Structural anomalies in the Española Basin: New Mexico Geological Society Guidebook 35, p. 59–62.

Blakely, R.J., 1995, Potential theory in gravity and magnetic applications: New York City, Cambridge University Press, 441 p.

Borchert, C.I., Skotnicki, S., and Read, A.S., 2003 (orig. publ. 1998), Preliminary geologic map of the Tesuque 7.5-minute quadrangle: New Mexico Bureau of Geology and Mineral Resources Open-File Geologic Map OF–GM–47, scale 1:24,000.

Broxton, D.E., and Vaniman, D.T., 2005, Geologic framework of a groundwater system on the margin of a rift basin, Pajarito Plateau, north-central New Mexico: Vadose Zone Journal, v. 4, p. 522–550. doi:10.2136/vzj2004.0073

Caine, J.S., Minor, S.A., and Johnson, P.S., 2008, Preliminary characterization of fault zones and potential impacts on ground-water resources—Española Basin, New Mexico [abs.], *in* Borchert, C.I., ed., Geologic and Hydrologic Framework of the Española Basin—Proceedings of the 6th Annual Española Basin Workshop, March 6, 2007: New Mexico Bureau of Geology and Mineral Resources Open-File Report 508, p. 4.

Cather, S.M., 1992, Suggested revisions to the Tertiary tectonic history of north-central New Mexico: New Mexico Geological Society Guidebook 43, p. 109–122.

Cather, S.M., 2004, Laramide orogeny in central and northern New Mexico and southern Colorado, *in* Mack, G.H., and Giles, K.A., eds., The Geology of New Mexico: New Mexico Geological Society Special Publication 11, p. 203–248.

Cavazza, William, 1986, Miocene sediment dispersal in the central Española Basin, Rio Grande rift, New Mexico, USA: Sedimentary Geology, v. 51, p. 119–135.

Cole, G.L., Baldridge, W.S., Burnette, L., and Hollis, D., 2006, The 2001 airborne electromagnetic survey of the Pajarito Plateau and its application to groundwater investigations: Los Alamos National Laboratory Report LA–UR–06–3059, CD-ROM.

Cordell, Lindrith, 1976, Aeromagnetic and gravity studies of the Rio Grande graben in New Mexico between Belen and Pilar: New Mexico Geological Society Special Publication 6, p. 62–70.

Deszcz-Pan, Maria, Rodriguez, B.D., Doucette, J.P., Godbout, M., Williams, J.M., Sawyer, D.A., Stone, B.D., Grauch, V.J.S., and Geoterrex-Dighem, Inc., 2000, Digital airborne time domain electromagnetic data from surveys over Cochiti Pueblo, Rio Puerco and Rio Rancho, New Mexico: U.S. Geological Survey Open-File Report 00–0502, *http://pubs.usgs.gov/of/2000/ofr-00-0502/*

Dethier, D.P., 2003, Geologic map of the Puye quadrangle, Los Alamos, Rio Arriba, Sandoval, and Santa Fe Counties, New Mexico: U.S. Geological Survey Miscellaneous Field Studies Map MF–2419, version 1.0, scale 1:24,000.

Dethier, D.P., and Koning, D.J., 2007, Preliminary geologic map of the White Rock quadrangle, Santa Fe, Sandoval, and Los Alamos Counties, New Mexico: New Mexico Bureau of Geology and Mineral Resources Open-File Geologic Map OF–GM–49, scale 1:24,000.

Erskine, D.W., and Smith, G.A., 1993, Compositional characterization of volcanic products from a primarily sedimentary record—The Oligocene Espinaso Formation, north-central New Mexico: Geological Society of America Bulletin, v. 105, p. 1214–1222.

Evans, T.C., and Lindline, Jennifer, 2004, Petrologic comparison of Precambrian rocks in the Las Vegas and Santa Fe areas, southern Sangre de Cristo Mountains, New Mexico [abs.]: Geological Society of America Abstracts with Programs, v. 36, no. 5, p. 508.

Faulds, J.E., and Varga, R.J., 1998, The role of accommodation zones and transfer zones in the regional segmentation of extended terranes, *in* Faulds, J.E., and Stewart, J.H., eds., Accommodation zones and transfer zones—The regional segmentation of the Basin and Range Province: Geological Society of America Special Paper 323, p. 1–45.

Ferguson, J.F., Baldridge, W.S., Braile, L.W., Biehler, S., Gilpin, B., and Jiracek, G.R., 1995, Structure of the Española Basin, Rio Grande rift, New Mexico, from SAGE seismic and gravity data: New Mexico Geological Society Guidebook 46, p. 105–110.

Ferguson, J.F., Baldridge, W.S., and Grauch, V.J.S., 2007, Structural framework and Tertiary history of the southern Española Basin, New Mexico, USA, interpreted from seismic reflection profiles [abs.]: Geological Society of America Abstracts with Programs, v. 39, no. 6, p. 364.

Ferguson, J.F., Felch, R.N., Aiken, C.L.V., Oldow, J.S., and Dockery, H., 1988, Models of the Bouguer gravity and geologic structure at Yucca Flat, Nevada: Geophysics, v. 53, no. 2, p. 231–244.

Finch, S.T., 2008, Hydrogeologic characteristics of the Tertiary-age Galisteo Formation, Santa Fe County, New Mexico [abs.], *in* Borchert, C.I., ed., Geologic and Hydrologic Framework of the Española Basin—Proceedings of the 6th Annual Española Basin Workshop, March 6, 2007: New Mexico Bureau of Geology and Mineral Resources Open-File Report 508, p. 8.

Frost, J.P., 2006, NM OSE ground water monitoring well program in the Santa Fe region [abs.], *in* McKinney, K.C., ed., Geologic and Hydrogeologic Framework of the Española Basin—Proceedings of the 5th Annual Española Basin Workshop, Santa Fe, New Mexico, March 7–8, 2006: U.S. Geological Survey Open-File Report 2006–1134, p. 6.

Giles, D.L., 1995, Cerrillos mining district, *in* Bauer, P.W., Maynard, S.R., Smith, G.A., Giles, D.L., Lucas, S.G., Barker, J.M., Smith, E.W., and Kottlowski, F.E., eds., Third-day road log, from Santa Fe to the Cerrillos Hills, Cerrillos, and Ortiz Mountains: New Mexico Geological Society Guidebook 46, p. 61–62.

Golombek, M.P., 1983, Geology, structure, and tectonics of the Pajarito fault zone in the Española Basin of the Rio Grande rift, New Mexico: Geological Society of America Bulletin, v. 94, no. 2, p. 192–205.

Grant, P.R., Jr., 1999, Subsurface geology and related hydrologic conditions, Santa Fe embayment and contiguous areas, New Mexico: New Mexico Geological Society Guidebook 50, p. 425–435.

Grauch, V.J.S., and Bankey, V., 2003, Aeromagnetic interpretations for understanding the hydrogeologic framework of the southern Española Basin, New Mexico: U.S. Geological Survey Open-File Report 03–124, 44 p. *http://pubs.usgs.gov/of/2003/ofr-03-124*,

Grauch, V.J.S., and Cordell, Lindrith, 1987, Limitations of determining density or magnetic boundaries from the horizontal gradient of gravity or pseudogravity data: Geophysics, v. 52, p. 118–121.

Grauch, V.J.S., and Hudson, M.R., 2007, Guides to understanding the aeromagnetic expression of faults in sedimentary basins—Lessons learned from the central Rio Grande rift, New Mexico: Geosphere, v. 3, no. 6, p. 596–623. doi:10.1130/ges00128.1.

Grauch, V.J.S., and Keller, G.R., 2004, Gravity and aeromagnetic expression of tectonic and volcanic elements of the southern San Luis Basin, New Mexico and Colorado: New Mexico Geological Society Guidebook 55, p. 230–243.

Grauch, V.J.S., Sawyer, D.A., Hudson, M.R., Minor, S.A., and Thompson, R.A., 2006, Gravity and aeromagnetic studies in the Santo Domingo Basin area, *in* Minor, S.A., ed., The Cerrillos uplift, the La Bajada constriction, and hydrogeologic framework of the Santo Domingo Basin, Rio Grande rift, New Mexico, U.S. Geological Survey Professional Paper 1720–D, p. 63–86. *http://pubs.usgs.gov/pp/1720/downloads/pdf/p1720D.pdf*

Hansen, R.O., Racic, L., and Grauch, V.J.S., 2005, Magnetic methods in near-surface geophysics, *in* Butler, D.K., ed., Near-surface geophysics—Investigations in Geophysics 13, Society of Exploration Geophysicists, p. 151–175.

Hansen, R.O., and Simmonds, M., 1993, Multiple-source Werner deconvolution: Geophysics, v. 58, p. 1792–1800.

Heywood, C.E., 1992, Isostatic residual gravity anomalies of New Mexico: U.S. Geological Survey Water-Resources Investigations Report 91–4065, 27 p.

Hudson, M.R., Grauch, V.J.S., and Minor, S.A., 2008, Rock magnetic characterization of faulted sediments with associated magnetic anomalies in the Albuquerque Basin, Rio Grande rift, New Mexico: Geological Society of America Bulletin, v. 120, p. 641–658.

Jachens, R.C., and Moring, B.C., 1990, Maps of the thickness of Cenozoic deposits and the isostatic residual gravity over basement for Nevada: U.S. Geological Survey Open-File Report 90–404, 15 p., 2 plates, scale 1:1,000,000.

Jiracek, G.R., Baldridge, W.S., Biehler, Shawn, Braile, L.W., Ferguson, J.F., Gilpin, B.E., McPhee, D.K., and Pellerin, Louise, 2008, SAGE celebrates 25 years of learning geophysics by doing geophysics: The Leading Edge, v. 27, no. 10, p. 1241–1375.

Johnson, P.S., and Frost, Jack, 2004, Hydrologic conditions in the southeastern Española Basin based on recent data collection near Santa Fe, New Mexico—A view from midstream [abs.], *in* Hudson, M.R., ed., Geologic and Hydrogeologic Framework of the Española Basin—Proceedings of the 3rd Annual Española Basin Workshop, Santa Fe, New Mexico, March 2–3, 2004: U.S. Geological Survey Open-File Report 2004–1093, p. 2.

Kautz, P.F., Ingersoll, R.V., Baldridge, W.S., Damon, P.E., and Shafiqullah, M., 1981, Geology of the Espinaso Formation (Oligocene), north-central New Mexico—Summary: Geological Society of America Bulletin, Part I, v. 92, p. 980–983.

Kelley, V.C., 1952, Tectonics of the Rio Grande depression of central New Mexico: New Mexico Geological Society Guidebook 3, p. 92–105.

Kelley, V.C., 1978, Geology of Española Basin, New Mexico: New Mexico Bureau of Mines and Mineral Resources Geologic Map 48, scale 1:125,000.

Koning, D.J., 2005a (orig. publ. 2003), Preliminary geologic map of the Chimayó 7.5-minute quadrangle, Rio Arriba and Santa Fe counties, New Mexico: New Mexico Bureau of Geology and Mineral Resources Open-File Geologic Map OF–GM–71, scale 1:24,000.

Koning, D.J., 2005b (orig. publ. 2002), Preliminary geologic map of the Española 7.5-minute quadrangle, Rio Arriba and Santa Fe counties, New Mexico: New Mexico Bureau of Geology and Mineral Resources Open-File Geologic Map OF–GM–54, scale 1:24,000.

Koning, D.J., and Aby, S.B., 2005, Proposed members of the Chamita Formation, north-central New Mexico: New Mexico Geological Society Guidebook 56, p. 258–278.

Koning, D.J., Connell, S.D., Morgan, G.S., Peters, L., and McIntosh, W.C., 2005, Stratigraphy and depositional trends in the Santa Fe Group near Española, north-central New Mexico—Tectonic and climatic implications: New Mexico Geological Society Guidebook 56, p. 237–257.

Koning, D.J., Connell, S.D., Pazzaglia, F.J., and McIntosh, W.C., 2002, Redefinition of the Ancha Formation and Plio-Pleistocene deposition in the Santa Fe embayment, north-central New Mexico: New Mexico Geology, v. 24, no. 3, p. 75–87.

Koning, D.J., and Hallett, R.B., 2001 (orig. publ. 2000), Preliminary geologic map of the Turquoise Hill 7.5-minute quadrangle, Santa Fe County, New Mexico: New Mexico Bureau of Geology and Mineral Resources Open-File Geologic Map OF–GM–41, scale 1:24,000.

Koning, D.J., and Johnson, P.S., 2006, Locations and textural contrasts of Tesuque Formation lithostratigraphic units in the southern Española Basin, New Mexico, and hydrogeologic implications [abs.], *in* McKinney, K.C., ed., Geologic and hydrogeologic framework of the Española Basin—Proceedings of the 5th annual Española Basin workshop, Santa Fe, New Mexico, March 7–8, 2006: U.S. Geological Survey Open-File Report 2006–1134, p. 24.

Koning, D.J., and Maldonado, F., 2003 (orig. publ. 2001), Preliminary geologic map of the Horcado Ranch 7.5-minute quadrangle, Santa Fe County, New Mexico: New Mexico Bureau of Geology and Mineral Resources Open-File Geologic Map OF–GM–44, scale 1:24,000.

Koning, D.J., Nyman, M., Horning, R., Eppes, M., and Rogers, S., 2005 (orig. publ. 2002), Preliminary geologic map of the Cundiyo 7.5-minute quadrangle, Santa Fe County, New Mexico: New Mexico Bureau of Geology and Mineral Resources Open-File Geologic Map OF–GM–56, scale 1:24,000.

Koning, D.J., Read, A.S., Grauch, V.J.S., and Minor, S.A., 2005, Intrabasinal architecture of the southern Española Basin [abs.], *in* McKinney, K.C., ed., Geologic and hydrogeologic framework of the Española Basin—Proceedings of the 4th Annual Española Basin Workshop, Santa Fe, New Mexico, March 1–3, 2005: U.S. Geological Survey Open-File Report 2005–1130, p. 21.

Koning, D.J., Read, A.S., Grauch, V.J.S., and Minor, S.A., 2006, Late Oligocene-Miocene structures in and west of the Santa Fe embayment, New Mexico, and inferences regarding tectonism and paleo-topography [abs.], *in* McKinney, K.C., ed., Geologic and hydrogeologic framework of the Española Basin—Proceedings of the 5th Annual Española Basin Workshop, Santa Fe, New Mexico, March 7–8, 2006: U.S. Geological Survey Open-File Report 2006–1134, p. 25.

Kucks, R.P., Hill, P.L., and Heywood, C.E., 2001, New Mexico aeromagnetic and gravity maps and data—A web site for distribution of data, version 1.0: U.S. Geological Survey Open-File Report 01–0061. *http://pubs.usgs.gov/of/2001/ofr-01-0061/.*

Kuhle, A.J., and Smith, G.A., 2001, Alluvial-slope deposition of the Skull Ridge Member of the Tesuque Formation, Española Basin, New Mexico: New Mexico Geology, v. 23, p. 30–37.

Lewis, A.C., and West, F., 1995, Conceptual hydrologic systems for Santa Fe County: New Mexico Geological Society Guidebook 46, p. 299–306.

Lisenbee, A.L., 1999, Preliminary geologic map of the Galisteo 7.5-minute quadrangle, Santa Fe County, New Mexico: New Mexico Bureau of Geology and Mineral Resources Open-File Geologic Map OF–GM–30, scale 1:24,000.

Los Alamos National Laboratory, 2006, 2006 hydrogeologic site atlas: Los Alamos National Laboratory Report LA–UR–06–3058, 112 p.

Lucas, S.G., Cather, S.M., Abbott, J.C., and Williamson, T.E., 1997, Stratigraphy and tectonic implications of Paleogene strata in the Laramide Galisteo Basin, north-central New Mexico: New Mexico Geology, v. 19, p. 89–95.

Manley, Kim, 1979, Stratigraphy and structure of the Española Basin, Rio Grande rift, New Mexico, *in* Riecker, R.E., ed., Rio Grande rift–Tectonics and magmatism: American Geophysical Union, p. 71–86.

Maynard, S.R., Lisenbee, A.L., and Rogers, John, 2002, Geology of the Picture Rock 7.5-minute quadrangle, Santa Fe County, New Mexico: New Mexico Bureau of Geology and Mineral Resources Open-File Geologic Map OF–GM–51, scale 1:24,000.

Milsom, John, 1989, Field geophysics—Geological Society of London Handbook: London, Open University Press and New York, Halsted Press (Wiley), 182 p.

Minor, S.A., ed., 2006, The Cerrillos uplift, the La Bajada constriction, and hydrogeologic framework of the Santo Domingo Basin, Rio Grande rift, New Mexico: U.S. Geological Survey Professional Paper 1720, 189 p.

Minor, S.A., and Hudson, M.R., 2006, Regional survey of structural properties and cementation patterns of fault zones in the northern part of the Albuquerque Basin, New Mexico—Implications for ground-water flow: U.S. Geological Survey Professional Paper 1719, 44 p.

Minor, S.A., Hudson, M.R., Grauch, V.J.S., and Sawyer, D.A., 2006, Structure of the Santo Domingo Basin and La Bajada constriction area, New Mexico, *in* Minor, S.A., ed., The Cerrillos uplift, the La Bajada constriction, and hydrogeologic framework of the Santo Domingo Basin, Rio Grande rift, New Mexico: U.S. Geological Survey Professional Paper 1720–E, p. 91–115. *http://pubs.usgs.gov/pp/1720/downloads/pdf/p1720E.pdf.*

Mourant, W.A., 1980, Hydrologic maps and data for Santa Fe County, New Mexico: New Mexico State Engineer Basic Data Report, Santa Fe, 180 p.

Muehlberger, W.R., 1979, The Embudo fault between Pilar and Arroyo Hondo, New Mexico—An active intracontinental transform fault: New Mexico Geological Society Guidebook 30, p. 77–82.

Myer, Caroline, and Smith, G.A., 2006, Stratigraphic analysis of the Yates #2 La Mesa well and implications for southern Española Basin tectonic history: New Mexico Geology, v. 28, no. 3, p. 75–83.

Nabighian, M.N., Ander, M.E., Grauch, V.J.S., Hansen, R.O., LaFehr, T.R., Li, Y., Pearson, W.C., Peirce, J.W., Phillips, J.D., and Ruder, M.E., 2005, The historical development of the gravity method in exploration: Geophysics, v. 70, p. 63ND–89ND.

Nabighian, M.N., Grauch, V.J.S., Hansen, R.O., LaFehr, T.R., Li, Y., Peirce, J.W., Phillips, J.D., and Ruder, M.E., 2005, Historical development of the magnetic method in exploration: Geophysics, v. 70, p. 33ND–61ND.

Nabighian, M.N., and Hansen, R.O., 2001, Unification of Euler and Werner deconvolution in three dimensions via the generalized Hilbert transform: Geophysics, v. 66, p. 1805–1810.

New Mexico Bureau of Geology and Mineral Resources, 2003, Geologic map of New Mexico: New Mexico Bureau of Geology and Mineral Resources, scale 1:500,000.

Nowell, D.A.G., 1996, Gravity modelling of the Valles caldera: New Mexico Geological Society Guidebook 47, p. 121–128.

Phillips, J.D., 1997, Potential-field geophysical software for the PC, version 2.2: U.S. Geological Survey Open-File Report 97–725; unpaged. *http://pubs.usgs.gov/of/1997/ofr-97-0725/.*

Phillips, J.D., 2000, Locating magnetic contacts—A comparison of the horizontal gradient, analytic signal, and local wavenumber methods [abs.]: Annual International Meeting of Society of Exploration Geophysicists, 70th, Expanded Abstracts, v. 19, p. 402–405. *http://seg.org/publications/archive/exAbsHist/abs_pdf/2000/ea200004020405.pdf.*

Phillips, J.D., 2001, Designing matched bandpass and azimuthal filters for the separation of potential field anomalies by source region and source type [abs.]: Geophysical Conference and Exhibition of Australian Society of Exploration Geophysicists, 15th, Extended Abstracts, CD-ROM.

Phillips, J.D., 2002, Two-step processing for 3D magnetic source locations and structural indices using extended Euler or analytic signal methods: Society of Exploration Geophysicists, 2002 Technical Program Expanded Abstracts, 4 p.

Phillips, J.D., and Grauch, V.J.S., 2004, Thickness of Santa Fe Group sediments in the Española Basin south of Santa Fe, New Mexico, as estimated from aeromagnetic data: U.S. Geological Survey Open-File Report 2004–1354, 24 p. *http://pubs.usgs.gov/of/2004/1354/*.

Phillips, J.D., Hansen, R.O., and Blakely, R.J., 2007, The use of curvature in potential-field interpretation: Exploration Geophysics, v. 38, p. 111–119.

Read, A.S., Koning, D.J., and Johnson, P.S., 2005 (orig. publ. 2004), Generalized geologic map of the southern Española Basin, Santa Fe County, New Mexico: New Mexico Bureau of Geology and Mineral Resources Open-File Report 481, scale 1:50,000, CD-ROM.

Read, A.S., Koning, D.J., Smith, G.A., Ralser, S., Rogers, J., and Bauer, P.W., 2003 (orig. publ. 2000), Preliminary geologic map of the Santa Fe 7.5-minute quadrangle: New Mexico Bureau of Geology and Mineral Resources Open-File Geologic Map OF–GM–32, scale 1:24,000.

Read, A.S., Rogers, J.B., Ralser, S., Ilg, B.R., and Kelley, S., 2004, (orig. publ. 1999), Preliminary geologic map of the Seton Village 7.5-minute quadrangle, Santa Fe County, New Mexico: New Mexico Bureau of Geology and Mineral Resources Open-File Geologic Map OF–GM–23, scale 1:24,000.

Reid, A.B., Allsop, J.M., Granser, H., Millett, A.J., and Somerton, I.W., 1990, Magnetic interpretation in three dimensions using Euler deconvolution: Geophysics, v. 55, p. 80–91.

Reynolds, R.L., Rosenbaum, J.G., Hudson, M.R., and Fishman, N.S., 1990, Rock magnetism, the distribution of magnetic minerals in the Earth's crust, and aeromagnetic anomalies: U.S. Geological Survey Bulletin 1924, p. 24–45.

Robinson, B.A., Broxton, D.E., and Vaniman, D.T., 2005, Observations and modeling of deep perched water beneath the Pajarito Plateau: Vadose Zone Journal, v. 4, p. 637–652. doi:10.2136/vzj2004.00168

Rodriguez, B.D., Deszcz-Pan, M., and Sawyer, D.A., 2006, Electromagnetic studies and subsurface mapping of electrical resistivity in the La Bajada constriction area, New Mexico, *in* Minor, S.A., ed., The Cerrillos uplift, the La Bajada constriction, and hydrogeologic framework of the Santo Domingo Basin, Rio Grande rift, New Mexico: U.S. Geological Survey Professional Paper 1720–F, p. 118–162. *http://pubs.usgs.gov/pp/1720/downloads/pdf/p1720F.pdf*.

Rodriguez, B.D., and Sawyer, D.A., 2007, Correlation of magnetotelluric resistivity soundings and regional borehole geophysical rock properties to stratigraphy of the northern Rio Grande rift, New Mexico: Geological Society of America Abstracts with Programs, v. 39, no. 6, p. 494.

Sauer, R.R., 1999, Petrochemistry and geochronology of plutons relative to tectonics in the San Pedro–Ortiz porphyry belt, New Mexico: University of Colorado, Boulder, M.S. thesis, 115 p.

Sawyer, D.A., 2004, Processed Landsat 7 satellite imagery of the Española Basin region, New Mexico: U.S. Geological Survey Open-File Report 2004–1040–A, CD-ROM.

Sawyer, D.A., and Minor, S.A., 2006a, Geologic setting of the La Bajada constriction and Cochiti Pueblo area, New Mexico, *in* Minor, S.A., ed., The Cerrillos uplift, the La Bajada constriction, and hydrogeologic framework of the Santo Domingo Basin, Rio Grande rift, New Mexico: U.S. Geological Survey Professional Paper 1720–A, p. 1–23. *http://pubs.usgs.gov/pp/1720/downloads/pdf/p1720A.pdf*.

Sawyer, D.A., and Minor, S.A., 2006b, Hydrogeologic framework of the La Bajada constriction area, New Mexico—Integration of subsurface and surface geology, *in* Minor, S.A., ed., The Cerrillos uplift, the La Bajada constriction, and hydrogeologic framework of the Santo Domingo Basin, Rio Grande rift, New Mexico: U.S. Geological Survey Professional Paper 1720–G, p.167–189. *http://pubs.usgs.gov/pp/1720/downloads/pdf/p1720G.pdf*.

Sawyer, D.A., Minor, S.A., Grauch, V.J.S., Rodriguez, B.D., and Thompson, R.A., 2006, Geologic cross sections spanning the La Bajada constriction and northern Cerrillos uplift, New Mexico (plate 6), *in* Minor, S.A., ed., The Cerrillos uplift, the La Bajada constriction, and hydrogeologic framework of the Santo Domingo Basin, Rio Grande rift, New Mexico: U.S. Geological Survey Professional Paper 1720, scale 1:50,000.

Sawyer, D.A., Minor, S.A., Thompson, R.A., Shroba, R.R., Smith, G.A., Dethier, D.P., Grauch, V.J.S., and Brandt, T.R., 2006, Geologic map of the Cochiti Pueblo area, New Mexico (plate 2), *in* Minor, S.A., ed., The Cerrillos uplift, the La Bajada constriction, and hydrogeologic framework of the Santo Domingo Basin, Rio Grande rift, New Mexico: U.S. Geological Survey Professional Paper 1720, scale 1:50,000.

Sawyer, D.A., Shroba, R.R., Minor, S.A., and Thompson, R.A., 2002, Geologic map of the Tetilla Peak quadrangle, Santa Fe and Sandoval Counties, New Mexico: U.S. Geological Survey Miscellaneous Field Studies Map MF–2352, scale 1:24,000, version 1.0.

Shroba, R.R., Thompson, R.A., Minor, S.A., Grauch, V.J.S., and Brandt, T.R., 2005, Geologic map of Agua Fria quadrangle, Santa Fe County, New Mexico: U.S. Geological Survey Scientific Investigations Map 2896, scale 1:24,000. *http://pubs.usgs.gov/sim/2005/2896*.

Simpson, R.W., Jachens, R.C., Blakely, R.J., and Saltus, R.W., 1986, A new isostatic residual gravity map of the conterminous United States with a discussion on the significance of isostatic residual anomalies: Journal of Geophysical Research, v. 91, no. B8, p. 8348–8372.

Smith, G.A., 2000, Oligocene onset of Santa Fe Group sedimentation near Santa Fe, New Mexico [abs.]: New Mexico Geology, v. 22, no. 2, p. 43.

Smith, G.A., Larsen, D., Harlan, S.S., McIntosh, W.C., Erskine, D.W., and Taylor, S., 1991, A tale of two volcaniclastic aprons—Field guide to the sedimentology and physical volcanology of the Oligocene Espinaso Formation and Miocene Peralta Tuff, north-central New Mexico, *in* Julian, Betsy, and Zidek, Jiri, Field guide to geologic excursions in New Mexico and adjacent areas of Texas and Colorado: New Mexico Bureau of Mines and Mineral Resources Bulletin 137, p. 87–103.

Smith, R.S., Thurston, J.B., Dai, Ting-Fan, and MacLeod, I.N., 1998, iSPI™—The improved source parameter imaging method: Geophysical Prospecting, v. 46, p. 141–151.

Spiegel, Zane, and Baldwin, Brewster, 1963, Geology and water resources of the Santa Fe area, New Mexico, *with contributions by* F.E. Kottlowski and E.L. Barrows *and a section on geophysics* by H.A. Winkler: U.S. Geological Survey Water-Supply Paper 1525, 258 p.

Sweeney, R.E., Grauch, V.J.S., and Phillips, J.D., 2002, Merged digital aeromagnetic data for the Albuquerque and southern Española Basins, New Mexico: U.S. Geological Survey Open-File Report 02–205, 15 p. *http://pubs.usgs.gov/of/2002/ofr-02-0205*.

Syberg, F.J.R., 1972, A Fourier method for the regional-residual problem of potential fields: Geophysical Prospecting, v. 20, p. 47–75.

Talwani, Manik, 1965, Computation with the help of a digital computer of magnetic anomalies caused by bodies of arbitrary shape: Geophysics, v. 30, no. 5, p. 797–817.

Thompson, D.T., 1982, EULDPH—A new technique for making computer-assisted depth estimates from magnetic data: Geophysics, v. 47, p. 31–37.

Thompson, R.A., Sawyer, D.A., Hudson, M.R., Grauch, V.J.S., and McIntosh, W.C., 2006, Cenozoic volcanism of the La Bajada constriction region, *in* Minor, S.A., ed., The Cerrillos uplift, the La Bajada constriction, and hydrogeologic framework of the Santo Domingo Basin, Rio Grande rift, New Mexico: U.S. Geological Survey Professional Paper 1720–C, p. 41–60. *http://pubs.usgs.gov/pp/1720/downloads/pdf/p1720C.pdf*.

Thurston, J.B., and Smith, R.S., 1997, Automatic conversion of magnetic data to depth, dip, and susceptibility contrast using the SPI™ method: Geophysics, v. 62, p. 807–813.

U.S. Geological Survey, Sander Geophysics, Ltd., and Geoterrex, Inc., 1999, Digital data from the Sandoval–Santa Fe, Belen, and Cochiti aeromagnetic surveys, covering areas in Sandoval, Santa Fe, Rio Arriba, Valencia, and Socorro Counties, New Mexico: U.S. Geological Survey Open-File Report 99–404, CD-ROM.

Wilkins, D.W., 1998, Summary of the southwest alluvial basins regional aquifer-system analysis in parts of Colorado, New Mexico, and Texas: U.S. Geological Survey Professional Paper 1407–A, p. A1–A49.

Appendixes

Appendix 1. Well Data Used to Constrain Three-Dimensional Integrated Model and Gravity Inversion.

[Depths picked for various geologic formations in wells that penetrate the base of the Santa Fe Group. Eastings and northings are based on a Universal Transverse Mercator Projection, zone 13, North American Datum of 1927. Formation codes: Mz, Mesozoic clastic rocks; PC, Precambrian basement rocks, Pz, Paleozoic clastic and carbonate rocks; SFG, Santa Fe Group; Tgd, Eocene Galisteo and late Paleocene Diamond Tail Formations; Ti, Tertiary intrusive rocks; Tov, Tertiary older volcanic rocks. Tgd, Mz, and Pz constitute the pre-rift sedimentary section. Ti depth intervals may indicate sills within older units. TD, total depth of well; NMBGMR, New Mexico Bureau of Geology and Mineral Resources; USGS, U.S. Geological Survey]

Site identifier (oil exploration well name, if applicable)	Easting (meters)	Northing (meters)	Elevation (feet)	Total depth of well (feet)	Formations in well	Depth to SFG base (feet)	Depth to top of formation (feet)					Ti depth interval (feet)	Data source*
							Tov	Tgd	Mz	Pz	PC		
96–1	419028	3931921	6,908	405	SFG/Pz/PC	200				200	220		[1]
96–4	417801	3931928	6,821	470	SFG/Pz	280				280			[1]
castlewig1 (Castle Wigzell Kelly Federal #1).	413180	3981070	6,040	2,703	SFG/Tov/Pz/ PC.	2,380	2,380			2,420	2,700		[2]
CKZ#1–G–7 (John Gianardi #1).	402260	3930730	6,210	7,773	SFG/Tgd/Mz/Pz.	175		175	1,659	7,109			[3]
EB–001	398579	3935004	6,063	221	SFG/Tgd	72		72					[1]
EB–002	399120	3935618	6,070	380	SFG/Ti	210						210–TD	[1]
EB–007	403983	3929089	6,190	146	SFG/Tov	96	96						[1]
EB–020	414999	3943065	7,043	658	SFG/Tov	349	349						[1]
EB–106–RSL#1	416860	3929416	6,705	1,490	SFG/Mz	110			110				[1]
EB–118	416160	3943637	7,141	600	SFG/Tov/Tgd	80	80	240					[1]
EB–139–RSL#2	417190	3928776	6,680	1,558	SFG/Mz	74			74				[1]
EB–202	410066	3926479	6,318	156	SFG/Tov	111	111						[1]
EB–209	405075	3922945	6,105	276	SFG/Tov	23	23						[1]
EB–211	407315	3926117	6,267	200	SFG/Tov	90	90						[1]
EB–214	401271	3932150	6,186	210	SFG/Tgd	130		130					[1]
EB–344	407223	3930261	6,316	400	SFG/Tov	70	70						[1]
EB–371	416308	3954596	7,209	980	SFG/PC	955					955		[1]
EB–374	403678	3928978	6,178	200	SFG/Tov	110	110						[1]
EB–378	400527	3933618	6,121	110	SFG/Tov	75	75						[1]

Appendix 1. Well Data Used to Constrain Three-Dimensional Integrated Model and Gravity Inversion.—Continued

[Depths picked for various geologic formations in wells that penetrate the base of the Santa Fe Group. Eastings and northings are based on a Universal Transverse Mercator Projection, zone 13, North American Datum of 1927. Formation codes: Mz, Mesozoic clastic rocks; PC, Precambrian basement rocks, Pz, Paleozoic clastic and carbonate rocks; SFG, Santa Fe Group; Tgd, Eocene Galisteo and late Paleocene Diamond Tail Formations; Ti, Tertiary intrusive rocks; Tov, Tertiary older volcanic rocks. Tgd, Mz, and Pz constitute the pre-rift sedimentary section. Ti depth intervals may indicate sills within older units. TD, total depth of well; NMBGMR, New Mexico Bureau of Geology and Mineral Resources; USGS, U.S. Geological Survey]

Site identifier (oil exploration well name, if applicable)	Easting (meters)	Northing (meters)	Elevation (feet)	Total depth of well (feet)	Formations in well	Depth to SFG base (feet)	Depth to top of formation (feet)					Ti depth interval (feet)	Data source*
							Tov	Tgd	Mz	Pz	PC		
EB–404	403062	3927680	6,140	150	SFG/Tgd	79		79					[1]
EB–412	404975	3931598	6,274	510	SFG/Tov	350	350						[1]
EUI#13–95–1	417735	3932199	6,860	1,000	SFG/Pz	230				230			[1]
EUI#14–96–2	417620	3932675	6,851	400	SFG/Pz	200				200			[1]
EUI#15–96–3	417949	3931921	6,852	400	SFG/Pz	240				240			[1]
G2–4	409750	3925300	6,343	2,010	SFG/Tov/Tgd	100	100						[4]
G–8A‡	401569	3925678	6,083	820	Tov/Tgd		0	485					[1]
G–11A	412817	3933958	6,612	460	SFG/Tov	200	200						[1]
G–12	405230	3923870	6,183	1,000	SFG/Tov	135	135						[1]
G–16	405710	3924566	6,161	170	SFG/Tov	100	100						[1]
G–25	404386	3931835	6,277	150	SFG/Tov	139	139						[1]
G–64	405767	3929190	6,262	927	SFG/Tov/Tgd	170	170	850					[1]
G–112	399569	3934917	6,121	160	SFG/Tov	120	120						[1]
G–178	414743	3930998	6,624	580	SFG/Tov	120	120						[1]
G–179/EB–581	415097	3928250	6,584	600	SFG/Tgd	80		80					[1]
G–181	415664	3931321	6,709	500	SFG/Tov	280	280						[1]
G–182	414060	3931538	6,625	500	SFG/Tov	170	170						[1]
G–205	406143	3926773	6,223	600	SFG/Tov	190	190						[1]
G–206	406949	3927579	6,264	600	SFG/Tov	105	105						[1]
G–214	406910	3927125	6,246	500	SFG/Tov	110	110						[1]
G–215	406540	3926575	6,260	1,000	SFG/Tov	200	200						[1]
G–218	406800	3926621	6,263	415	SFG/Tov	120	120						[1]

Appendix 1. Well Data Used to Constrain Three-Dimensional Integrated Model and Gravity Inversion.—Continued

[Depths picked for various geologic formations in wells that penetrate the base of the Santa Fe Group. Eastings and northings are based on a Universal Transverse Mercator Projection, zone 13, North American Datum of 1927. Formation codes: Mz, Mesozoic clastic rocks; PC, Precambrian basement rocks, Pz, Paleozoic clastic and carbonate rocks; SFG, Santa Fe Group; Tgd, Eocene Galisteo and late Paleocene Diamond Tail Formations; Ti, Tertiary intrusive rocks; Tov, Tertiary older volcanic rocks. Tgd, Mz, and Pz constitute the pre-rift sedimentary section. Ti depth intervals may indicate sills within older units. TD, total depth of well; NMBGMR, New Mexico Bureau of Geology and Mineral Resources; USGS, U.S. Geological Survey]

Site identifier (oil exploration well name, if applicable)	Easting (meters)	Northing (meters)	Elevation (feet)	Total depth of well (feet)	Formations in well	Depth to SFG base (feet)	Depth to top of formation (feet)					Ti depth interval (feet)	Data source*
							Tov	Tgd	Mz	Pz	PC		
JAILWell	405056	3935836	6,341	1,365	SFG/Tov	1,214	1,214						[1]
Lot12–2	415009	3927268	6,603	480	SFG/Tgd	135		135					[5]
Lot14–3	414539	3926850	6,584	510	SFG/Tgd	125		125					[5]
Lot7–1	416025	3927090	6,662	510	SFG/Mz	70			70				[5]
McMillan	414140	3930160	6,491	640	SFG/Tov	160	160						[6]
merrblk2 (Merrion Blackshare #2).	383255	3918401	6,010	6,820	SFG/Tov/Tgd/ Ti/Tgd/Mz.	2,150	2,150	3,534	6,407			5,253–6,305	[7]
MonteAltoPlaza	417200	3933170	6,870	1,000	SFG/Pz	255				255			[6]
ND1	399600	3939334	6,220	900	SFG/Tov	790	790						[1]
ND9	409491	3932823	6,419	1,717	SFG/Tov	475	475						[1]
ND10	412409	3932369	6,510	1,117	SFG/Tov	115	115						[1]
ND38	401379	3937859	6,200	1,145	SFG/Tov	600	600						[1]
ND49	406741	3925436	6,200	660	SFG/Tov	80	80						[1]
ND85	401047	3938905	6,150	750	SFG/Tov	710	710						[1]
OB–A	407775	3939338	6,475	1,802	SFG/Tov	1,710	1,710						[1]
peltblk1 (Pelto Blackshare #1).	384765	3917614	6,034	7,025	SFG/Tov/Tgd/Mz.	1,480	1,480	3,230	4,300				[7]
peltort1 (Pelto Ortiz #1).	403901	3919011	5,804	7,450	SFG/Tgd/Mz	79		79	4,679				[3]
R1A	420247	3931136	6,886	232	SFG/Pz/PC	42				42	225		[1]
R1–EUI#8	419757	3930646	6,844	325	SFG/Pz	95				95			[1]
R3	418445	3931260	6,860	258	SFG/Pz	164				164			[1]
R5	419145	3930326	6,818	332	SFG/Pz	176				176			[1]
R36	416780	3934540	6,845	405	SFG/Pz	146				146			[1]

Appendix 1. Well Data Used to Constrain Three-Dimensional Integrated Model and Gravity Inversion.—Continued

[Depths picked for various geologic formations in wells that penetrate the base of the Santa Fe Group. Eastings and northings are based on a Universal Transverse Mercator Projection, zone 13, North American Datum of 1927. Formation codes: Mz, Mesozoic clastic rocks; PC, Precambrian basement rocks, Pz, Paleozoic clastic and carbonate rocks; SFG, Santa Fe Group; Tgd, Eocene Galisteo and late Paleocene Diamond Tail Formations; Ti, Tertiary intrusive rocks; Tov, Tertiary older volcanic rocks. Tgd, Mz, and Pz constitute the pre-rift sedimentary section. Ti depth intervals may indicate sills within older units. TD, total depth of well; NMBGMR, New Mexico Bureau of Geology and Mineral Resources; USGS, U.S. Geological Survey]

Site identifier (oil exploration well name, if applicable)	Easting (meters)	Northing (meters)	Elevation (feet)	Total depth of well (feet)	Formations in well	Depth to SFG base (feet)	Depth to top of formation (feet)					Ti depth interval (feet)	Data source*
							Tov	Tgd	Mz	Pz	PC		
R37	416904	3933297	6,836	540	SFG/Pz	180				180			[1]
R49	418178	3934458	6,937	129	SFG/Pz	42				42			[1]
R50	417744	3934277	6,900	440	SFG/Pz	79				79			[1]
R–51	417390	3934580	6,890	311	SFG/Pz	91				91			[1]
SVTD205	415460	3938710	6,912	205	SFG/PC	78					78		[8]
TH3C	415850	3929575	6,680	800	SFG/Mz	95			95				[1]
tomckee1‡ (Trans-Ocean McKee #1).	410103	3916593	5,936	8,128	Tgd/Mz/Pz			0	335	5,350			[3]
ULURU	419527	3932746	6,996	770	SFG/PC	190					190		[1]
W2A	416154	3934587	6,796	330	SFG/Pz	285				285			[1]
W3–EUI#3	417888	3934408	6,918	324	SFG/Pz/PC	62				62	311		[1]
W4–EUI#4	417829	3934581	6,931	375	SFG/Pz/PC	52				52	369		[1]
W–9/WX2E	412842	3932575	6,535	322	SFG/Tov	80	80						[1]
WX11W	419440	3929255	6,765	260	SFG/Mz	80			80				[1]
WX9S/X9N	414451	3928591	6,556	325	SFG/Tov	62	62						[1]
X10N	416990	3928739	6,665	220	SFG/Mz	80			80				[1]
X11A	419744	3929610	6,815	300	SFG/Mz	100			100				[1]
X3C1/2S	415715	3928965	6,635	200	SFG/Mz	120			120				[1]
X3C3/4S	416055	3928777	6,620	260	SFG/Mz	50			50				[1]
X3CE	416690	3930015	6,741	260	SFG/Mz?	153			153				[1]
X3CN	415970	3930380	6,700	240	SFG/Mz?	210			210				[1]
X3CS	415872	3929550	6,680	800	SFG/Mz	97			97				[1]

Appendix 1. Well Data Used to Constrain Three-Dimensional Integrated Model and Gravity Inversion.—Continued

[Depths picked for various geologic formations in wells that penetrate the base of the Santa Fe Group. Eastings and northings are based on a Universal Transverse Mercator Projection, zone 13, North American Datum of 1927. Formation codes: Mz, Mesozoic clastic rocks; PC, Precambrian basement rocks, Pz, Paleozoic clastic and carbonate rocks; SFG, Santa Fe Group; Tgd, Eocene Galisteo and late Paleocene Diamond Tail Formations; Ti, Tertiary intrusive rocks; Tov, Tertiary older volcanic rocks. Tgd, Mz, and Pz constitute the pre-rift sedimentary section. Ti depth intervals may indicate sills within older units. TD, total depth of well; NMBGMR, New Mexico Bureau of Geology and Mineral Resources; USGS, U.S. Geological Survey]

Site identifier (oil exploration well name, if applicable)	Easting (meters)	Northing (meters)	Elevation (feet)	Total depth of well (feet)	Formations in well	Depth to SFG base (feet)	Depth to top of formation (feet)					Ti depth interval (feet)	Data source*
							Tov	Tgd	Mz	Pz	PC		
X3CW	414945	3929323	6,619	250	SFG/Tov	155	155						[1]
X3DW/WX3DE	413418	3931155	6,560	345	SFG/Tov	95	95						[1]
YLM#2 (Yates La Mesa #2).	405534	3949690	6,610	7,710	SFG/Tov/Pz/PC.	3,966	3,966			6,018	7,534		[9]
YLM#3 (Yates La Mesa #3).	406009	3932807	6,336	4,740	SFG/Tov/Ti/Mz.	393	393	2,300	3,739			3,128–3,739	[10]

*Data sources: [1] Database compiled by P.S. Johnson and D.J. Koning, NMBGMR, accessed May, 2008; [2] Koning, Nyman, and others (2005); [3] D.J. Koning, NMBGMR, unpub. data, 2007; [4] Lisenbee (1999); [5] D.J. Koning, NMBGMR, unpub. data, 2006; [6] Meghan Hodgins, Glorieta Geoscience, Inc., written commun., 2007; [7] D.A. Sawyer, USGS, written commun., 2007; [8] Read and others (2004); [9] Myer and Smith (2006); [10] D.A. Sawyer, USGS, and D.J. Koning, NMBGMR, written commun., 2008.

‡G8–A and tomckee1 were not used in the gravity inversion because Santa Fe Group is not reported in those wells.

Appendix 2. Well Data Used to Guide Three-Dimensional Integrated Model.

[Data for wells that do not penetrate below Santa Fe Group. Total depths provide minimum depths to base of Santa Fe Group. Data compiled and maintained by P.S. Johnson and D.J. Koning, New Mexico Bureau of Geology and Mineral Resources; accessed May 2008. Coordinates are in Universal Transverse Mercator Projection, zone 13, North American Datum of 1927]

Site identifier	Easting (meters)	Northing (meters)	Elevation (feet)	Total depth of well (feet)
ArchMW	413260	3953571	7,200	1,153
BuckMW	398638	3961316	5,960	2,500
EB–004	411115	3935891	6,594	560
EB–111	414112	3940815	6,909	650
EB–117	415600	3943321	7,042	465
EB–244/SF–1	412888	3946766	6,879	2,020
EB–358/CDEX	409417	3939620	6,555	1,500
EB–385	404356	3936059	6,302	802
G–55	413428	3942801	6,921	495
G–176	412172	3934258	6,579	410
G–180	412022	3934341	6,568	440
ND2	410939	3942442	6,700	1,000
ND3	409556	3941015	6,559	1,000
ND4	411129	3939205	6,660	1,490
ND5	407873	3937626	6,440	995
ND6	406018	3936207	6,385	1,600
ND7	401411	3936858	6,185	680
ND8	404028	3936442	6,305	1,000
ND11	402226	3939282	6,180	1,000
ND12	405955	3947056	6,519	980
ND17	401742	3946125	6,320	1,985
ND36	403661	3939279	6,260	1,400
ND40	400416	3941083	6,280	970
ND41	402439	3942100	6,330	2,000
ND43	401461	3944117	6,322	1,000
ND46	404520	3944262	6,400	1,940
ND52	402455	3940876	6,220	1,000
ND53	401422	3939470	6,140	1,000
ND54	402855	3939482	6,220	1,200
ND55	407108	3942283	6,450	1,450
ND59	401199	3940058	6,260	1,000
ND69	401407	3938451	6,205	1,200
ND76	401636	3939705	6,180	1,140
ND77	401021	3939656	6,240	1,000
ND80	400799	3939253	6,202	800
ND81	400412	3939492	6,190	800
ND82	400595	3939474	6,170	800
ND83	400834	3939664	6,230	1,000
ND84	400202	3939506	6,230	775
ND86	400617	3939083	6,150	810

Appendix 2. Well Data Used to Guide Three-Dimensional Integrated Model.—Continued

[Data for wells that do not penetrate below Santa Fe Group. Total depths provide minimum depths to base of Santa Fe Group. Data compiled and maintained by P.S. Johnson and D.J. Koning, New Mexico Bureau of Geology and Mineral Resources; accessed May 2008. Coordinates are in Universal Transverse Mercator Projection, zone 13, North American Datum of 1927]

Site identifier	Easting (meters)	Northing (meters)	Elevation (feet)	Total depth of well (feet)
ND87	401225	3939290	6,160	840
ND88	402023	3939079	6,170	980
ND89	399902	3940244	6,250	920
ND90	400830	3940309	6,250	1,000
ND91	401631	3939089	6,160	900
ND92	401384	3938854	6,170	800
ND93	401188	3938661	6,150	670
ND94	400803	3939298	6,220	760
ND95	400899	3939494	6,220	975
ND96	400585	3938884	6,120	705
ND97	400814	3939543	6,230	795
R2B	416345	3934450	6,804	260
R11	414271	3934563	6,684	925
SVX8	414817	3938660	6,883	300
W1–EUI#1	411867	3934697	6,556	719
W2–EUI#2	414206	3934726	6,666	350
WX3BN–EUI#6	415869	3932198	6,752	280
WX3N–EUI#7	416683	3931104	6,761	270
X1E	412637	3934197	6,584	300

Appendix 3. Magnetic Depth Estimation Methods Used in This Study.

Factor	Method		
	Multisource Werner	**Local wavenumber**	**Two-step extended Euler**
Input type	Magnetic profile data	Magnetic profile data or gridded magnetic data.	Gridded magnetic data.
Approach	Complex linear regression within sliding windows using the profile and its derivatives.	The local wavenumber profile or grid is calculated from the derivatives of the magnetic (or other potential) field. Local curvature is used to locate the ridge crests of the local wavenumber and estimate the depth, strike (for grids), and structural index.	Step one—Least squares solution of Euler's homogeneity equation within small or moderate-sized windows using the magnetic field, its first derivatives, its Hilbert transform components, and their first derivatives. Step two—Correct or discard solutions above a user-defined minimum depth surface, such as the ground surface or a surface representing the depth to a particular magnetic unit interpreted independently by use of other subsurface information.
Assumptions	Magnetic anomalies within the analysis window are all produced by multiple sources having the same integer structural index (N). Sources are two-dimensional Strikes of sources are perpendicular to the profile azimuth. Total magnetization is parallel to the inducing Earth field.	Magnetic anomalies within small data windows are produced by a single isolated two-dimensional source. Sources strike perpendicular to the profile azimuth, for profile analysis. Total magnetization is parallel to the inducing Earth field.	Magnetic anomalies within small or moderate-sized data windows are produced by single isolated sources satisfying Euler's homogeneity equation. A minimum depth surface is available for testing and correcting solutions. All solutions below the minimum depth surface have a single known structural index (usually N=0). Solutions above the minimum depth surface can be corrected by increasing their structural index (N>0) until their depth estimates match the minimum depth surface or discarded if the required adjustment results in values of N considered too high by the interpreter.
Required input parameters	Window length (a multiple of 22) Number of sources contributing to the anomaly within the window (we used two or three for this study). Integer structural index of the sources (usually N=0 or 1). Clustering radius (as a percentage of depth). Profile azimuth Earth field strength and direction (optional).	Minimum and maximum acceptable structural index (N).	Window size. Initial (minimum) structural index value (usually N=0). Threshold (maximum) structural index value (usually N=1 for geologic sources or N=3 for anthropogenic sources). Maximum allowable error in the depth (typically 15 percent). Minimum depth surface in grid form.

Appendix 3. Magnetic Depth Estimation Methods Used in This Study.—Continued

Factor	Method		
	Multisource Werner	**Local wavenumber**	**Two-step extended Euler**
Output	Source locations. Estimated dip and magnetic susceptibility contrast are provided if Earth field is specified. Clustering of sources is an indication of reliability, so that solutions are usually averaged within clusters.	Source locations and structural indices. Strikes of sources are provided for grids. Estimated dip and magnetic susceptibility contrast are provided for profile data.	Source locations, error estimates, estimated structural indices for sources on the minimum depth surface.
Limitations	Cannot be used to determine the "best" structural index, so it is up to the interpreter to decide between the shallow "contact" solution or the deeper "sheet" solution typically produced by each source. 3D sources will not give accurate results. Depths will be overestimated if strike is not perpendicular to the profile. Dip and susceptibility contrast will be in error if remanent component contributes to a total magnetization that is oblique to Earth field direction. Deeper sources are hard to identify and locate. Error estimates are not provided.	Interference from multiple nearby sources and noise can produce inaccurate results. Topographic and other 3D sources will produce inaccurate results. For profile data, depths will be overestimated if strike is not perpendicular to the profile. For profile data, dip and susceptibility contrast will be in error if remanent component contributes to a total magnetization that is oblique to Earth field direction. Deeper sources are hard to identify and locate. Error estimates are not provided	Anomalies resulting from interfering sources will produce unreliable results. Shallow solutions are strongly controlled by the minimum depth surface. Solution depths below the minimum depth surface depend strongly on the assumed minimum structural index. Solutions from adjacent windows tend to scatter and may require averaging within clusters.
Advantages	Provides a robust multisource method. Generally works better than other (single-source) methods on profile data.	Provides a robust method for estimating source locations and structural indices. Solutions from grid data tend to follow linear magnetic sources, for which strike estimates are provided.	Error estimates, which are derived from the least-squares regression, are provided. 3D sources are permitted.
References	Hansen and Simmonds (1993)	Thurston and Smith (1997) Phillips (2000) Phillips (2002) Phillips and others (2007)	Reid and others (1990). Nabighian and Hansen (2001). Phillips (2002). Phillips and Grauch (2004).

Appendix 4. Other Point-Located Data.

[Depths to the base of the Santa Fe Group at single sites within or surrounding the study area from well data, representative depth picks from seismic-reflection and refraction sections, and 2D resistivity models from magnetotelluric soundings. Well data listed without a formal reference correspond to data available from the Petroleum Library at the New Mexico Bureau of Geology and Mineral Resources. m/s, meters per second; MT, magnetotelluric; SFG, Santa Fe Group]

Site identifier	Easting[1] (meters)	Northing[1] (meters)	Depth to base of SFG (feet)	Location code[2]	Data source
Well data outside the study area used to constrain the gravity inversion					
cpfed	384792	3908568	80	G	Colorado Plateau Federal exploration well.
davtam1y	344677	3916345	5,600	G	Davis Tamara 1-Y exploration well.
lanlaet4	350565	3962027	184	G	AET-4, Goff and others (1988).
lanlfh2	348957	3971676	433	G	FH-2.
lanlgt1	349289	3974409	160	G	GT-1, Goff and others (1988).
lanljs1	346622	3958867	73	G	JS-1, Goff and others (1988).
lanlpc1	349970	3971314	193	G	PC-1, Goff and others (1988).
lanlpc2	348012	3971285	394	G	PC-2, Goff and others (1988).
lanltsta	349590	3971692	155	G	LANL Test Hole A.
lanltstb	350871	3978961	440	G	LANL Test Hole B.
lanltstc	353558	3981670	580	G	LANL Test Hole C.
lanltstd	345529	3972980	120	G	LANL Test Hole D.
lanlvc1	353666	3967306	1,107	G	VC-1, Goff and others (1988).
lanlvc2	354544	3974563	2,625	G	VC-2, Goff and others (1988).
shsfp1	348375	3913234	2,969	G	Shell Santa Fe Pacific #1.
shsfp3	332702	3910313	3,996	G	Shell Santa Fe Pacific #3.
shwmf	337593	3893194	8,540	G	Shell West Mesa Federal exploration well.
ugbaca12	356490	3970880	6,594	G	Union Geothermal Baca 12, Goff and others (1988).
ugbaca17	357565	3973780	5,479	G	Union Geothermal Baca 17.
ugbaca20	357720	3973315	5,335	G	Union Geothermal Baca 22.
ugbaca22	357408	3973515	5,331	G	Union Geothermal Baca 17.
ugbaca4	358240	3972680	5,971	G	Union Geothermal Baca 4, Goff and others (1988).
wc23-4	352763	3974904	550	G	WC 23-4, Goff and others (1988).
Point depth picks from seismic reflection data					
velarde3	414759	3998974	3,150	G	Ferguson and others (1995), Velarde line, using velocity=2,400 m/s.
velarde6	417121	3997224	2,440	M	Ferguson and others (1995), Velarde line, using velocity=2400 m/s.
EW1_005	399779	3959097	8,702	S	J. Ferguson, written commun., 2007, using velocity=2,526 m/s.
EW1_025	402548	3959175	7,550	S	J. Ferguson, written commun., 2007, using velocity=2,526 m/s.
EW2_010	402240	3947379	4,658	S	J. Ferguson, written commun., 2007, using velocity=2,526 m/s.
NS1_355	404990	3958358	5,917	S	J. Ferguson, written commun., 2007, using velocity=2,526 m/s.
NS1_425	403056	3965269	7,297	S	J. Ferguson, written commun., 2007, using velocity=2,526 m/s.
NS1_445	402154	3967204	7,840	S	J. Ferguson, written commun., 2007, using velocity=2,526 m/s.
NS1_495	401297	3972147	7,873	S	J. Ferguson, written commun., 2007, using velocity=2,526 m/s.
AB3559	381791	4008951	800	G	Baldridge and others (1994).
AB3725	383607	4009167	2,200	G	Baldridge and others (1994).
AB4176	387742	4009094	2,000	G	Baldridge and others (1994).

Appendix 4. Other Point-Located Data.—Continued

[Depths to the base of the Santa Fe Group at single sites within or surrounding the study area from well data, representative depth picks from seismic-reflection and refraction sections, and 2D resistivity models from magnetotelluric soundings. Well data listed without a formal reference correspond to data available from the Petroleum Library at the New Mexico Bureau of Geology and Mineral Resources. m/s, meters per second; MT, magnetotelluric; SFG, Santa Fe Group]

Site identifier	Easting[1] (meters)	Northing[1] (meters)	Depth to base of SFG (feet)	Location code[2]	Data source
Interpreted depth picks from magnetotelluric models at sounding locations					
MT_EB01	406752	3978388	3,937	S	B. Rodriguez, written commun., 2007.
MT4	391060	3938490	656	S	Rodriguez and others (2006).
MT5	393370	3946820	3,937	S	B. Rodriguez, written commun., 2007.
MT8	391127	3942655	820	S	Rodriguez and others (2006).
MT9	395221	3955517	4,921	S	B. Rodriguez, written commun., 2007.
MT11	392391	3945184	1,640	S	Rodriguez and others (2006).
MT12	374449	3958861	2,624	M	Rodriguez and others (2006).
MT14	389104	3948096	2,624	S	B. Rodriguez, written commun., 2007.
MT15	388902	3956023	4,593	S	B. Rodriguez, written commun., 2007.
MT17	376785	3949770	4,593	M	Rodriguez and others (2006).
MT23	394527	3952588	5,741	S	B. Rodriguez, written commun., 2007.
MT25	394185	3948914	5,741	S	B. Rodriguez, written commun., 2007.
MT27	395460	3960730	5,250	S	B. Rodriguez, written commun., 2007.
MT28	388978	3951444	4,593	S	B. Rodriguez, written commun., 2007.
MT29	388978	3944059	984	S	B. Rodriguez, written commun., 2007.
MT31	372461	3954777	1,640	M	B. Rodriguez, written commun., 2007.
MT32	372338	3960693	2,297	M	B. Rodriguez, written commun., 2007.
MT36	374863	3952577	1,640	M	B. Rodriguez, written commun., 2007.

[1]Sites are located by use of the Universal Transverse Mercator Projection, zone 13, North American Datum of 1927.

[2]Location code: G, located in an area covered only by the gravity inversion; M, located in an area covered by both the 3D model and gravity inversion; S, located in the study area.

Publishing support provided by:
Denver Publishing Service Center

For more information concerning this publication, contact:
Team Chief Scientist, USGS Crustal Imaging and Characterization
Box 25046, Mail Stop 964
Denver, CO 80225
(303) 236-1312

Or visit the Crustal Imaging and Characterization Team Web site at:
http://crustal.usgs.gov/

USGS

Grauch and others—**Geophysical Interpretations of the Southern Española Basin, New Mexico**—Professional Paper 1761

ISBN 978-141132365-0